CNWRA 94-012

STOCHASTIC ANALYSIS OF LARGE-SCALE UNSATURATED FLOW AND TRANSPORT IN LAYERED, HETEROGENEOUS MEDIA

Prepared for

Nuclear Regulatory Commission
Contract NRC-02-93-005

Prepared by

Center for Nuclear Waste Regulatory Analyses
San Antonio, Texas

June 1994

CNWRA 94-012

STOCHASTIC ANALYSIS OF LARGE-SCALE UNSATURATED FLOW AND TRANSPORT IN LAYERED, HETEROGENEOUS MEDIA

Prepared for

Nuclear Regulatory Commission
Contract NRC-02-93-005

Prepared by

Amvrossios C. Bagtzoglou and Michael Muller

Center for Nuclear Waste Regulatory Analyses
San Antonio, Texas

June 1994

ABSTRACT

This report presents a suite of plausible methods and tools necessary for the realistic modeling and analysis of the complex, heterogeneous flow and transport processes anticipated or hypothesized to occur in the far-field of the proposed high-level waste (HLW) repository at Yucca Mountain, Nevada. More specifically, a possible methodology to study and assess the variability in model parameters and the effect of this variability on various performance measures is discussed. In this study, the detailed evaluation of flow and advection-dispersion of solute in unsaturated, heterogeneous porous media is simulated to understand transport processes in the far-field of a two-layer, faulted system analogous, in some respects, to Yucca Mountain, Nevada.

CONTENTS

CONTENTS (Cont'd)

FIGURES

FIGURES (Cont'd)

FIGURES (Cont'd)

TABLES

ACKNOWLEDGMENTS

This report was prepared to document work performed by the Center for Nuclear Waste Regulatory Analyses (CNWRA) for the Nuclear Regulatory Commission (NRC) under Contract No. NRC-02-93-005. The activities reported here were performed on behalf of the NRC Office of Nuclear Regulatory Research, Division of Regulatory Applications under FIN B6664. The report is an independent product of the CNWRA and does not necessarily reflect the views or regulatory position of the NRC.

Data used in this report were not developed under the quality assurance (QA) program described in the CNWRA Quality Assurance Manual. Therefore, their respective sources should be consulted for determining their level of QA. The computer codes used to perform the analyses presented in this report are BIGFLOW, SLIM, TURN3D, and FLUX. Only BIGFLOW and SLIM are presently controlled under the CNWRA Software Configuration Procedure TOP-018. TURN3D has been developed by others (see Chapter 2). Pertinent references should be consulted regarding the current status of this code, since its application has been extensively documented in the peer-reviewed literature. FLUX is the CNWRA-developed post-processor which is not currently under formal configuration control.

The first author acknowledges the continuous collaboration and support by Drs. R. Ababou (CEA/CEN), D.E. Dougherty (University of Vermont), and A.F.B. Tompson (Lawrence Livermore National Laboratory), and discussions and early efforts by Mr. M.R. Islam (Washington State University). Expert secretarial services, beyond the call of duty, are credited to Mr. A. Ramos. The SwRI Publication Services provided editorial, artistic, and production assistance. The authors thank Ms. E. Cantu for her format review, Drs. A. Ghosh, P. Lichtner, and S. Stothoff for their technical reviews, and Dr. B. Sagar for his programmatic review. A part of the results presented in this work was enhanced through numerous discussions with Dr. V. Kapoor who provided also an informal review of this document. UZ-16 saturation data were kindly provided in electronic form by Mr. W. Ford of the NRC. Discussions with Dr. B. Gureghian are greatly appreciated. Finally, the authors gratefully acknowledge the contributions and encouragement of Mr. B. Baca, the Performance Assessment and Hydrologic Transport Element Manager, and Mr. T.J. Nicholson, the NRC Project Officer.

EXECUTIVE SUMMARY

The technical objective of the "Stochastic Analysis of Unsaturated Flow and Transport" Research Project, hereafter called Stochastic Project, is to provide and document the methods and tools necessary for realistic modeling and analysis of the complex, heterogeneous flow and transport processes anticipated or hypothesized to occur in the far-field of the proposed high-level waste (HLW) repository at Yucca Mountain, Nevada. These models and analyses will be necessary to predict the performance of the overall system (10 CFR 60.112), the Geologic Setting (10 CFR 60.113), and to evaluate compliance with siting criteria (10 CFR 60.122). The spatial variability of many processes and parameters affecting the long-term behavior of the flow system at the scale of the Yucca Mountain site is poorly known. More specifically, there is a lack of acceptable hydrogeologic parameters, theories, and conceptual and mathematical models that are considered applicable or computationally feasible for the conditions prevailing at Yucca Mountain. Even if such models are developed, there will be a variety of fundamental questions regarding their applicability over the spatial scales of the subregional and regional hydrologic systems. Moreover, some uncertainty will always remain in the value of hydrogeologic parameters because only a limited amount of data can be collected.

The Stochastic Project aims to address issues related to the quantitative characterization of large-scale flow and transport in unsaturated, highly fractured, heterogeneous rock. Information, methodologies, and numerical tools developed within this project will be used to support specific portions of the License Application Review Plan (LARP). Parameter heterogeneity effects on flow and transport at a scale similar to that of Yucca Mountain provide knowledge relevant to the Description of the Individual Systems and Characteristics of the Site (Sections 3.1.1, 3.1.2, and 3.1.3 of the LARP). Similarly, detailed numerical analyses of the flow processes occurring in highly fractured, heterogeneous rock provide the necessary framework for the development of the LARP specifically related to favorable hydrogeological conditions (Sections 3.2.2.3, and 3.2.2.4) and potentially adverse hydrogeological conditions (Sections 3.2.2.9, 3.2.2.11, 3.2.2.12, and 3.3.4.2). More specifically, review plans that deal with "Assessment of Compliance with the Groundwater Travel Time (GWTT) Performance Objective" and "Potentially Adverse Condition: Perched Water Bodies" have been judged to require a Type 5 review, and thus require independent research to resolve the following key technical uncertainties (KTUs): (i) uncertainty in evaluation of the potential for formation of future perched water bodies at Yucca Mountain, (ii) uncertainty in developing a unique conceptual groundwater flow model that is representative of the Yucca Mountain flow system, and (iii) uncertainties associated with determining characterization parameters.

Stochastic theory-based approaches provide a suitable platform to address issues related to the quantitative characterization of large-scale flow and transport in unsaturated, highly fractured, heterogeneous rock. Recent research demonstrating the applicability of stochastic theory approaches for addressing geologic uncertainty evaluation in a regulatory environment includes, but is not limited to, the work of Rautman and Treadway (1991), Rautman and Robey (1993), Tidwell et al. (1993), Robey (1993), Nichols and Freshley (1993). These approaches allow one to study and assess the variability in model parameters and the effect of the variability on various performance measures, such as GWTT. Tools to apply stochastic methods in the form of numerical models and executive codes, are being developed to examine compliance with the GWTT performance objective.

In this study, the detailed evaluation of flow and advection-dispersion of solute in unsaturated heterogeneous porous media is simulated to understand transport processes in the far-field of a two-layer

system analogous, in some respects, to Yucca Mountain, Nevada, the site of the proposed HLW repository. Generation and subsequent analysis of flow fields obeying basic constitutive and conservation laws in complex geologic media and an assessment of the impact of the flow field on solute transport is performed with the executive numerical code named Stochastic Analysis of Unsaturated FLow And Transport (SUFLAT) (Bagtzoglou et al., 1994a).

SUFLAT can be used to conduct large-scale, stochastic flow and transport simulations in order to assess uncertainty in GWTT estimates due to variability in hydrogeologic properties. The executive numerical code SUFLAT is capable of: (i) stochastically generating all appropriate three-dimensional (3D), cross-correlated hydrogeologic property fields using the Turning Bands Method (TBM) (Tompson et al., 1987a), as incorporated in the code MKPROP; (ii) solving the flow problem using the numerical code BIGFLOW (Ababou and Bagtzoglou, 1993); (iii) post-processing all flow results in order to calculate flux and velocity fields using the numerical code FLUX; and (iv) conducting particle transport simulations with SLIM (Tompson et al., 1987b; Bagtzoglou et al., 1991). The particle tracking method of SLIM is also used to study the impact of the complex flow fields (associated with highly heterogeneous hydraulic properties) on the distribution of solute undergoing advection and local dispersion. The evolution of the ensemble mean and variance of the concentration field is shown. All four of these activities are conducted in a repeated-realization (Monte Carlo) mode and independently of each other.

The Stochastic Project has produced two final reports. The first addressed the issue of effective hydraulic property calculations for unsaturated, fractured rock. A methodology was introduced, and advocated in the work of Bagtzoglou et al. (1994b), to lump the effects of fractures and matrix heterogeneity into spatially variable effective continuum parameters. This second of two final reports addresses the issue of large-scale flow and transport in unsaturated, heterogeneous media and presents one possible methodology for the assessment of the effects of model parameter variability on various performance measures, such as GWTT. It is organized as follows. Chapter 1 constitutes an introduction to various stochastic methods of unsaturated flow and transport. It continues with a description and a discussion of the Monte Carlo approach, the method of choice for uncertainty propagation in the present work. Chapter 2 presents the SUFLAT numerical code and discusses, in some detail: (i) generation of random hydraulic property fields, (ii) solution of the unsaturated flow problem, and (iii) solution of the transport problem with particle methods. Chapter 3 is a description of the specific flow and transport problem, tackled in the present work. Chapters 4 and 5 present results of flow and transport simulations with, or without, the presence of faulting under purely advective, or advective-dispersive, conditions for a heterogeneous two-layered system. Finally, Chapter 6 of this report summarizes the findings and presents some conclusions.

The primary findings of this study are: The interface between hydraulically distinct layers behaves, in general, as a capillary barrier, even in the presence of strong intra-layer heterogeneity. Associated with the capillary barrier is the existence of very strong, lateral flow velocities (in the order of 10 mm/yr). The integrity of this capillary barrier, however, is breached in a very localized fashion. The locations of the capillary barrier breaching regions depend greatly on the nature of the heterogeneity of the porous medium and are closely related to the range of suction-based crossing points in the unsaturated conductivity curves. The flow system behaves very differently in the presence of a persistent discontinuity, such as a fault zone. The effects of the fault on the flow system are prevalent to a region of at least 100 m around the fault zone. Furthermore, even though some recirculatory flow patterns are perceptible, the flow is pretty much focused through the fault zone (velocities in the order of 10^3 mm/yr). This work demonstrated that stochastic approaches can be readily used to infer the likelihood of perched zone development. It was found that only 20 percent of our flow simulations exhibited characteristics

associated with potential perched zone formation. The need to account for large variations in concentrations in the assessment of contaminant transport predictions is emphasized. This effort demonstrated that matrix-flow models lead to large travel times. However, these travel times are associated with large uncertainties.

1 STOCHASTIC METHODS OF FLOW AND TRANSPORT

1.1 HETEROGENEITY AND STOCHASTIC SIMULATION: SOME PREVIOUS WORK

In recent years, these is an increasing awareness that the spatial variability of porous medium properties has a significant impact on flow and transport within the medium. As an example, the saturated hydraulic conductivity of porous materials can exhibit a coefficient of variation in the range of 90 to 240 percent (Harr, 1987) and routinely varies by five or six orders of magnitude at a site (Freeze, 1975). Although other porous medium properties, such as porosity and compressibility are also variable, their degree of fluctuation is much less than that for hydraulic conductivity; consequently, hydraulic conductivity variation receives the most attention. Material variability translates to variability in corresponding hydraulic behavior, directly affecting the predictions of flow and transport in porous media. The irregularity and randomness of the aquifer skeleton makes a fully deterministic description of the solute transport phenomenon impossible; thus, arguably the best approach is to consider all possible displacements and their associated probabilities (Uffink, 1986). The performance assessment models, currently used, do not resolve small-scale variability which according to Pruess and Tsang (1994) "invariably lead[s] to localized ponding of water, and will cause water flow to be channelized...."

A useful representation of natural porous media involves a grid of macroscopic elements in which the value of the hydraulic conductivity is defined by frequency distributions (Freeze, 1975). A large number of investigators proposed a lognormal probability density function for hydraulic conductivity, and a fair number of measurements supports this proposition (Freeze, 1975). Based on this distribution, the expression for the hydraulic conductivity is given as:

$$K = \exp(\sigma_Y R_N + \mu_Y) \tag{1-1}$$

where μ_Y and σ_Y are the mean and standard deviation of lnK, and R_N is a random number taken from the zero-mean, unit variance normal distribution $N(0,1)$. Depending on the porous medium, K can range from 10^{-10} to 10^{3} m/day in various materials. Values for the standard deviation, σ_Y, range typically between 0.6 and 2.2 (Gelhar, 1986). Willardson and Hurst (1965), however, reported values of σ_Y up to 5.5 for some Imperial Valley, California soils.

As a preliminary, some definitions are now presented. Let $Y(x)$ denote the value of a random spatial variable, and let $\langle\ \rangle$ denote the expectation operator. A weakly stationary process is usually assumed to govern the behavior of such a random variable. Processes of this type have: (i) a constant first moment (mean) over the domain, independent of location x:

$$\langle Y(x) \rangle = \mu_Y \tag{1-2}$$

and (ii) a constant second moment (autocovariance) given by:

$$\langle (Y(x_1) - \mu_Y)(Y(x_2) - \mu_Y) \rangle = \mathrm{COV}_Y(x_1, x_2) \tag{1-3}$$

over the domain, which depends not upon the location of the two points x_1, and x_2 considered, but only upon the separation vector or lag, given by $\xi = x_2 - x_1$. That is:

$$\langle \left(Y(x_1) - \mu_Y\right)\left(Y(x_2) - \mu_Y\right) \rangle = \mathrm{COV}_Y(\xi) \tag{1-4}$$

where ξ is the lag vector. By definition, $\mathrm{COV}_Y(0)$ is the variance σ_Y^2. When the autocovariance depends upon the locations of the two variables, the process is called nonhomogeneous. If it is unaffected by the direction of the vector connecting these two points, the process is called isotropic. The semivariogram, defined by (Gómez-Hernández and Gorelick, 1989) as:

$$\gamma_Y(\xi) = \mathrm{COV}_Y(0) - \mathrm{COV}_Y(\xi) \tag{1-5}$$

is sometimes encountered, particularly when discussing *kriging*, a best linear unbiased estimate (BLUE) interpolator for weakly stationary fields (de Marsily, 1986). For an isotropic exponential covariance function, the correlation length is the distance at which the correlation between two points has been reduced by a factor of Euler's number, e. In a more general sense, the correlation length, λ, is the characteristic length over which variations of the log hydraulic conductivity are strongly correlated with each other (Figure 1-1). Depending on the porous medium, λ can range from 0.1 m to greater than 1,000 m (Gelhar and Axness, 1983). Most hydrogeologic properties are actually non-stationary. For example, porosity and permeability are often found to decrease with depth. Hoeksema and Kitanidis (1985) compiled and analyzed statistics of aquifer transmissivities, and found that the presumed stationary correlation structure of porous formations is not well defined for certain sites and/or for certain scales of observation. Since no satisfactory theory to deal with such variables is available, the assumption of weak stationarity is typically made. It should also be noted that in the case of normally distributed properties, weak stationarity is equivalent to strong (or strict) stationarity.

Warren and Price (1961) were the first to use a stochastic model of flow through porous media. They studied the effects of three-dimensional (3D) heterogeneities on flow across a cube. Their approach assumed that the hydraulic conductivity was lognormally distributed with a small variance and that it was spatially uncorrelated. The major weakness of this study was the lack of spatial correlation. More recently, a large number of studies on solute transport in saturated porous media have been reported. Dagan (1987), interpreting the experimental results from various test sites, suggested that it is the effective longitudinal dispersivity that dominates the spread of the solute body around its center of mass. This macrodispersivity, associated with the field scale, is much larger than the pore-scale dispersion. Dagan employed a Lagrangian representation, allowing a solute particle to move along a flow line. The total displacement of a particle is decomposed into convection by the mean velocity, convection by the velocity fluctuation, and a "Brownian motion" component (Dagan, 1987). Gelhar and Axness (1983) and Gelhar (1986) developed a perturbation-based spectral approach to obtain explicit analytical results for the head variance, effective hydraulic conductivity, and macrodispersivity. They reported that, in isotropic media, the longitudinal dispersivity, A, increases directly with the variance of the log hydraulic conductivity as follows:

$$A_{11} = \frac{\sigma_Y^2 \lambda}{\gamma^2}, \quad A_{22} = A_{33} = \frac{\sigma_Y^2 \alpha_L}{15\gamma^2}\left[1 + \frac{4\alpha_T}{\alpha_L}\right] \tag{1-6}$$

where λ is the correlation length in the direction of the mean flow, α_L and α_T are the longitudinal and transverse dispersivities, respectively, and γ is the ratio of the effective conductivity to the geometric mean of the conductivity, given by:

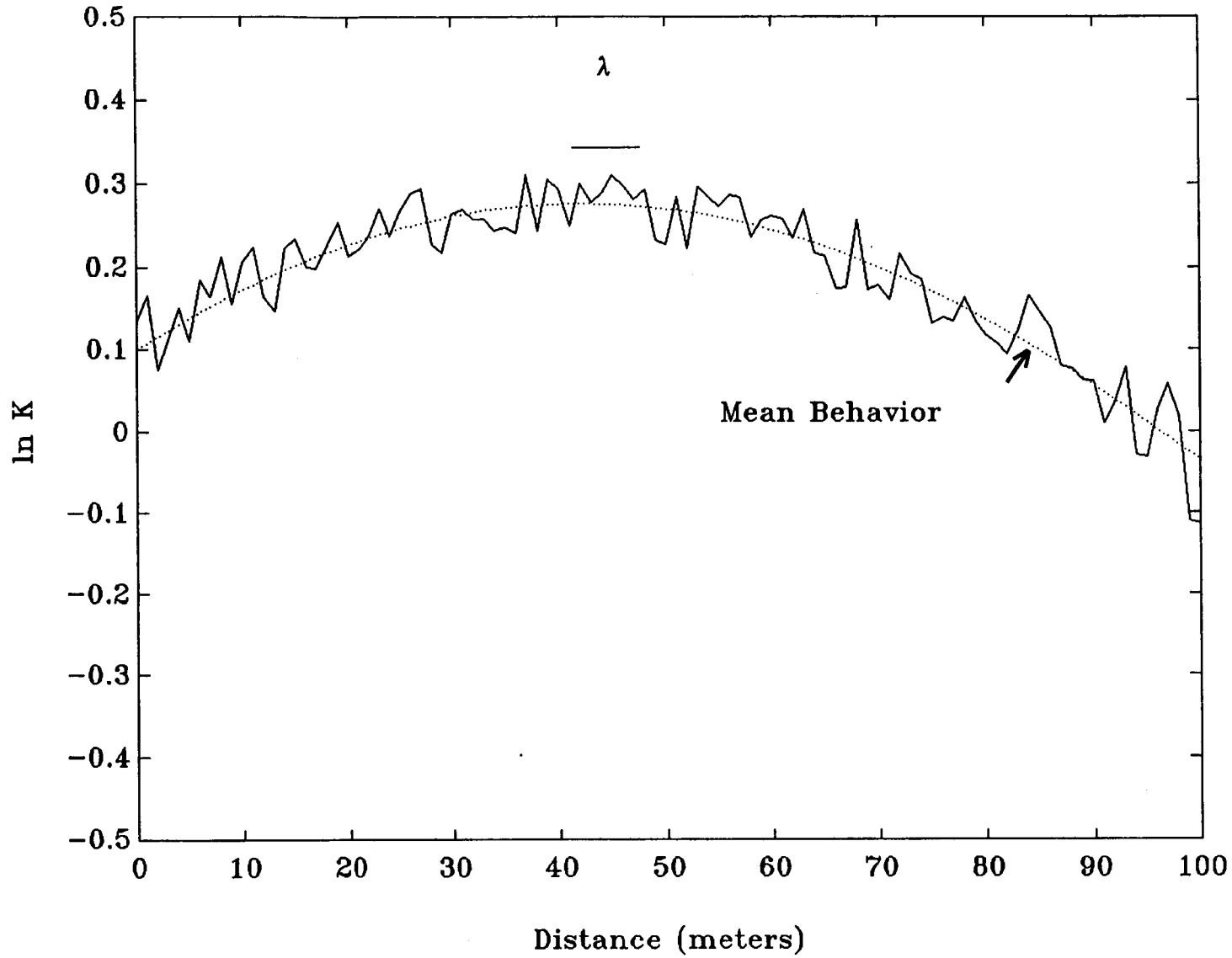

Figure 1-1. Spatial variation of the log hydraulic conductivity. Dotted lines represents the mean or trend behavior (Adapted from Tompson et al., 1987b).

$$\gamma = \exp\left[\frac{\sigma_Y^2}{6}\right] \tag{1-7}$$

The macrodispersivity estimate given by Eq. (1-6) is identical to Dagan (1984) when $\gamma=1$. It has also been shown that for large-length scales, macrodispersion eventually becomes insensitive to the local dispersivity, making the models of dispersion in porous media nonempirical (Chin, 1989).

Tang and Pinder (1977) used a semianalytical approach in which the medium parameters are split into a mean and a perturbed part. The governing partial differential equation is then solved using perturbation theory without relying on Monte Carlo analysis. A limitation of this method is that it can treat only linearized equations with relatively low degrees of uncertainty. The effects of macroscopic dispersion were simulated for uniform heterogeneous porous media subjected to one-dimensional (1D) flow by Schwartz (1977), who used idealized media consisting of low-conductivity obstacles within a higher-conductivity host medium. Schwartz found that when these inclusions are not arranged in a statistically homogeneous fashion, a unique dispersivity could not be defined. Moreover, dispersivity values decreased with decreasing conductivity contrast and regularization of the porous material structure.

Numerical work of a similar nature was performed by Smith and Schwartz (1980). In their effort, the macroscopic dispersion is attributed to spatial heterogeneities in hydraulic conductivity. The hydraulic conductivity field used in their work was generated as a two-dimensional (2D), spatially autocorrelated, first-order, nearest-neighbor stochastic process. Analyzing the behavior of tracer particles advected through this statistically homogeneous conductivity field, Smith and Schwartz (1980) concluded that constant dispersivity values could not be obtained. Chu et al. (1987) concluded that contaminant transport predictions are more sensitive to accurate estimation of transmissivity than to dispersivity estimation. An alternate mathematical method for solving the stochastic transport problem employs an ensemble approach that emphasizes the dispersion process and its direct relation to the spatial variation of flow velocity. Simmons (1982) performed such an analysis in 1D. The flow velocity is decomposed into a mean and a perturbed part:

$$V(x) = u(x) + \tilde{u}(x) \tag{1-8}$$

where $\langle \tilde{u}(x) \rangle = 0$. Then, assuming that the velocity fluctuation is weakly stationary with a known covariance function, solute transport solutions can be computed in a straightforward manner.

Stochastic analyses of heterogeneous porous media have been extended to treat unsaturated flows by Yeh et al. (1985a,b,c) who modeled 3D steady infiltration under the assumption of a lognormally distributed saturated hydraulic conductivity. Other notable efforts are the works of Mantoglou and Gelhar (1985; 1987a,b,c) and Polmann et al. (1988). More recently, Ünlü et al. (1990) conducted Monte Carlo numerical experiments to study the stochastic behavior of the 1D unsteady unsaturated flow. The saturated hydraulic conductivity was assumed to be lognormal and to be derived from a statistically homogeneous random field correlated in space *via* an isotropic exponential function. Finally, a series of simulations of unsaturated flow and conservative transport in a heterogeneous soil at the Las Cruces trench site in New Mexico was presented in the work of Rockhold (1993).

The moments of solute concentration are often calculated, since they are useful in interpreting transport simulation results. The global moments of the concentration serve as physically meaningful

descriptions of solute plume behavior. They are also quite easy to compute. Therefore, moment analysis is a popular and useful tool in the analysis of stochastic behavior. In Cartesian coordinates, the zeroth moment (M_{000}) measures the total mass contained in the plume, the first moment (M_{100}) measures the mean location of the plume in the x direction, and the second moment (M_{200}) measures the spreading of the plume about its mean position in the x direction. The moments of mass in the fluid phase of a porous medium of infinite extent can be defined as (Freyberg, 1986):

$$M_{ijk}(t) = \int_{-\infty}^{\infty}\int_{-\infty}^{\infty}\int_{-\infty}^{\infty} nc\,(x,y,z,t)x^i y^j z^k \,dx\,dy\,dz \tag{1-9}$$

where $c(x,y,z,t)$ is the concentration field and n is the porosity. The coordinates of the center of mass of the plume, which are functions of time, are given by:

$$\begin{aligned} X_c &= \frac{M_{100}}{M_{000}} \\ Y_c &= \frac{M_{010}}{M_{000}} \\ Z_c &= \frac{M_{001}}{M_{000}} \end{aligned} \tag{1-10}$$

The mean velocity vector is, then, written as:

$$V_{eff} = \left[u_{eff}, v_{eff}, w_{eff}\right]^T = \frac{d}{dt}\left(\left[X_c, Y_c, Z_c\right]^T\right) \tag{1-11}$$

Freyberg (1986) and Güven et al. (1984) applied the moment method of Aris and defined the 2D (vertically-averaged) effective longitudinal dispersion coefficient, D_{eff} as:

$$D_m + D_{eff} = \frac{1}{2}\frac{d}{dt}\left(\sigma_{xx}^2\right) \tag{1-12}$$

where D_m is the effective molecular diffusion coefficient for the porous medium (assumed to be zero in their works), and the macroscopically uniform flow is along the x direction. The variance $\left(\sigma_{xx}^2\right)$ of the depth-averaged concentration is:

$$\sigma_{xx}^2 = \frac{M_{200}}{M_{000}} - \left[\frac{M_{100}}{M_{000}}\right]^2 \tag{1-13}$$

The rate of change of the mean particle position equals the mean longitudinal velocity, in contrast to the particle position variance which depends on the size of the input zone (Valocchi, 1990). In realistic field problems, overall spreading of a reactive solute plume will result from both nonequilibrium and macrodispersive processes (Valocchi and Quinodoz, 1989). Consequently, for linear kinetics, the overall longitudinal plume variance is given by:

$$\sigma_x^2 = {}^K\sigma_x^2 + {}^H\sigma_x^2 \qquad (1\text{-}14)$$

where ${}^K\sigma_x^2$ represents the impact of kinetics on the longitudinal variance of the plume and ${}^H\sigma_x^2$ represents the variance due to the spatial heterogeneity of the hydraulic conductivity field.

Numerical simulations of the motion of inert solutes in 2D random lognormal conductivity fields have been conducted by Salandin and Rinaldo (1990). They employed a finite element model to solve the flow equation for each realization of the conductivity field and a particle-tracking method to solve the transport equation. They used a range of lognormal variance of conductivity from 0.2 to 2.0, and concluded that Dagan's linear theory may yield acceptable results even in high degrees of heterogeneity. Similar analyses were conducted by Bellin et al. (1992), who discuss the results of numerical simulations of dispersion in 2D heterogeneous porous formations.

Typically, modelers of field-scale problems restrict the problem to include a certain number of homogeneous zones which they treat as having constant hydraulic conductivities on either a node or an element basis. Since nature seldom abides by this assumption, model solutions tend to exhibit an average behavior on a scale larger than the scale of local variabilities. Thus, modelers using large grids may need to consider the effects of averaging behavior of the type described above. In one such formulation, Naff (1990) lumped the average variability in the concentration field into a global dispersive flux. Naff claimed that, even if the resulting stochastic process is not strictly ergodic, inferences about how the concentration is expected to behave can be made without sacrificing accuracy.

In assessing feasibility of waste disposal schemes in geologic media, the ultimate concern is the possible exposure of human beings to toxic substances. This requires estimating contaminant concentrations. The premise that the heterogeneity of the advective pathways will influence the assessment of the solute transport is unambiguously clear from results of large-scale solute transport experiments. In these experiments, hundreds of point measurements of concentrations were taken to construct 3D snapshots of contaminant plumes in the saturated zone at the Borden site in Canada (Freyberg, 1986; Sudicky, 1986), the Cape-Cod site in Massachusetts (LeBlanc et al., 1991; Garabedian et al., 1991), and at the Columbus site in Mississippi (Boggs et al., 1992; Adams and Gelhar, 1992). These large-scale experiments document the enhanced (compared to the laboratory scale) mass flux associated with transport in 3D varying hydraulic conductivity fields, and the concomitant complex 3D spatial distributions of solute concentration. The few large-scale experiments in unsaturated porous media (e.g., Butters and Jury, 1989) show that the features of enhanced mass transport and rugged concentration distributions are common to both the saturated and unsaturated zones.

An approach similar to the works of Salandin and Rinaldo (1990) and Bellin et al. (1992) is followed in the present work. Stochastic realizations of hydraulic property fields will be obtained, ultimately providing a stochastic velocity field which advects and disperses particles released at a point. This approach, also known as geostatistical simulation (Journel, 1989; Journel and Alabert, 1989; Rautman and Treadway, 1991), provides a powerful technique for quantifying the uncertainty associated with numerical representations of geological processes. Gotway (1994) has also advocated the power of stochastic simulation in association with nuclear waste site performance assessments. Under this approach, uncertainty in the site description is propagated through the performance assessment models and produces uncertainty in the modeled output (Rautman and Robey, 1994).

1.2 THE MONTE CARLO APPROACH

In various performance assessment methodologies, parameter uncertainty is treated by propagating the uncertainty *via* model calculations in order to identify the effects of uncertainty in model output (e.g., some performance measure). Extensive reviews of methods for the propagation of parameter uncertainty through models are given by Kozak et al. (1993), Zimmerman et al. (1990), and Gutjahr and Bras (1993). One limitation, perhaps the most important one, of stochastic models is that they are often based on some form of perturbation analysis which assumes negligible or small input variances (Gutjahr, 1992). However, Dagan (1985) and Gutjahr (1984) showed that perturbation techniques are applicable in certain cases even for large variances. Alternative methods, based on the limit-state formulation, have been explored by Wu et al. (1993) and showed that they can reach convergence in approximately 10 percent of the iterations required by the Monte Carlo approach. It should be noted, however, that in their analyses Wu et al. (1993) assumed a very modest coefficient of variation of 0.5 for all material properties.

According to Zimmerman et al. (1990), there are five important reasons for using Monte Carlo analysis in parameter uncertainty propagation: (i) it facilitates consistent propagation of uncertainties; (ii) it can be applied to a series of linked models, such as cascaded vaults or layered geologic media; (iii) it does not require extensive modifications to existing numerical codes; (iv) it is capable of handling large uncertainties in the input variable parameter space; and (v) it is appropriate for use in association with nonlinear models. Hopmans et al. (1988) classify the Monte Carlo approach as particularly attractive, since no stationarity assumptions are required.

Under the Monte Carlo framework, the quantity of interest (e.g., one of the hydraulic properties of the natural system) is considered to be a regionalized variable that is exhibiting spatially correlated or uncorrelated variability. Thus, it is dealt with by using a probabilistic framework consisting of an ensemble of realizations of equal probability. This ensemble of realizations constitutes a set of equally-likely representations of nature, the one and only true, being unknown, realization (Follin, 1992). Applications of Monte Carlo simulations to study the effect of heterogeneity on flow through naturally-occurring porous media were first used by Warren and Price (1961). Since then, numerous efforts have applied Monte Carlo techniques for parameter uncertainty propagation. Notable efforts include, but are not limited to, the works of Freeze (1975), Smith and Freeze (1979a,b), Clifton et al. (1985), Sagar and Clifton (1985), and Bonano et al. (1989). Recently, Nichols and Freshley (1993) conducted Monte Carlo numerical simulations of 1D unsaturated flow in the Calico Hills nonwelded zeolitic layer at Yucca Mountain, Nevada.

Monte Carlo analysis is criticized as being unrealistically excessive in its computational requirements. This is especially true in the case of variably saturated flow whereby a large number of internal nonlinear iterations are required for each time step. However, Monte Carlo analyses are becoming increasingly more attractive, especially since computing costs are dropping dramatically. As a result, the justifiable concerns regarding the feasibility of Monte Carlo analyses of variably saturated flow and transport are diminishing (Kozak et al., 1993). Furthermore, according to Rautman and Flint (1992), "layering corresponding to some degree of geologic subdivision almost certainly would be retained as the logical representation of known deterministic geologic processes." Having decoupled the generation of hydraulic property fields from one layer to the rest renders the computational requirements of Monte Carlo analysis of less importance, since information regarding the layering serves as a very strong type of conditioning or constraining of the parameter space. This implies that if Monte Carlo

analyses were to be conducted without the incorporation of any geological information (e.g., stratigraphy), the parameter sampling space would have to be drastically greater than in the case where such information is incorporated. The incorporation of cross-correlation algorithms for the generation of hydraulic properties, as it will be discussed in detail later, provides another very important and drastic form of conditioning. The end product of both forms of conditioning is that the parameter sampling space is drastically reduced, thereby limiting the need for extensive searches. Finally, prior experience with Monte Carlo analysis of groundwater travel time seems to indicate that there is very little, if any, statistically significant difference in the results obtained with 50 and 500 conditional simulations (Bonano et al., 1989).

2 THE STOCHASTIC ANALYSIS OF UNSATURATED FLOW AND TRANSPORT EXECUTIVE SUITE OF NUMERICAL CODES

A description of the executive numerical code SUFLAT is presented in this chapter. SUFLAT can be used in the conduct of large-scale, stochastic flow and transport simulations in order to assess uncertainty in performance measures, such as the GWTT estimates, as manifested by variability in hydrogeologic parameters. The executive numerical code SUFLAT is capable of: (i) stochastically generating all appropriate 3D cross-correlated hydrogeologic property fields using the Turning Bands Method (TBM) as incorporated in the module MKPROP, (ii) solving the flow problem using the numerical code BIGFLOW, (iii) post-processing all flow results in order to calculate flux and velocity fields using the module FLUX, and (iv) conducting particle transport simulations with the code SLIM. All four of these activities are conducted in a repeated realization (Monte Carlo) mode. A schematic flowchart of SUFLAT is depicted in Figure 2-1.

In this schematic, all links between the numerical modules are identified, together with a variety of data files associated with the inputs and/or outputs of SUFLAT. In the next sections, a detailed description of the three main components of SUFLAT is presented. These sections deal with: (i) random field generation, (ii) solution of the flow problem, and (iii) solution of the transport problem. Some material on the theoretical background of the methods involved is presented, followed with discussions justifying the selection of particular conceptual models. For example, a discussion is presented on: (i) the issue of preferring particle methods for the conduct of solute transport simulations; (ii) the use of the exponential covariance model which some researchers consider physically meaningless; and (iii) the role of sub-scale heterogeneity (e.g., micro-fracturing) and its numerical representation as a nugget effect, closely related to a dispersion process in the solute transport context.

2.1 RANDOM HYDRAULIC CONDUCTIVITY FIELD GENERATION

Monte Carlo simulations of stochastic transport require that sample fields of log-conductivity be developed. Numerous methods of random field generation exist and have been applied successfully. Smith and Schwartz (1980) assume that hydraulic conductivity, K, is lognormally distributed. Then, the nearest-neighbor autoregressive relation was given by:

$$Y_{ij} = \alpha_x\left(Y_{i-1,j} + Y_{i+1,j}\right) + \alpha_y\left(Y_{i,j-1} + Y_{i,j+1}\right) + \epsilon_{ij} \qquad (2\text{-}1)$$

where Y_{ij} is a random variable equal to $ln\ K_{ij}$; α_x, α_y are autoregressive parameters expressing the degree of spatial dependence of Y_{ij} on its two neighbors in the x and y direction, respectively; and ϵ_{ij} is a white noise-like normal random variable uncorrelated in space. If $\alpha_x = \alpha_y$, the material is classified as stochastically isotropic. Ünlü et al. (1990) used a modified version of the nearest-neighbor model to generate the second-order stationary soil hydraulic properties for a 1D study of flow in unsaturated soils. Unfortunately, it is difficult to ensure that any specific autocovariance function is reproduced using the nearest-neighbor approach (Tompson et al., 1987a). Clifton and Neuman (1982), and more recently Jones (1990), performed Monte Carlo analysis for flow in random 2D aquifers. The variates of the log-transmissivity for each simulation were generated using a method based on the decomposition of the covariance matrix of Y. Introduced by Matalas (1967), the decomposition method is convenient only if the field to be generated is small, the computer being used has very large memory, or the covariance matrix is sparse (i.e., the covariance is zero for most values of the lag vector). Given the autocovariance function, the Fourier transform can be applied to obtain the spectrum of the autocovariance. Random

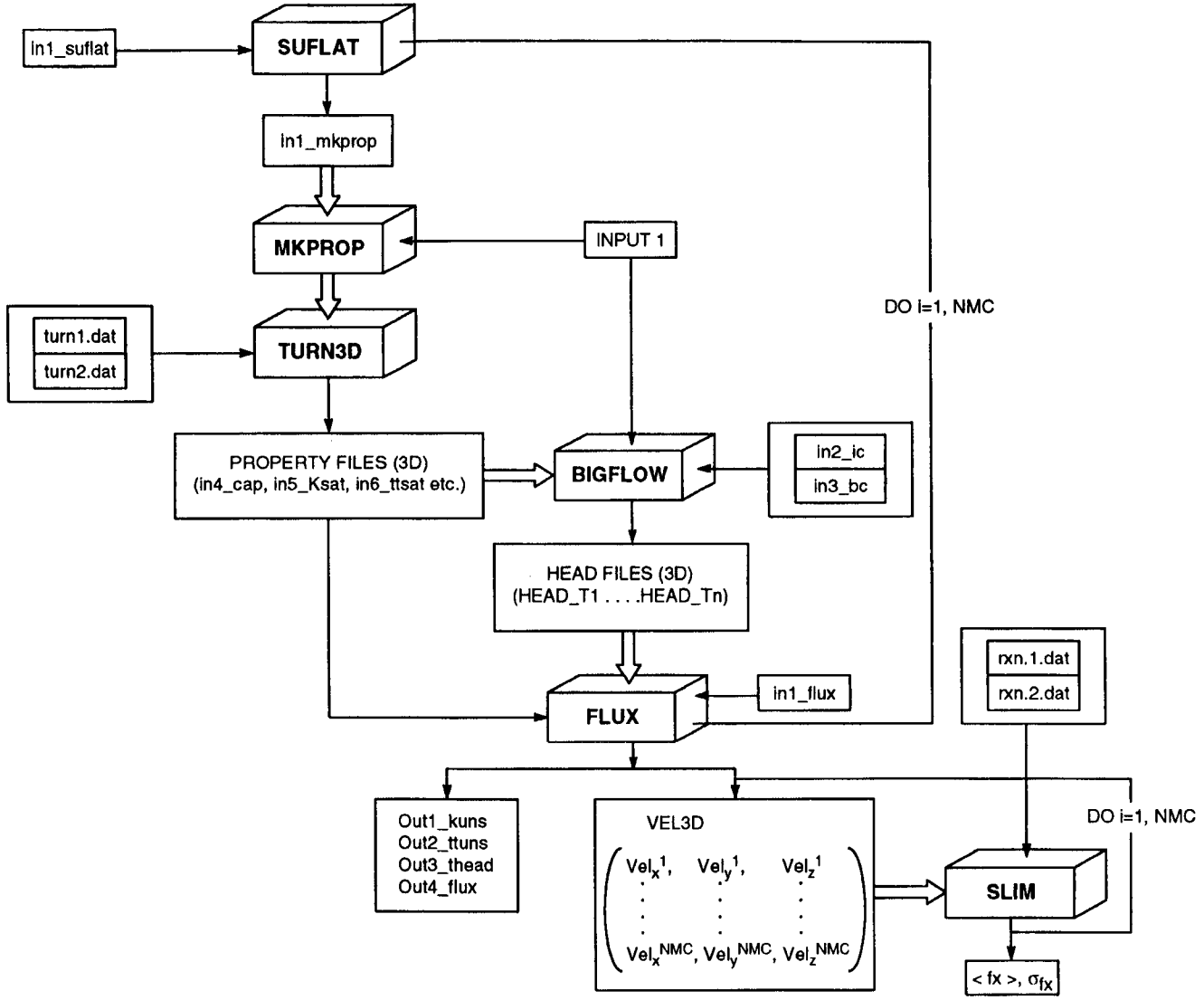

Figure 2-1. Schematic representation of flowchart for SUFLAT

fields can be constructed from the spectral properties of the autocovariance and then transformed from Fourier to physical space. Multidimensional Fourier transforms are often used to accomplish this task. Other methods include, but are not limited to, the sequential Gaussian simulation algorithm (Deutsch and Journel, 1992; Rosenblatt, 1952) and the stochastic indicator techniques (Journel, 1983; Rautman and Robey, 1994).

Another method, employed in this work, is the TBM. A thorough description of the method is given by Mantoglou and Wilson (1982) and by Tompson et al. (1987a, 1989). Assuming the field to be simulated is second-order stationary, a series of 1D simulations along numerous lines is performed. These simulations use a uni-dimensional covariance function corresponding to the actual 2D or 3D behavior. Once the series of simulations is completed, a weighted sum of the corresponding line process values results in the stochastic field at each point of interest (Mantoglou and Wilson, 1982; Tompson et al., 1989; Tompson and Gelhar, 1990). The computer program developed by Tompson et al. (1987a) is used to generate 3D stochastic realizations of the conductivity field, assuming a lognormal K distribution and an exponentially-decaying spatial covariance structure. The line processes are generated using the method of Shinozuka and Jan (1972).

Kapoor (1993) presented an analysis of data collected on a cross-bedded sandstone from a carboniferous outcrop in Scotland on a 1 mm scale. In the analysis by Kapoor, the autocorrelation function of log-permeability is plotted against the separation distance. Kapoor indicated the "strikingly unambiguous" upward convexity of the correlation function, a clear characteristic of a Gaussian covariance model. Kapoor further pointed to the "zero microscale(s)" assumption, denying continuum differentiability, associated with exponential correlation functions, and cautioned the reader of the upper and lower bounds imposed on the wave numbers of the log-permeability spectra due to limited sampling, that is lack of data at very fine or coarse scales. However, as discussed in Section 2.1.1 [for details one can also refer to the work by Ababou et al. (1994)], it is precisely at very small separation lags that the Gaussian model creates difficulties in the numerical solution process. Whether the popular exponential covariance model's unrealistic implication of a zero microscale has more deleterious effects than the very large (theoretically infinite) condition number of a Gaussian covariance model is still unknown. This work, especially since it deals with the generation of very large (tens of thousands) number of computational nodes, assumes inherently that computational efficiency and accuracy outweighs possible theoretical implications until such time when evidence to the contrary is made available.

The numerical implementation of geostatistical estimation and random field generation requires solving dense linear systems involving a covariance matrix. The computational tractability of these algebraic systems can be characterized by the condition number of the covariance matrix, which depends on the underlying covariance structure and on the spatial configuration of measurements (location of data points). The covariance matrix arises in the process of solving kriging systems for the posterior mean, or BLUE, of a given set of geostatistical data. Essentially, kriging is a particular type of spatial interpolation based on some assumed spatial structure. In ordinary kriging, the spatial structure is characterized by a stationary mean and a stationary two-point covariance function, usually with the implicit assumption that the observed variable has the statistical distribution of a Gaussian random field. In the case of inherently positive variables such as conductivity, porosity, etc., a one-to-one transform such as $ln(x)$ can be used to make the Gaussian assumption more realistic.

Kriging is also used for conditional simulation of random fields by a superposition method (Delhomme, 1979; Journel and Huijbregts, 1978). The superposition method produces random fields conditioned on a set of measurements by linearly combining unconditioned random fields with kriged fields. As shown in the work of Ababou et al. (1994), kriging calculations involve the repeated solution

of covariance matrix systems. This can be achieved by computing (only once) a triangular factorization of the matrix and by using the triangular factors in a recursive backward-forward solution scheme for any (of the many) right-hand side vector(s). Kriging or conditional simulation algorithms are not, at present, included in the SUFLAT suite of codes.

Finally, one of the simplest methods for generating Gaussian random fields, although not necessarily the most efficient one, is the "multivariate Gaussian method" which also requires factoring a covariance matrix. Specifically, the method consists of factoring the covariance matrix into a product of two triangular matrices $\boldsymbol{M}$ and $\boldsymbol{M}^T$. The random field is then generated by multiplying $\boldsymbol{M}$ by a vector of replicates of independent normalized Gaussian variables. The covariance matrix can be either the prior covariances among all grid points (unconditional generation) or the posterior covariances among all simulation points conditioned on measurement data where the "simulation points" do not include the data points themselves (conditional generation). See Dagan (1982a) for an example of application of this technique to stochastic subsurface hydrology.

Inasmuch as perfect knowledge of needed field data cannot be attained, linear estimation and conditional simulation play an important role in processing, interpolating, and statistically interpreting data. These methods are particularly important for spatially distributed models of hydrological processes, such as space-time rainfall fields, and large-scale contaminant migration in heterogeneous geological formations. In all the methods reviewed above, the feasibility of factorization (or inversion), and hence the accuracy of the generated fields, depends on the covariance matrix being invertible. More precisely, the numerical stability and accuracy of matrix factorization (or inversion) depend on the condition number of the covariance matrix. The condition number ranges from one, for an identity matrix, to infinity, for a noninvertible matrix. A large condition number means that the systems to be solved are very sensitive to small perturbations, in which case the estimation or simulation procedures become impractical.

In geostatistics, the estimated field is usually obtained by solving a kriging system that contains the covariance matrix as sub-matrix (Journel and Huijbregts, 1978; de Marsily, 1986; Isaaks and Srivastava, 1989; O'Dowd, 1991). The latter author pointed out that the condition number of the kriging matrix is always larger than, or at best equal to, the condition number of the prior covariance matrix. The condition number of this matrix intrinsically characterizes the computational difficulty, and associated errors, of the problem.

2.1.1 Ill-Conditioning of Covariance Matrices

The spectral condition number of the covariance matrix can be used to characterize the numerical feasibility of inversion or factorization algorithms required in the simulation and kriging problems mentioned above. For a given matrix $\boldsymbol{A}$, the spectral condition number $\kappa(\boldsymbol{A})$ is defined as the ratio of largest to smallest eigenvalues, each taken in absolute value (Golub and Van Loan, 1989, or Press et al., 1986). That is:

$$\kappa(A) = \frac{\text{Max} \mid \lambda_k(A) \mid}{\text{Min} \mid \lambda_k(A) \mid} \tag{2-2}$$

To be more specific, let us assume from now on that the prior covariance function of the spatial field being simulated or estimated is stationary, that is $C(x_1,x_2)=C(\xi)$ where $\xi=x_2-x_1$ is the two-point separation or lag vector, and has unit variance, that is $C(0)=\sigma^2=1$. The associated covariance matrix is symmetric positive-definite. It turns out that $\kappa(\boldsymbol{A})$ can be quite sensitive to the shape of the covariance

function $C(\xi)$. Eckstrom (1973), Lewis (1987), Posa (1989), and O'Dowd (1991) all indicate (in different ways) the ill-conditioned nature of Gaussian covariance systems in the context of linear estimation. Posa (1989) computed the condition number of the kriging matrix numerically for Gaussian, exponential, and spherical covariances, and concluded that the condition number of the Gaussian covariance was the worst, for several configurations of the data points. Lewis (1987) and O'Dowd (1991) noticed that the ill-conditioned nature of the Gaussian covariance matrix (and of the associated kriging matrix) is related to the infinitely differentiable property of Gaussian covariance random fields. One curious consequence of this property is that, given information on the random field and all its derivatives at only one point, one can extrapolate the field with perfect accuracy to any other point (Yaglom, 1962). The extremely smooth nature of this random field is related to the very fast Gaussian decay of its spectral density at large wave numbers (high spatial frequencies). Based on these observations, it may be expected that under certain conditions to be determined (e.g., oversampling), the discrete eigenvalue spectrum of the Gaussian covariance matrix includes near-zero eigenvalues. These near-zero eigenvalues would lead to a very large condition number according to Eq. (2-2). Qualitative arguments along these lines were developed in a paper by Eckstrom (1973) for the case of numerical deconvolution of signals with highly continuous and smooth kernels.

It should be noted that several random field simulation procedures do not depend on the condition number of the covariance matrix. For instance, the multidimensional TBM of Mantoglou and Wilson (1982) and Tompson et al. (1987a, 1989) generates stationary, unconditional random fields without any matrix inversion. Indeed, the TBM is based on 1D Fourier transforms and multidimensional projections, neither of which requires matrix inversion. On the other hand, as explained earlier, inversion or factorization of a covariance matrix is required for: (i) random field generation by the multivariate Gaussian method, (ii) conditional random field generation by the superposition method, and (iii) geostatistical estimation or kriging. The inversion of covariance-type matrices is also required in signal processing packages.

2.1.2 Covariance Functions and Spectral Density Functions

Figure 2-2 depicts different types of 1D covariance functions. The exponential covariance corresponds to a first-order Markovian time process, and the linear-exponential corresponds to a second-order Markovian process in 1D space (Vanmarcke, 1983). The exponential and Gaussian models are frequently used in geostatistics and hydrology. There exist, however, a number of other covariance models that have been extensively used in geostatistics. Examples are the triangular model, the spherical model, and the cubic model which is parabolic at the origin and thus more robust than the Gaussian.

Multidimensional counterparts to these covariance functions can also be defined, although care must be taken to satisfy certain admissibility conditions (Vanmarcke, 1983; Christakos, 1984). For example, the ellipsoidal-anisotropic Gaussian covariance function is defined for any number of spatial dimensions by:

$$C(\xi) = \sigma^2 \prod_{m=1}^{m=D} \exp\left\{-\frac{1}{2}\left[\frac{\xi_m}{l_m}\right]^2\right\} \qquad (2\text{-}3)$$

where ξ is the separation vector, D is the dimension of space (D=1, 2, or 3), and l_m is a characteristic fluctuation scale along direction x_m. An alternative set of length scales, the integral correlation scales, can be obtained by integrating the covariance function to infinity and dividing by the variance. Thus, the one-sided integral correlation scale, λ_m, is related to the defined fluctuation scales by the relation:

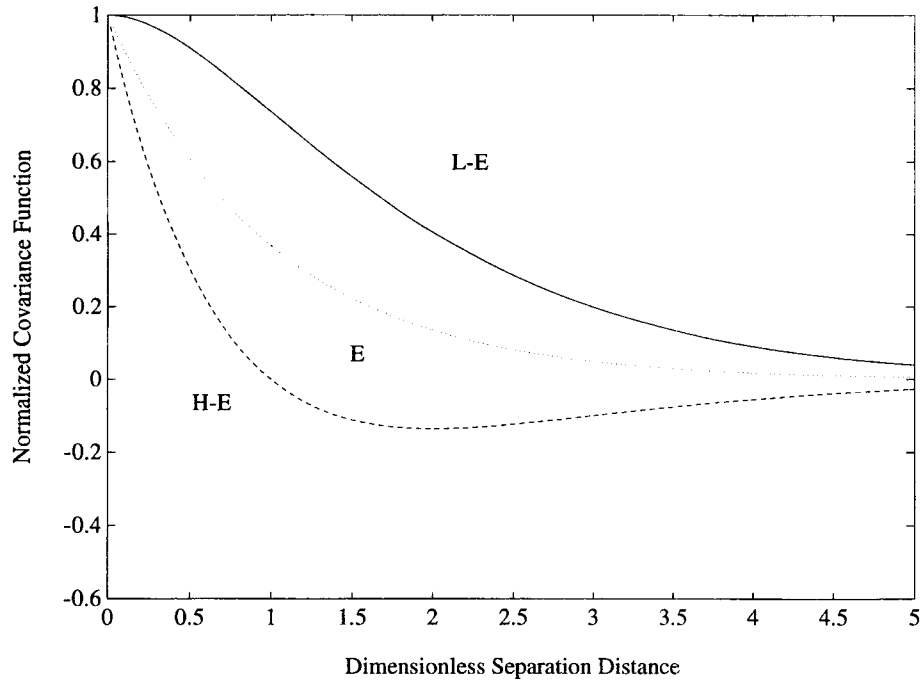

(a)

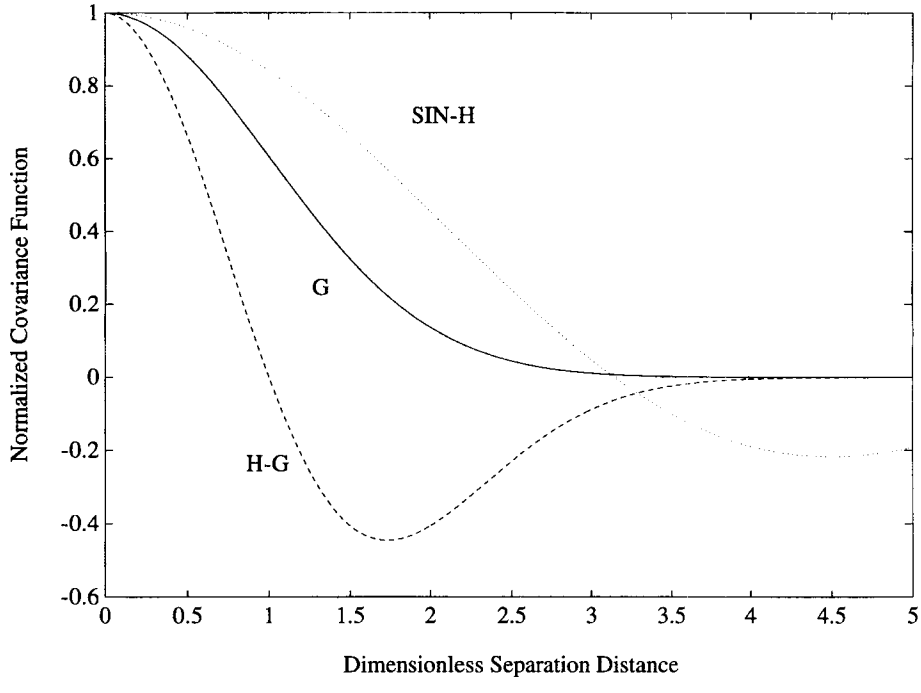

(b)

Figure 2-2. One-dimensional covariance functions: (a) solid: linear-exponential (Markovian); dot: exponential; dash: hole-exponential; (b) solid: Gaussian; dash: Hole-Gaussian; dot: Hole-sinusoidal

$$\lambda_m = l_m \left[\frac{\pi}{2}\right]^{1/2} \simeq 1.25\, l_m \tag{2-4}$$

However, the integral scales can vanish for other types of covariance functions. Therefore, we prefer to use the fluctuation scales, l_m, rather than the integral correlation scales, λ_m, as characteristic length scales of heterogeneity.

The spectral density function can be obtained from the Wiener-Khintchine theorem (Yaglom, 1962) by computing the Fourier transform of the covariance function. In the case of the Gaussian covariance, the spectral density is also Gaussian, that is

$$S(k) = \sigma^2 \prod_{m=1}^{m=D} \left[\frac{l_m}{\sqrt{2\pi}}\right] \exp\left\{-\frac{1}{2}(k_m l_m)^2\right\} \tag{2-5}$$

where k represents the wave vector. Note in particular that both $C(\xi)$ and $S(k)$ must be even functions, that is $C(-\xi)=C(\xi)$ and $S(-k)=S(k)$, regardless of the particular form of the covariance function at hand (Vanmarcke, 1983).

The 1D covariance functions in Figure 2-2 are plotted as functions of the dimensionless lag, ξ/l. Selected covariances are also given analytically in Table 2-1, along with the associated spectral densities. Both were normalized for a unit-variance field and a unit fluctuation scale; to obtain dimensional expressions, let $\xi \leftarrow \xi/l$, $k \leftarrow kl$, $C \leftarrow \sigma^2 C$ and $S \leftarrow \sigma^2 lS$ in Table 2-1. Important differences exist among the five models. The hole-Gaussian and hole-exponential covariances exhibit negative correlation at intermediate lags $\xi \approx l$, while the other functions exhibit positive correlations for all lags. The hole-sinusoidal exhibits negative correlation at lags $\xi > \pi$ with the maximum negative correlation at $\xi = 3\pi/2$. Some functions decay to zero at large lags $\xi >> l$ (Gaussian and hole-Gaussian). Other functions decay quickly at small lags $\xi << l$ (exponential and hole-exponential). The linear-exponential covariance decays slowly, both at small lags and large lags. These differences suggest that similar differences may exist in the eigenvalue spectra and condition numbers of the corresponding covariance matrices. Furthermore, the covariance structure is often corrupted in practice by the nugget effect or small-scale noise. The effect of adding a nugget to the above covariance models will be examined briefly in terms of conditioning in Section 2.1.3. A detailed analysis of the dependence of the condition number on the covariance models and various parameters was conducted and results can be found in the paper by Ababou et al. (1994). In what follows, a summary of some of the most important results is presented.

Results from these analyses are presented in Figure 2-3. Based on these results, the covariance models listed in Table 2-1 were ranked as follows, from best to worst in terms of condition numbers: (i) hole-exponential, (ii) exponential, (iii) linear-exponential, (iv) hole-Gaussian, and (v) Gaussian. This ranking is based mainly upon condition number comparisons in the region of ill-conditioning, that is at small-to-moderate sampling distances.

Table 2-1. One-dimensional covariance functions C(ξ) and spectral density functions *S(k)* (dimensionless formulation)

Covariance Model	Covariance Function	Spectral Density Function
1. Hole-exponential	$(1-\lvert\xi\rvert)\ \exp\{-\lvert\xi\rvert\}$	$\frac{2}{\pi}\ \frac{k^2}{(1+k^2)^2}$
2. Exponential	$\exp\{-\lvert\xi\rvert\}$	$\frac{1}{\pi}\ \frac{1}{1+k^2}$
3. Linear-exponential	$(1+\lvert\xi\rvert)\ \exp\{-\lvert\xi\rvert\}$	$\frac{2}{\pi}\ \frac{1}{(1+k^2)^2}$
4. Hole-Gaussian	$(1-\lvert\xi^2\rvert)\ \exp\left\{-\frac{1}{2}\lvert\xi^2\rvert\right\}$	$\frac{1}{\sqrt{2\pi}}\ k^2\ \exp\left\{-\frac{1}{2}k^2\right\}$
5. Gaussian	$\exp\left\{-\frac{1}{2}\lvert\xi^2\rvert\right\}$	$\frac{1}{\sqrt{2\pi}}\ \exp\left\{-\frac{1}{2}k^2\right\}$

2.1.3 Nugget Covariance and Its Effect on the Condition Number

For any of the covariance models considered, a pure nugget covariance reflecting the presence of small-scale noise can be added (Journel and Huijbregts, 1978). In terms of the random field itself, $y(x)$ corresponds to a decomposition into two independent fields, $y(x)=y_0(x) + y_1(x)$. Here, $y_0(x)$ represents the nugget effect or small-scale variability corresponding to measurement scale, assumed less than the smallest measurement spacing being considered, and $y_1(x)$ represents larger scale variability. The resulting covariance of $y(x)$ can be expressed as:

$$C(\xi) = C_{00}(\xi) + C_{11}(\xi) \tag{2-6}$$

where $C_{11}(\xi)$ is the covariance corresponding to large-scale variability with variance σ^2. The nugget covariance $C_{00}(\xi)$ can be represented as a coarsened white noise with variance, σ_0^2, as is usually done in geostatistical applications:

$$C_{00}(\xi) = \begin{matrix} \sigma_0^2 \text{ for } \lvert\xi\rvert \le \ell_0 \\ 0 \text{ for } \lvert\xi\rvert > \ell_0 \end{matrix} \tag{2-7}$$

where ℓ_0 is the smallest measurement scale. In the limit, $\ell_0 \to 0$, as a pure white noise covariance with intensity, s_0^2:

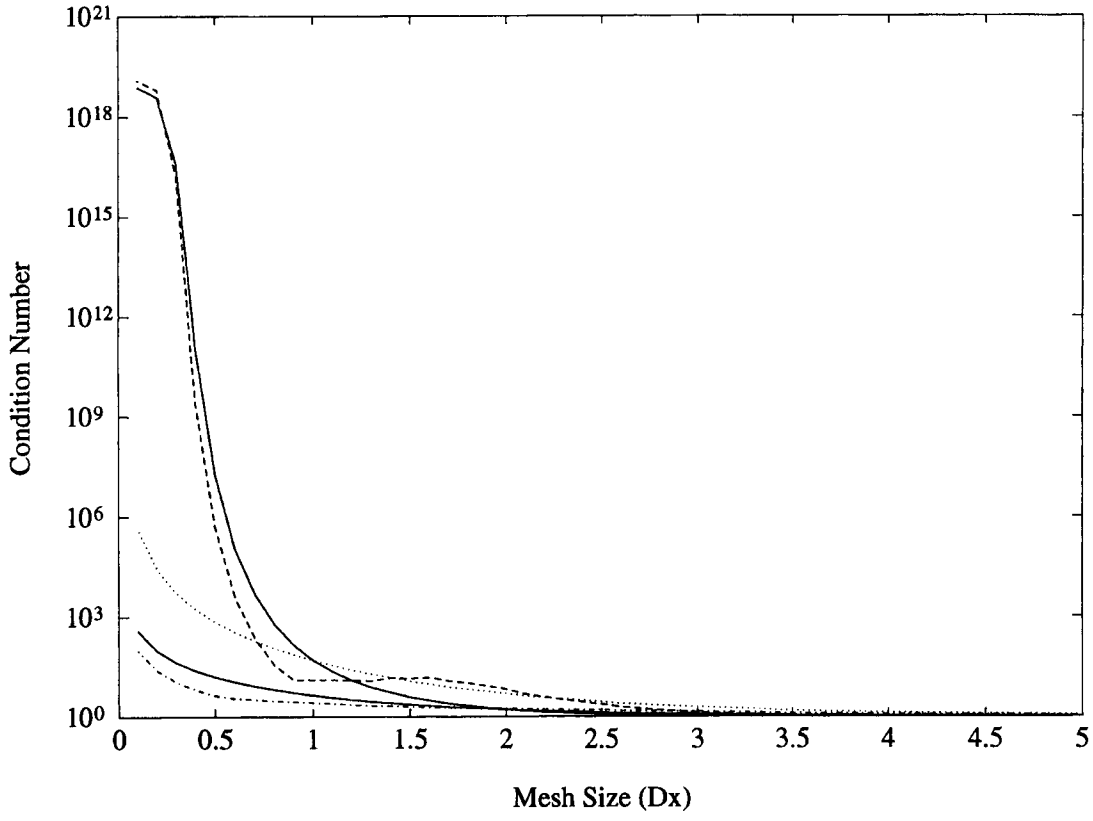

Figure 2-3. Condition number versus mesh size Δx in the case of a fixed domain size for various covariance functions. Solid: Gaussian; dash: Hole-Gaussian; dot: Linear-exponential (Markovian); Solid: Exponential; dash-dot: Hole-exponential.

$$C_{00}(\xi) = s_0^2\, \delta(\xi) \tag{2-8}$$

where $\delta(\xi)$ is the Dirac function. It is important to recognize that there is a definite relation between the two formulations which conveys the fact that Eq. (2-7) is a coarsened version of Eq. (2-8):

$$\sigma_0^2 = s_0^2/(2\ell_0) \tag{2-9}$$

Therefore, for a given intensity, the apparent nugget variance depends in fact on the small scale ℓ_0 (scale of measurement). It is advocated here that one can view the nugget variance as a representation of subscale heterogeneity, that is a form of noise resulting from variability at a scale smaller than the scale of observation. Generalizing this argument, one can postulate the relationship between regionalized variables, such as hydraulic conductivity or permeability, and a level of heterogeneity which is impossible to account for (i.e., at a scale smaller than the sampling scale).

Fractures, which cannot be fully characterized are another form of such heterogeneity. Field evidence at unsaturated fractured rock sites [e.g., the Apace Leap Tuff Site (ALTS)] and at saturated nonfractured sites indicate that there exists a great deal of variability that current (or feasible) techniques

cannot fully characterize; hence it is grouped all together in the form of a nugget variance. Guzman et al. (1993) have presented ALTS data on log-permeability (air) semivariograms that clearly exhibit a nested structure (i.e., prone to scale dependence) and a high (≈2.5/6.6) degree of otherwise unclassified variability. The recognition that the rock is fractured results in the postulation of a semivariogram which is the summation of effects from two other regionalized variables: (i) the matrix, γ_m; and (ii) the persistent or large fractures, γ_f. Faults are excluded from this concept, since there is no clear evidence to justify their regionalized nature. All remaining variability is lumped under the nugget variance. As will be demonstrated later, the subscale heterogeneity is very closely related to an apparent dispersivity concept. Both concepts, however, contribute to a reduction in the amplification of uncertainty as it is propagated through the physical system.

It could be expected intuitively that adding a small-scale variance to the diagonal of the covariance matrix improves its condition number. Using the spectral (continuum) approximation presented in Ababou et al. (1994) one confirms this is true at least in the case of monotonic covariance models. Note that the Fourier Transform of the pure white noise is a constant. Thus, the spectral density is:

$$S(k) = S_{00}(k) + S_{11}(k) = \frac{s_0^2}{2\pi} + S_{11}(k) \tag{2-10}$$

where $S_{00}(k)$ and $S_{11}(k)$ are the spectral densities corresponding to covariances $C_{00}(\xi)$ and $C_{11}(\xi)$, respectively. For monotonic models, Ababou et al. (1994) presented the following approximate expression for the condition number (κ):

$$\kappa(\sigma_0) \approx \frac{S\left[\frac{\pi}{L}\right]}{S\left[\frac{\pi}{\Delta x}\right]} \approx \frac{\sigma_0^2 + \frac{\pi}{\ell_0} S_{11}\left[\frac{\pi}{L}\right]}{\sigma_0^2 + \frac{\pi}{\ell_0} S_{11}\left[\frac{\pi}{\Delta x}\right]} \tag{2-11}$$

For example, using the exponential covariance model:

$$\kappa(\sigma_0) \approx \frac{\sigma_0^2\, \ell_0 + \left\{1 + \left[\frac{\pi}{L}\right]^2\right\}^{-1}}{\sigma_0^2\, \ell_0 + \left\{1 + \left[\frac{\pi}{\Delta x}\right]^2\right\}^{-1}} \tag{2-12}$$

Based on the above equations, the following remarks can be made regarding the condition number:

- κ goes to unity in the limit of a pure nugget; thus, it tends to improve as the nugget variance increases.

- κ increases to a finite value in the limit of infinite domain with fixed sampling density. This result holds with and without a nugget, but it can be shown that the limit value of κ is smaller when a nugget is present.

- κ increases to a finite value in the limit of infinite sampling density with fixed domain size provided a nugget is present. If the nugget variance vanishes, then we obtain a condition number that increases indefinitely as sampling density increases. The nugget, therefore, eliminates this singular behavior of κ.

These theoretically derived results can be verified numerically for the case of an exponential covariance model with variance $\sigma^2=1.0$. A nugget variance $C_0=\sigma_0^2$ of 0.1 and 1.0 is added to the main diagonal of the covariance matrix, and the condition number κ is calculated. Then the ratio $\frac{[\kappa]^{C_0=0}}{[\kappa]^{C_0\neq 0}}$ is calculated as a function of mesh size, Δx. This result is depicted in Figure 2-4. As shown earlier, the nugget variance improves the condition number of the covariance matrix, especially for small Δx. For $\Delta_x = 0.1$, for example, the condition number of the exponential covariance model is three and twenty times better for $\sigma_0^2=0.1$ and $\sigma_0^2=1.0$, respectively.

2.2 SOLUTION OF THE UNSATURATED FLOW EQUATION

Variably saturated flow in a heterogeneous porous medium is assumed to be governed at the local scale by the mass conservation equation, and by the generalized Darcy or Darcy-Buckingham equation relating flux to the pressure gradient. This relation is linear for saturated flow and nonlinear or quasilinear for unsaturated flow. In both cases, the coefficient of proportionality is called the hydraulic conductivity of the medium. Local mass conservation in a slightly compressible and variably saturated porous medium without source/sink terms is expressed by the equation:

$$\frac{\partial}{\partial t}\left[M(h) + \theta(h)\right] = -\frac{\partial q_i}{\partial x_i} \qquad (i = 1,2,3) \qquad (2\text{-}13)$$

where q_i is the flux vector or specific discharge rate (L/T) in the direction x_i, h is the water pressure head, $\theta(h)$ is the volumetric soil water content (L^3/L^3) relative to the incompressed soil matrix, and $M(h)$ is an elastic storage term (L^3/L^3) due to the combined compressibility of water and solid porous matrix. This term may be assumed negligible for unsaturated flow ($M=0$ if $h<0$) and proportional to pressure head for saturated flow ($M=S_s h$ if $h>0$, where S_s is the specific storage coefficient).

The generalized Darcy equation for variably saturated flow can be expressed in an arbitrary (x_1, x_2, x_3) coordinate system as:

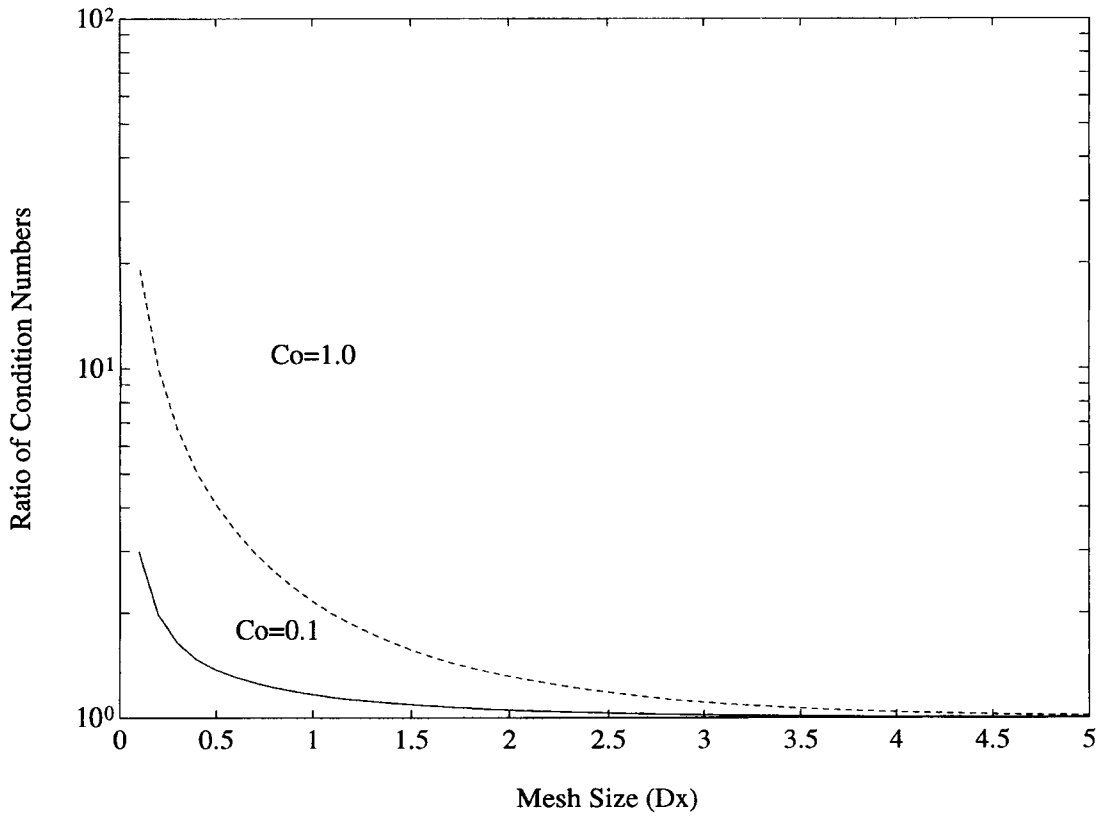

Figure 2-4. Ratio of condition number without a nugget variance over condition number with a nugget variance versus mesh size Δx in the case of a fixed domain for an exponential covariance. Solid: $C_0=\sigma_0^2=0.1$; dash: $C_0=\sigma_0^2=1.0$.

$$q_i = - K(h) \frac{\partial}{\partial x_i} (h + z) \tag{2-14}$$

where implicit summation on repeated indices is used. In Eq. (2-14), $K(h)$ is the unsaturated hydraulic conductivity (L/T); and h is the water pressure head relative to atmospheric pressure, negative in the unsaturated zone and positive in the saturated zone (L). Note that the water content $\theta(h)$ and the conductivity $K(h)$ are, in general, spatially variable functions of pressure head h.

Equations (2-13) and (2-14) are applicable in principle to the general case of variably saturated flow. That is, they are applicable to the case where the flow domain is partially saturated and partially unsaturated. However, the present discussion can be simplified by considering separately: (i) purely saturated flow ($h \geq 0$), and (ii) purely unsaturated flow ($h \leq 0$). The assumption of purely unsaturated flow is justified only if it can be shown that positive pressures do not appear at any time within the flow domain. This is indeed the case for sufficiently low-rate infiltration in dry soils, even in the presence of significant heterogeneity.

Inserting the Darcy equation into the mass conservation equation yields the Richards' equation of unsaturated flow

$$\frac{\partial \theta(h)}{\partial t} - \frac{\partial}{\partial x_i}\left[K(h)\left[\frac{\partial h}{\partial x_i} + \frac{\partial z}{\partial x_i}\right]\right] = 0 \qquad (2\text{-}15)$$

On the other hand, in the case of saturated flow ($h \geq 0$), a new variable H for the total hydraulic potential is introduced

$$H = h + z \qquad (2\text{-}16)$$

The actual numerical computations implemented in BIGFLOW are based on a single modularly structured program that can either solve the general problem of transient variably saturated flow or more specialized flow problems such as saturated and/or steady-state flows.

2.2.1 Finite Difference Discretization in Three-Dimensional Space

In the case of highly heterogeneous or random porous media, and in the case of highly nonlinear flows, the fine details of the flow field must be adequately resolved in all three spatial dimensions in order to obtain meaningful solutions. High-order discretization schemes such as pseudo-spectral methods, spectral finite elements, and some other weighted residual schemes, may work well for relatively smooth flow fields. In the heterogeneous case, however, fine grid resolution remains a necessary requirement even when using high-order schemes; these schemes can therefore require a very significant increase of computational work relative to lower-order schemes (for similar levels of accuracy).

The BIGFLOW code is based on a low-order, seven-point centered finite difference scheme in space, and a fully implicit one-step (Euler backwards) finite difference scheme in time. The spatial mesh can be rectangular but must be uniform along each direction. On the other hand, the time step can be variable. The resulting coefficient matrix is symmetric and very sparse, having only seven nonzero diagonals. The finite difference discretization scheme for both unsaturated and saturated flow is developed in the following, keeping in mind that the latter can be obtained by specializing the former. The analogy between saturated and unsaturated flow leads to the introduction of a single designation P for the pressure head h and hydraulic head $H=h+z$. Indeed, this is the strategy adopted for implementing the saturated-unsaturated equations in the BIGFLOW code. Accordingly, let $P=h$ for unsaturated flow and $P=H$ for saturated flow. In addition, let the vector ∇ designate the gradient operator

$$\nabla(\cdot) = \left[\frac{\partial(\cdot)}{\partial x_1}, \frac{\partial(\cdot)}{\partial x_2}, \frac{\partial(\cdot)}{\partial x_3}\right] \qquad (2\text{-}17)$$

With these notations, the unsaturated flow Eq. (2-15) becomes

$$\frac{\partial \theta}{\partial t} - \nabla\left[K\nabla(P)\right] - g \cdot \nabla(K) = 0 \qquad (2\text{-}18)$$

where in general $\theta=\theta(P,x)$, and $K=K(P,x)$; and g is the unit vector for unsaturated flow, and zero for saturated flow.

Now, the seven-point centered finite difference approximation of Eq. (2-18) in 3D space will be developed briefly. Start with the flux discretization. Recall that the first component of the flux vector is given by the generalized Darcy equation

$$q_1 = - K(P,x) \left[\frac{\partial P}{\partial x_1} + g \right] \tag{2-19}$$

This flux component is now approximated by a two-point centered difference scheme as follows

$$q_1 \left[x_{i+\frac{1}{2},j,k} \right] \approx - K_{i+\frac{1}{2},j,k} \left[\frac{P_{i+1,j,k} - P_{i,j,k}}{\Delta x_1} + g \right] \tag{2-20}$$

where the pressure is evaluated at the nodes $x(i,j,k)$ of the regular orthogonal finite difference grid, while the flux and the conductivity are both evaluated at the mid-nodal points $x(i+1/2,j,k)$, which define a staggered grid distinct from the original grid (i,j,k). A similar scheme is used for discretizing the flux divergence. For instance, $\partial q_1/\partial x_1$ is approximated at the grid points by the two-point centered finite difference

$$\frac{\partial q_1}{\partial x_1} \left(x_{i,j,k} \right) \approx \frac{q_1 \left(x_{1+\frac{1}{2},j,k} \right) - q_1 \left(x_{1-\frac{1}{2},j,k} \right)}{\Delta x_1} \tag{2-21}$$

Using similar approximations for q_2, q_3, $\partial q_2/\partial x_2$, and $\partial q_3/\partial x_3$, a seven-point finite difference approximation of the spatial operators of Eq. (2-18) in terms of the nodal pressure P evaluated at the grid points, $x(i,j,k)$ is finally obtained. By the same token, the flux components q_1, q_2 and q_3 are evaluated on three different staggered grids, one for each flux component. Nevertheless, there is a provision in the postprocessing modules for generating cell-averaged flux components. This alternative form of the flux is useful for subsequent simulations of solute transport, for example, by particle tracking methods (PTMs).

The boundary conditions implemented in BIGFLOW are of three types. The following classification is based on physics (the mathematical classification is indicated in parentheses).

(i) pressure condition (Dirichlet) — $P=P_B(x)\ x\in\Gamma_1$

(ii) normal flux condition (Neumann) — $q\cdot n=q_B(x)\ x\in\Gamma_2$

(iii) gravity drainage or null pressure gradient (Neumann) — $\nabla P\cdot n=0\ x\in\Gamma_3$

In these equations, n represents the vector normal to the boundary Γ_i, and $\Gamma_1+\Gamma_2+\Gamma_3 = \Gamma$ (the entire boundary). Each Γ_i may consist of a disconnected set of boundary nodes. That is, the different types of boundary conditions can co-exist on any of the six planar faces composing the boundary of the hexahedral domain. In the case of unsaturated flow, note that the second and third types of conditions are nonlinear. Since the boundary condition equations are eliminated by a process known as matrix condensation, they

become part of the interior domain equations, which are thereafter linearized by Picard-type iterations. In short, the implication is that the nonlinear boundary conditions are themselves linearized by the same iterative process. Therefore, the correct solution of the original nonlinear boundary value problem is obtained as the number of iterations increases, provided the Picard iterations do not diverge.

There is no particular difficulty in accommodating Dirichlet-type conditions in the above equations, since fixed pressure conditions can be enforced exactly at the boundary nodes. However, Neumann-type conditions (fixed flux or pressure gradient) must be approximated by using a centered finite difference scheme. The order of accuracy of this approximation is the same as that in the interior of the domain, provided that the physical boundary is assumed to be located precisely at a mid-nodal point rather than at a node. The third type of condition, gravity drainage, is peculiar to unsaturated flow. In BIGFLOW, it can be implemented only for the lower horizontal boundary. It was noted in the literature (McCord, 1991) that BIGFLOW (Ababou, 1988; Ababou and Bagtzoglou, 1993) is one of a few multidimensional flow codes which provide the gravity drainage condition.

The centered mid-nodal formulation of Neumann-type conditions has the advantage of preserving the sparsity structure, symmetry, and positive definite characteristics of the finite difference system, as obtained after elimination of boundary pressures from the system and linearization. More precisely, note that the condensed matrix will be positive-definite if at least one boundary node is under fixed pressure. It is worth noting this important algebraic property holds not only for saturated flow but also for linearized unsaturated flow. More precisely, this is true in the case of a Picard-type nonlinear iterative solver as used in BIGFLOW.

2.2.2 Time Discretization

Having developed the spatial discretization scheme, one can now proceed to discretize the transient equation of unsaturated flow in time. A fully implicit one-step finite difference scheme known to be first order accurate in time is implemented. From Eq. (2-18), this choice leads to the fully discretized equation:

$$\frac{\theta^{n+1}(P) - \theta^{n}(P)}{\Delta t_{n+1}} - \nabla \left[K(P)\nabla P\right]^{n+1} - g \cdot \nabla \left[K(P)\right]^{n+1} = 0 \qquad (2\text{-}22)$$

where

$$\Delta t_{n+1} = t_{n+1} - t_n \qquad (2\text{-}23)$$

is the variable time step. For clarity, the direct dependence of θ and K on spatial location has been omitted, as well as the discrete-space index (i, j, k). It is understood that, in general, $\theta=\theta(P_{ijk}, x_{ijk})$, $K=K(P_{ijk}, x_{ijk})$, and that P stands for P_{ijk}.

The fully implicit Euler backward scheme was selected among other one-step implicit schemes in view of numerical experiments reported in the literature (e.g., Vauclin et al., 1979). The Euler forward explicit scheme was ruled out because of the well known fact that it requires a stringent stability condition, $\Delta t \leq 2D\Delta x^2$ for the linear diffusion equation (a similar condition is likely required for the nonlinear diffusion equation). In the case of unsaturated flow, the nonlinear soil moisture diffusivity

$D=K/C$, where C is the soil moisture capacity, may become quite large in wet soils. Thus, the time step may have to be dramatically small in order to satisfy the explicit scheme stability condition; there may also be additional instabilities due to the nonlinear gravitational term.

On the other hand, it can be shown by Fourier analysis that implicit schemes are linearly stable, regardless of time step size (unconditionally stable). However, for nonlinear diffusion problems, the proof of unconditional stability is based on Fourier analysis assuming frozen coefficients. Due to this approximation, one should keep in mind that the nonlinear stability of the implicit scheme is not truly guaranteed for strongly nonlinear equations like unsaturated flow. It is nonetheless probable that the implicit scheme allows larger time steps than the explicit scheme, as demonstrated experimentally by Vauclin et al. (1979) and others.

2.2.3 Iterative Linearization

In the case of unsaturated flow, an approximate linearized solution method must be devised to deal with the nonlinear system. For instance, implementing a Picard iteration scheme will transform the sparse and symmetric nonlinear system into a more tractable sequence of equally sparse and symmetric matrix systems. The question of solving large symmetric matrix systems and of coupling the matrix solution process with the nonlinear iteration process will be discussed later. Here, the iterative linearization approach that transforms the nonlinear system into a sequence of linear systems is developed.

The modified Picard iteration scheme defined in the following approximates the unsaturated flow equation as a sequence of systems ($k=0, 1, 2....$) where the unsaturated conductivities appear linearly at each iteration level

$$\frac{\theta^{n+1,k+1} - \theta^{n+1,k}}{\Delta t_n + 1} - \nabla \left[K^{n+1,k} \nabla \left(P^{n+1,k+1} - P^{n+1,k} \right) \right] \approx$$

$$- \left[\frac{\theta^{n+1,k} - \theta^{n}}{\Delta t_{n+1}} - \nabla \left(K^{n+1,k} \nabla P^{n+1,k} \right) - g \cdot \nabla \left(K^{n+1,k} \right) \right] \qquad (2\text{-}24)$$

Note that $k+1$ represents the current iteration level, while $n+1$ represents the current time step. The residual term on the right-hand side of Eq. (2-24) is known since it depends only on the previous iteration level $n+1, k$. The spatial operator on the left-hand side operates on a pressure increment rather than pressure itself. This incremental formulation, or modified Picard scheme, was obtained by subtracting known quantities from both sides of the standard Picard equation. The modified Picard scheme is not only more elegant but also computationally more stable than the standard Picard scheme with respect to round-off errors (Ababou, 1988).

There remains a pressure-dependent moisture content in Eq. (2-24). To obtain a fully linear system at each iteration level, the storage term is now linearized by using a first-order difference approximation of the $\theta(P)$-increment. Specifically, one may construct a chord-slope approximation of the soil moisture capacity, $C=\partial\theta/\partial P$, which is now inserted in a first order difference approximation of the $\theta(P)$-increment

$$\frac{\theta^{k+1} - \theta^k}{\Delta t_{n+1}} \approx \frac{\mathbb{C}\left(P^k\right)}{\Delta t_{n+1}} \left(P^{k+1} - P^k\right) \tag{2-25}$$

where all variables are implicitly taken at time level $n+1$, except for P^0 which is the pressure at iteration level (0), that is the solution of the previous time step. Note the resulting finite difference system is a discrete approximation of the mixed form equation, rather than the pressure-based Richards' equation. This mixed form is identical to that developed in Ababou (1988) and similar to that adopted by Bouloutas (1989) and Celia et al. (1990).

In the case of unsaturated flow, let $\mathbb{C}$ be the diagonal matrix of specific moisture capacities, K the matrix of unsaturated conductivities, δp the vector of incremental pressures, and b the right-hand side vector. The latter includes the residual term on the right-hand side, as well as additional terms obtained after elimination of boundary values from the linearized system (matrix condensation). With these notations, the iterative sequence of linearized unsaturated flow systems can be written equivalently as:

$$\left[\frac{\mathbb{C}^{n+1,k}}{\Delta t_{n+1}} + K^{n+1,k}\right] \delta p^{n+1,k+1} = b^{n+1,k} \tag{2-26}$$

The case of saturated flow leads to a similar algebraic equation, with $\mathbb{C}$ a diagonal matrix of storativities rather than moisture capacities, and K a matrix of saturated rather than unsaturated conductivities. The more general case of variably saturated flow also leads to a similar equation, with $\mathbb{C}$ a diagonal matrix containing both storativities and moisture capacities.

2.3 SOLUTION OF THE TRANSPORT PROBLEM WITH PARTICLE TRACKING METHODS

2.3.1 Advection-Diffusion-Equation

Solute transport in porous media may be represented by the advection-diffusion-equation (ADE)

$$\frac{\partial c}{\partial t} + \nabla \cdot (vc) - \nabla \cdot (D \cdot \nabla c) = 0 \tag{2-27}$$

where the porosity is constant, c is the solute concentration, v is the flow velocity (Darcy flux divided by porosity), and D is the anisotropic velocity-dependent dispersion tensor.

Over the years, this equation has been extensively investigated and numerically approximated by numerous methods. It is conventionally solved by finite difference or finite element techniques. The method of characteristics (MOC) is an Eulerian-Lagrangian method, treating advection by looking along characteristics and diffusion by a conventional grid approach. This technique allows the diffusion-free motion of the solutes to be represented accurately by tracking the flow lines. A disadvantage of the MOC method is that it requires one to solve for the characteristics, which may be extremely difficult in 3D problems. Allowing miniscule particles to follow the flow lines, one can bypass the problem of finding the flow characteristics. Pinder and Cooper (1970) were among the first to apply a particle-oriented model

in hydrological applications, and studied the transient position of the saltwater front in coastal aquifers. A large collection of computer-generated particles, with each particle assigned a value of concentration, moves along streamlines. These concentration values are mapped on a grid and a standard Eulerian diffusion problem is solved *via* finite difference or finite element techniques. Practice has shown this method often leads to mass conservation errors, especially during the first time increments. The method is, also, extremely sensitive to the initial number of particles and the time step (Konikow and Bredehoeft, 1978), as there is no attempt to redistribute particles in the presence of diverging or converging flow fields.

2.3.2 Origin and Applications of the Particle Tracking Method

According to Hockney and Eastwood (1988), the term *particle models* is generic and used for the class of simulation models in which the discrete representation of physical phenomena involves the use of interacting particles. Each particle may have a set of attributes such as mass, charge, position, momentum, heat, or vorticity. The basic concept behind this method is to represent the distribution of an extensive quantity (e.g., the mass of the solute species or a packet of water) as a large collection of particles (Tompson and Dougherty, 1988). Each one of these particles can be translated by diffusive-dispersive and/or advective driving forces over discrete time steps. The mass of each particle or the number of particles can be altered depending on the reaction terms involved. Particle tracking methods (PTMs) were originally introduced by Harlow in the 1950s to facilitate the solution of complicated problems in fluid dynamics. PTMs have been used to solve partial differential equations in various areas of application such as fluid dynamics involving large distortions of the fluid, supersonic flow of gases past cylinders (Harlow, 1964), plasma gun simulations (Morse, 1970), and studies of spiral structure in thin disk galaxies (Hockney and Eastwood, 1988).

Since Ahlstrom et al. (1977) first applied this technique to numerical investigations of groundwater contaminant hydrology, many other investigators (Todorovic, 1970; Smith and Schwartz, 1980, 1981); Prickett et al., 1981; Schwartz et al., 1983; Uffink, 1986, 1987; Tompson et al., 1987b; Tompson and Dougherty, 1988, 1992; Kinzelbach, 1988; Ackerer, 1988; Bagtzoglou and Dougherty, 1990; Dougherty and Tompson, 1990; Bagtzoglou et al., 1991, 1992a,b; and Andricevic and Foufoula-Georgiou, 1990) have used particle methods with success. The PTM has also been effectively applied to transport studies in fractured rock (Wollrath and Zielke, 1990), stratified formations (Cvetkovic and Shapiro, 1989), and anisotropic heterogeneous aquifers (Dagan, 1988); bed sediment dispersion studies in natural and/or artificial waterways (Todorovic, 1975); simulation of alluvial fan deposition (Price, 1974); and studies of roughness of drainage networks (Seginer, 1969).

Unlike the conventional Eulerian methods, PTMs have no unacceptable grid Peclet numbers or grid orientation effects and are traditionally considered well-suited for advection-dominated simulations (Ahlstrom et al., 1977). The practical time step size is limited by the ability of the algorithm to accurately track the flow characteristics.

2.3.3 The Random Walk Method and Its Application in Heterogeneous Fields

One of the more popular particle methods, which has been extensively applied in solute transport in hydrology, is based on a random walk approach. The theoretical basis of the random walk model has its origin in Einstein's explanation of Brownian motion (Einstein, 1926) describing the motions of suspended particles under the influence of a fluctuating force. The motion of a Brownian particle

experiencing random changes in acceleration is described by the Langevin equation given by (Srinivasan and Vasudevan, 1971)

$$m\frac{dv}{dt} = -\varphi v + F(t) \tag{2-28}$$

where v is the velocity of the particle and m is the mass. The right-hand side of Eq. (2-28) represents the influence of the surrounding medium, comprising a fluctuating force $F(t)$ (random part) and a dynamic friction $-\varphi v$ (deterministic part). Eq. (2-28) can be written in terms of any state variable $X(t)$ which evolves probabilistically with time t. Therefore, it can be rewritten in the form of a position instead of a force balance equation. Then, changes of the variable X in time (i.e., the motion of the particle, for X being the position vector) will be modeled by:

$$\frac{dX}{dt} = A(X,t) + B(X,t) \cdot \xi(t) \tag{2-29}$$

where $\xi(t)$ is a Gaussian process. Assuming that $B(t)$ varies very rapidly compared to X, the Fokker-Planck equation (FPE) can be obtained (Haken, 1983; Gardiner, 1985)

$$\frac{\partial f}{\partial t} + \nabla \cdot (Af) - \nabla \cdot \left[\nabla \cdot \left[\frac{1}{2} B \cdot B^T f \right] \right] = 0 \tag{2-30}$$

where f is some extensive quantity, A is a deterministic forcing vector, and B is a deterministic scaling (square) matrix.

In order to make Eq. (2-30) analogous to Eq. (2-27), the following assignments have to be made:

$$f = f(x,t) \Leftrightarrow c \tag{2-31}$$

$$A = A(x,t) \Leftrightarrow v + \nabla \cdot D \tag{2-32}$$

$$B \cdot B^T = B(x,t) \cdot B^T(x,t) \Leftrightarrow 2D \tag{2-33}$$

Imposing Eq. (2-32) is necessary to correct the unrealistic/unreliable results obtained with commercially used random walk models in regions of strong velocity gradients (Kinzelbach, 1989). Russo and Dagan (1991) discussed the possibility of unsaturated transport variability being governed by similar laws as saturated transport, and concluded that "Lagrangian analysis ... is of general nature and applies to saturated and unsaturated flow as well." In the case of unsaturated flow, Eq. (2-32) should have an extra term added to the right-hand side, namely the moisture dependent term $D \cdot \nabla(ln\theta)$ which accounts for the influence of moisture content variability. The effect of this term is small in most applications, except in the case of steep wetting fronts and rapidly draining characteristic curves. The moisture content should also be accounted for in the velocity term, that is $v=q/\theta$.

The difference form of Eq. (2-29), over a time period Δt, takes the form (Sposito et al., 1986)

$$X(t + \Delta t) - X(t) = A\left[X(t),t\right] \cdot \Delta t + \int_t^{t+\Delta t} B\left[X(s),s\right] \cdot \xi(s)\,ds \tag{2-34}$$

With the understanding that the relaxation time Δt is very large compared with the time in which random force fluctuations occur, the stochastic process described by a conditional probability function satisfying the FPE is equivalent to the *Itô* stochastic differential equation (Bhattacharya and Gupta, 1983)

$$dX(t) = A\left[X(t),t\right] \cdot dt + B\left[X(t),t\right] \cdot dW(t) \tag{2-35}$$

where it was inherently assumed that

$$\int_t^{t+\Delta t} B\left[X(s),s\right] \cdot \xi(s)\,ds = B\left[X(t),t\right] \int_t^{t+\Delta t} \xi(s)\,ds = B\left[X(t),t\right] \cdot dW(t) \tag{2-36}$$

The above equation can be written in the form of the following discrete-step equation:

$$X^{n+1} = X^n + A\left(X^n,t_n\right)\Delta t + B\left(X^n,t_n\right)W(t_n) \tag{2-37}$$

where the index n indicates time t_n; X is the particle position vector; A and B are as previously described; x is the grid position vector; and $W(t_n)$ is a random forcing vector given by $W(t_n) = Z^n\sqrt{\Delta t}$, where Z^n is a random number sampled from a normal distribution, at each time t_n, with mean of zero and unit variance.

Consider the case of a heterogeneous random formation (see Figure 2-5). A particle, which at time t=0 is located at X_o, moves to its new location X at time t. This new location X can be considered a random variable, and similarly the evolution of the trajectory $X=X(X_o, t)$ that this particle followed is a random process. According to Dagan (1982a,b), the random vector X is characterized by a probability density function $f_X(X,t;\ X_o)$ such that the probability for a particle, originally released from X_o at t=0, to end up within the elementary volume $d\Omega_e$ surrounding X at t is given by:

$$P = \int_{\Omega_e} f_X\,d\Omega \tag{2-38}$$

Then for the domain Ω, at any time t

$$P = \int_{\Omega} f_X\,d\Omega = 1 \tag{2-39}$$

with

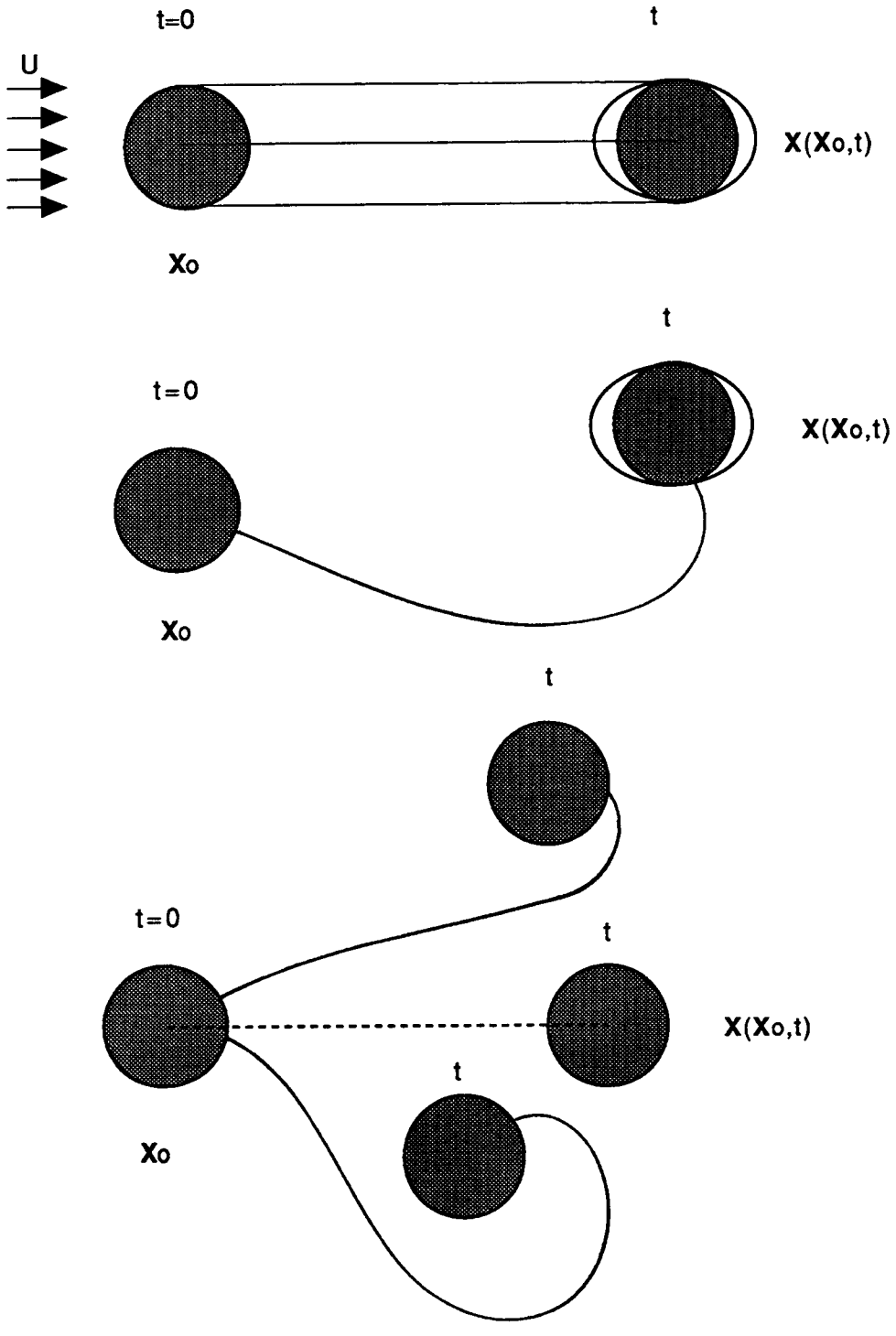

Figure 2-5. Schematical representation of solute body transport: (i) homogeneous formation, uniform flow; (ii) heterogeneous deterministic formation; (iii) various realizations for heterogeneous random formation (Adapted from Dagan, 1982b). The circular body boundary represents the advection influence, whereas the elliptical boundary represents the pore-scale dispersion influence.

$$f_X(X,0;X_o) = \frac{1}{\Delta V_o} \tag{2-40}$$

for $X \epsilon \Delta V_o$, where ΔV_o is the volume of particle release and

$$f_X(X,0;X_o) = 0 \tag{2-41}$$

for X elsewhere. Alternatively one can write

$$\int_{\Omega_e} f_X \, d\Omega = P\,(X \in \Omega_e) \tag{2-42}$$

and

$$\int_{\Omega_e} f_{X_o} \, d\Omega = 1 \tag{2-43}$$

It follows that the solute concentration $c(X,t)$ is also a random variable, and its probability density function (*pdf*) f_c is entirely determined in terms of f_X. Dagan (1982b) and Dagan and Nguyen (1989) prove that the expected value of concentration resulting from the release of mass M in an aquifer of porosity n and initially at concentration 0 can be given by:

$$\langle\, c(X,t) \,\rangle = \frac{M}{n} f_X\,(X, t; X_o) \tag{2-44}$$

Here, $\langle\, c \,\rangle$ is the expected value of the concentration field for a series of random hydraulic conductivity field realizations. Equation (2-44) establishes the direct proportionality between $\langle\, c \,\rangle$ (or $\langle\, c \,\rangle / M$) and f_X. Because of the interest in travel time estimation methodologies, note that the roles of concentration and particle density can be reversed. That is, the *pdf* $f_X(X,t;\, X_o)$ can be sought describing the probability that a particle, originated at position X_o at time t=0 is located at X after a time t has elapsed. Soerjadi (1981) was one of the first to make use of moving particle density functions and their relations as they evolve in time.

The *pdf* f_X may be interpreted as the concentration field arising from the release of a unit of mass at X_o at time 0. The *pdf* f_{X_o} conversely, may be interpreted as the probability that a unit of mass, which originated at time 0 from X_o, is observed at X at time t. In each case, the variance of the *pdf*, except possibly in initial short time intervals, increases as the amount of time from source (the term after the semicolon) to the target (the term before the semicolon) increases. Smith and Schwartz (1981) have implemented a similar approach and calculated regional probability plots for moving reference particles.

As became evident in the discussion of Section 2.1, microfracturing at a scale below detection constitutes a white-noise type of variability which can often be lumped under a nugget variance effect. It was also shown that this nugget has a very positive effect on the stability of the system (at least as far as the condition number of the covariance matrix is concerned). One can also view this noise as an indicator of lack of information. Obviously, if one could fully account for the geometric and hydraulic

characteristics of fractured rock, then a semivariogram without the presence of a nugget would have been obtained. Bagtzoglou et al. (1994b) presented examples of such variograms in the case of stochastically generated, yet fully described, fracture networks. It has also been advocated by Neuman et al. (1987) and Neuman (1990) that the effective dispersion coefficient is essentially an artifact of our lack of knowledge even though this type of induced dispersion is a macroscopic one at a small scale. Nevertheless, one could postulate the usage of such an effective dispersion as an analog to the mixing induced by microfracturing at a scale smaller than that of dominant persistent features (e.g., layers and fault zones).

Smith and Schwartz (1993) presented analyses of results from numerical experiments of transport in fractured media conducted by Robertson (1990). Figure 2-6 depicts results of a simulation of solute mass distribution within a discrete fracture network comprising two vertical sets of fractures with variable lengths and aligned to the cartesian coordinate system. Simulation time since a solute pulse injection was 35 days, and the inferred longitudinal dispersivity was 0.44 m over 200 statistically equally likely realizations. Smith and Schwartz (1993) commented on the uncertainties related to the prediction of breakthrough curves by emphasizing that the simulation results are highly uncertain when the fracture geometry "promote[s] relatively tortuous (indirect) connections across the network." Similar observations were made by Moreno (1985) who fitted curves produced by a hydrodynamic dispersion model and a discrete fracture-channeling model with success. However, a word of caution on the lumping of heterogeneity effects under the concept of dispersion coefficients was voiced by Rubin (1991) who claimed that "the effects of local(ized) parameter configurations ... are consequential for less-than-ergodic plumes."

2.3.4 Computational Details

2.3.4.1 Moving Particles Around

Equation (2-37) can be used to move a particle, initially located at X_o, through space over small discrete time steps, Δt, to its final position, X_n (Figure 2-7). Each step consists of a deterministic displacement $A \cdot \Delta t$ and an independent, random displacement $B \cdot dW$. If the experiment were to be conducted N times, the same particle (located initially at X_o) will end up at N locations, X_n^*. Then, the spatial density of the points, evaluated at $t=t_n$, will be $f(X,t)$, the extensive quantity involved in the FPE. The same results would be obtained if, instead, N particles all located at the same initial location X_o at time $t=t_o$ were to independently move according to Eq. (2-37) up to time $t=t_n$ (Figure 2-8). This is the approach employed by the SUFLAT numerical code.

2.3.4.2 Time Step Selection

In spatially varying flows, the choice of the time step is of importance. Selection of large time steps may lead to overshoot errors, thus eventually distorting the results. This problem can be bypassed if the time steps used force the Courant number $C_o = v\Delta t / \Delta x$ to be less than one in any computational cell. Selection of Δt small enough so that the Courant number is always less than 0.1 ensures that the maximum overshoot is always less than $0.1\Delta x$ (Tompson et al., 1987b). This of course requires extensive computations in order to move a single particle across a cell.

(a)

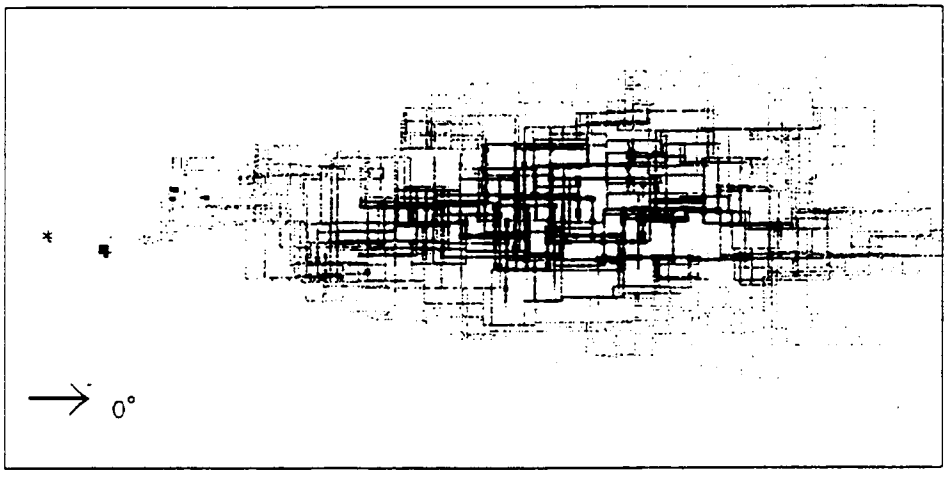

(b)

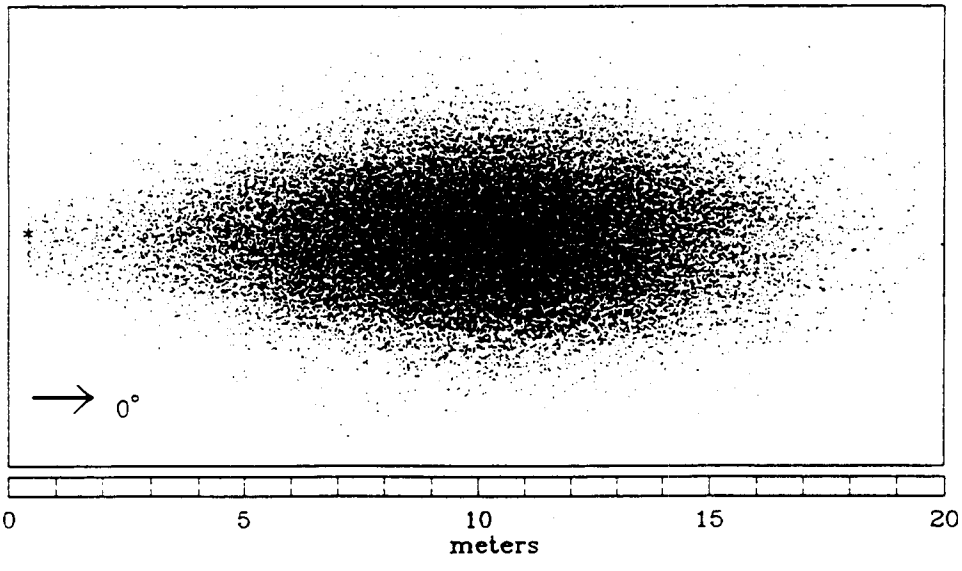

Figure 2-6. Simulation of the mass distribution at t=35 days after injection within: (a) a discrete fractured network, and (b) an equivalent porous medium (Adapted from Robertson, 1990)

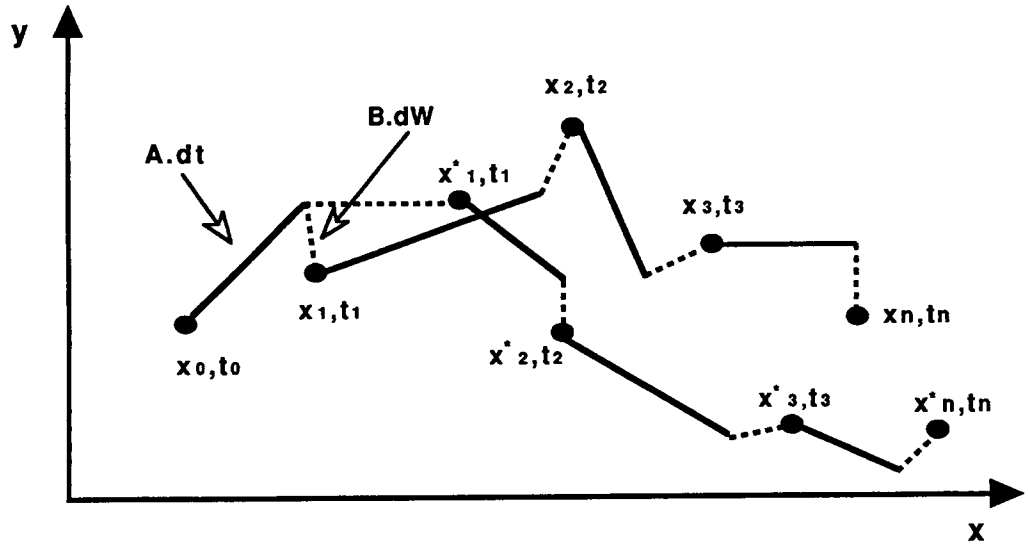

Figure 2-7. Two realizations of one particle moving during N steps

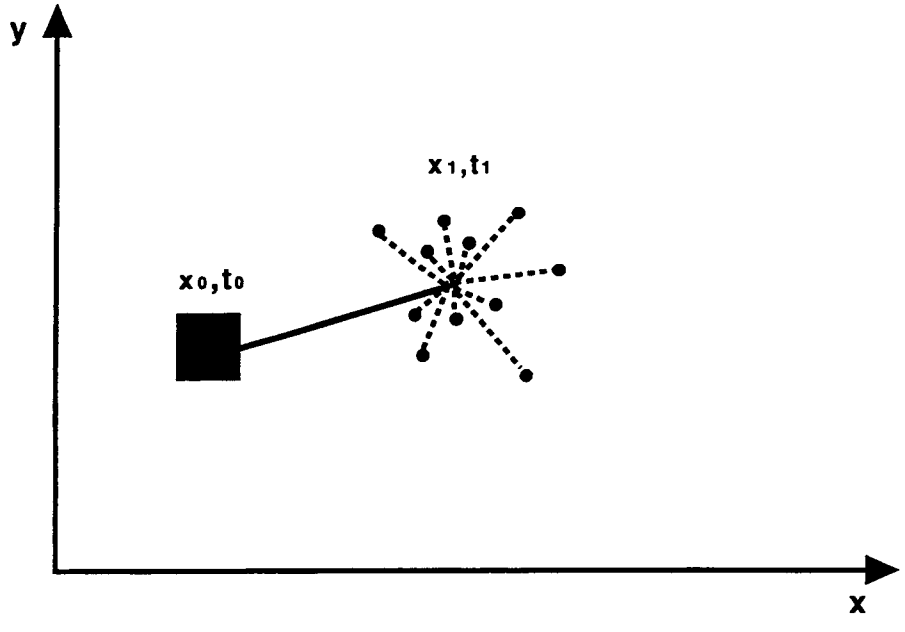

Figure 2-8. Single realization of N particles moving during one step

2.3.4.3 Initial and Boundary Conditions

Within the particle method framework, initial and boundary conditions are treated by constraining either the number or the movement of particles. Instantaneous spills can be readily simulated by introducing a certain number of particles within the domain. Dirichlet boundary conditions are imposed by simply assigning a certain number of particles in each cell of a boundary layer $\Omega 1$ (Figure 2-9) and letting them move under the influence of the velocity field. After all particle displacements have taken place, a fresh batch of N_b particles is reimposed within $\Omega 1$ such that:

$$c_{\Omega 1} = \frac{N_b m_p}{V_{\Omega 1}} \tag{2-45}$$

where $c_{\Omega 1}$, is the imposed concentration boundary condition; m_p is the mass per particle; and $V_{\Omega 1}$ is the volume of the boundary layer. Neuman boundary conditions can be imposed by forcing a certain number of particles to enter the computational domain through the boundary over a discrete time step. No-flux boundary conditions can be assigned by treating the boundary $\Omega 3$ as a reflection plane (Figure 2-10) where the particles bounce back into the domain in a billiard-ball fashion. Finally, infinite-domain behavior can be simulated by treating the boundaries as absorbing and allowing particles to freely exit the computational domain.

2.3.5 Accuracy of Particle Tracking Methods

2.3.5.1 Problem Specification

In this section we compare single-realization simulations using a PTM with six other methods. Four classical methods are used: (i) centered finite difference (CFD), (ii) upwind finite difference (UFD), (iii) Lax-Wendroff (LW), and (iv) Fromm (FR), all described by Roache (1976). In addition, two nonlinear flux-limiting schemes are employed: piecewise parabolic method (PPM) (Collela and Woodward, 1984), and flux-corrected transport (FCT) (Boris and Book, 1973). One widely used test problem, the advancing front problem, was developed for the Convection-Dispersion Forum held at the International Conference on Computational Methods in Water Resources (Baptista et al., 1988). The problem is specified as follows:

$$\frac{\partial c}{\partial t} + v\frac{\partial c}{\partial x} - D\frac{\partial^2 c}{\partial x^2} = 0 \tag{2-46}$$

for $0 \le x \le \infty$, and subject to

$$\begin{aligned} c(x,0) &= 0 \\ c(0,t) &= 1 \end{aligned} \tag{2-47}$$

and

$$c(\infty,t) = 0 \tag{2-48}$$

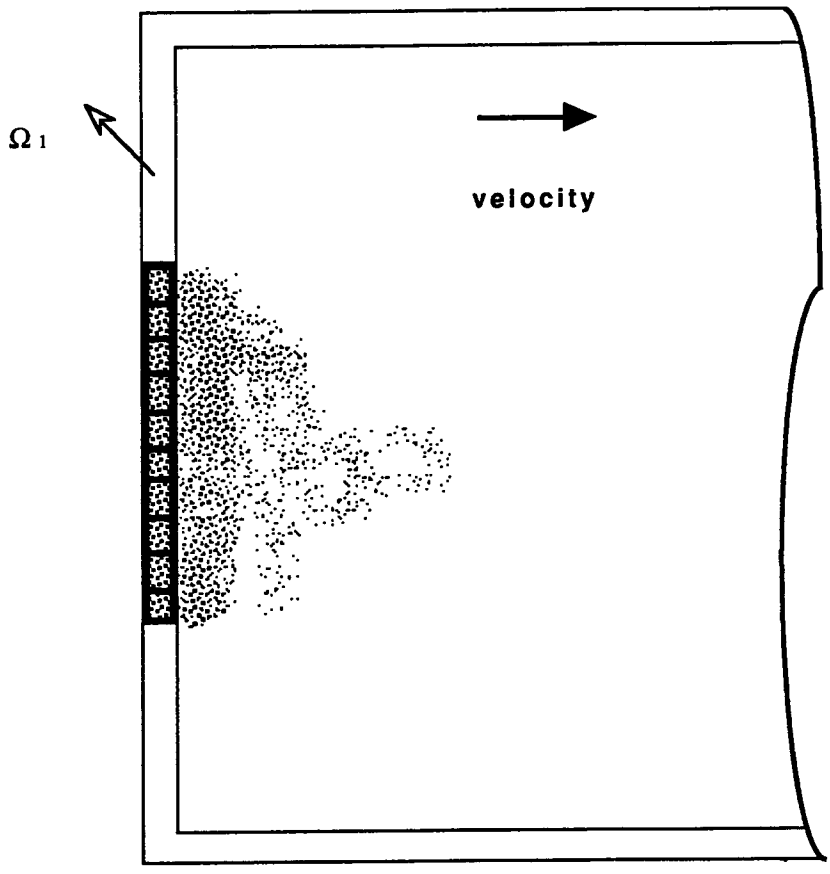

Figure 2-9. Dirichlet boundary Ω1 (Adapted from Tompson et al., 1987b)

The analytical solution for this problem is (Ogata and Banks, 1961; van Genuchten and Alves, 1982)

$$c(x,t) = \frac{1}{2}\left[\text{erfc}\left[\frac{x-vt}{\sqrt{4Dt}}\right] + \exp\left[\frac{vx}{D}\right]\text{erfc}\left[\frac{x+vt}{\sqrt{4Dt}}\right]\right] \tag{2-49}$$

The numerical simulations are performed on $x \in [0, 12{,}800]$ with a grid spacing Δx=200; a flow velocity v=0.5; a time step Δt=96; a total simulation time of 9,600; and a dispersion coefficient D = 50. Thus, a grid Peclet number defined as:

$$P_e = \frac{v\Delta x}{D} \tag{2-50}$$

of 2 is considered. For spatially and temporally invariant v and D in 1D, Eq. (2-37) can be simplified to:

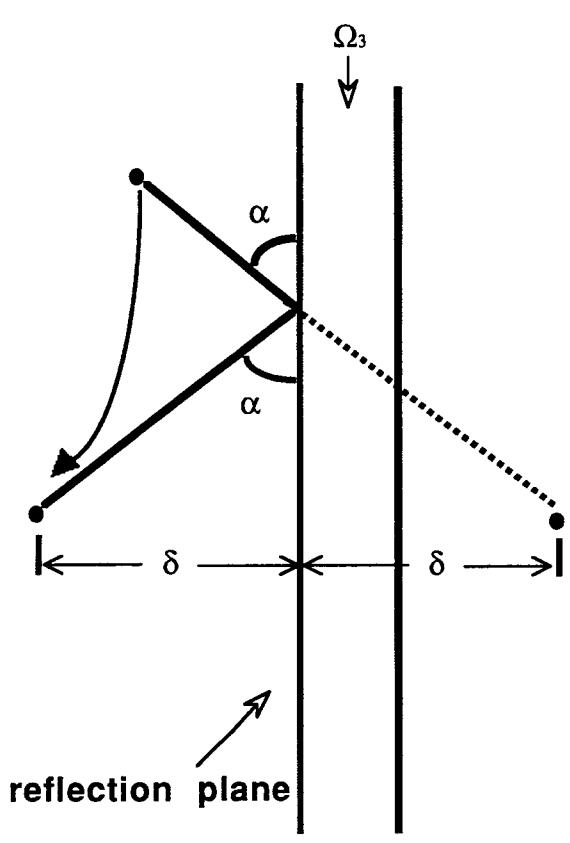

Figure 2-10. No-flux boundary Ω3 (Adapted from Tompson et al., 1987b)

$$X^{n+1} = X^n + v\Delta t + \sqrt{2D\Delta t}\, Z^n \tag{2-51}$$

where all variables have been previously defined. The random forcing vector is usually sampled from a uniform distribution, due to computing time requirements (Ackerer, 1988). Then, Eq. (2-51) can be written as:

$$X^{n+1} = X^n + v\Delta t + \sqrt{24D\Delta t}\,(0.5 - R^n) \tag{2-52}$$

where R^n is a random number uniformly distributed between 0 and 1.

The second test problem under consideration is the rectangular wave propagation problem which is governed by:

$$\frac{\partial c}{\partial t} + v\frac{\partial c}{\partial x} - D\frac{\partial^2 c}{\partial x^2} = 0 \tag{2-53}$$

with $x \in [-\infty, \infty]$ and initial and boundary conditions described by:

$$\begin{aligned} c(x,0) &= 0 \quad \forall\ x < 1{,}400 \text{ and } 2{,}600 < x \\ c(x,0) &= 1 \quad \forall\ 1{,}400 < x < 2{,}600 \\ c(\infty,t) &= 0 \quad \forall\ t > 0 \end{aligned} \tag{2-54}$$

where v and D are constant. The parameters used in the simulations are similar to those used for the advancing front problem. The analytic solution for this problem is given by (Neuman, 1981)

$$c(x,t) = \frac{1}{2}\left[\text{erf}\left[\frac{b-x+vt}{2\sqrt{Dt}}\right] + \text{erf}\left[\frac{b+x-vt}{2\sqrt{Dt}}\right]\right] \tag{2-55}$$

where $2b$=(2,600−1,400) is the width of the rectangular wave initial condition. The subdomain considered for numerical simulation is from 0 to 12,800.

Over the years, both problems have been extensively studied by numerous investigators. Stone and Brian (1963) employed a cyclic use of a set of difference equations, which yielded wave propagation rates with an optimum harmonic decay for linear problems. Konikow and Bredehoeft (1978) solved the solute transport equation by approximating the convective transport *via* particle tracking and by a two-step explicit procedure to solve the diffusion equation *via* finite-differences. Cheng et al. (1984) investigated the applicability of an Eulerian-Lagrangian approach, a technique that Yeh (1990) enhanced with the use of zoomable hidden fine-meshes. Celia et al. (1989) presented the application of algebraic theory to the discretization of the spatial derivatives of the ADE and developed a semidiscrete system which was solved by standard marching algorithms. Allen and Curran (1989) incorporated an adaptive grid refinement procedure within the framework of a finite-element collocation solution of the advection-dominated solute transport. Bentley et al. (1989) employed a least squares collocation Eulerian-Lagrangian method with great success for purely advective flows. Similar work has been reported by Neuman (1981) who used an Eulerian-Lagrangian method with conjugate space-time grids, and by Cady and Neuman (1985) who combined a modified method of characteristics with a finite element formulation.

In this work, all seven numerical schemes mentioned earlier are applied to the advancing front test problem, whereas only the particle tracking, PPM and FCT are tested for the rectangular wave problem. A description of the seven numerical schemes can be found in Appendix A. For these flow and discretization parameters the grid Courant number, $C_o = v\Delta t/\Delta x$, is equal to 0.24. The particle method does not involve repeated simulations. This is in order to make its results comparable to the single-run, deterministic, standard numerical methods. The particle method simulations involve N_p=400 particles, and one grid cell as support for the particle-to-grid projection.

2.3.5.2 Discussion of Results

The analytical and numerical solutions to these standard test problems are shown in Figures 2-11 and 2-12 for the advancing front and rectangular wave propagation problems, respectively. For all tests, the domain was evenly discretized into 65 nodes. The classical methods lead to excessive smearing of the front and, especially for higher velocities, oscillations. The particle method, because of the finite number of particles used (here 400), yields noisy solutions unless the diffusion is negligible. Note that the modern methods provide excellent solutions. Implicit-in-time methods have not been considered here because it is well known that they have high truncation errors for large time steps. Time steps that provide sufficiently reduced truncation errors require more effort than explicit methods for this linear problem.

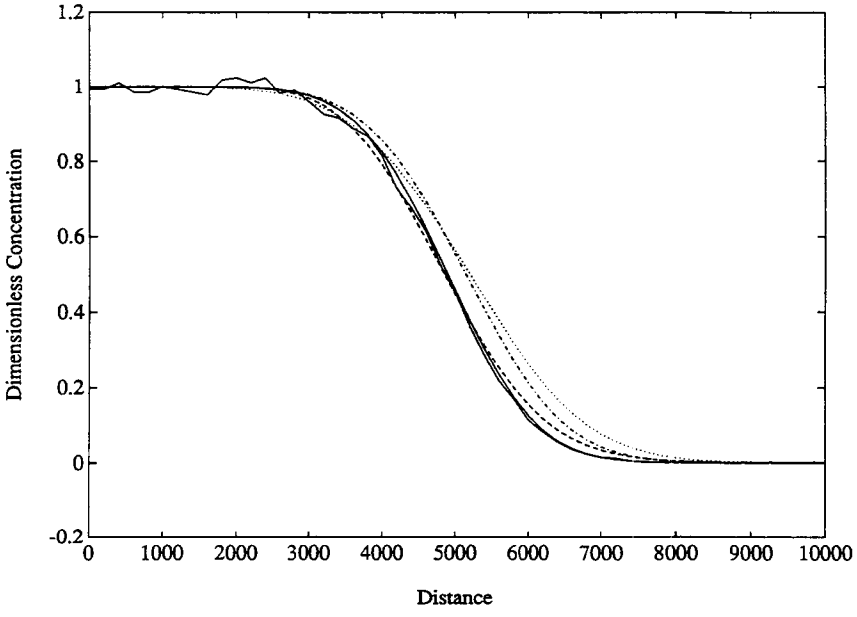

(a)

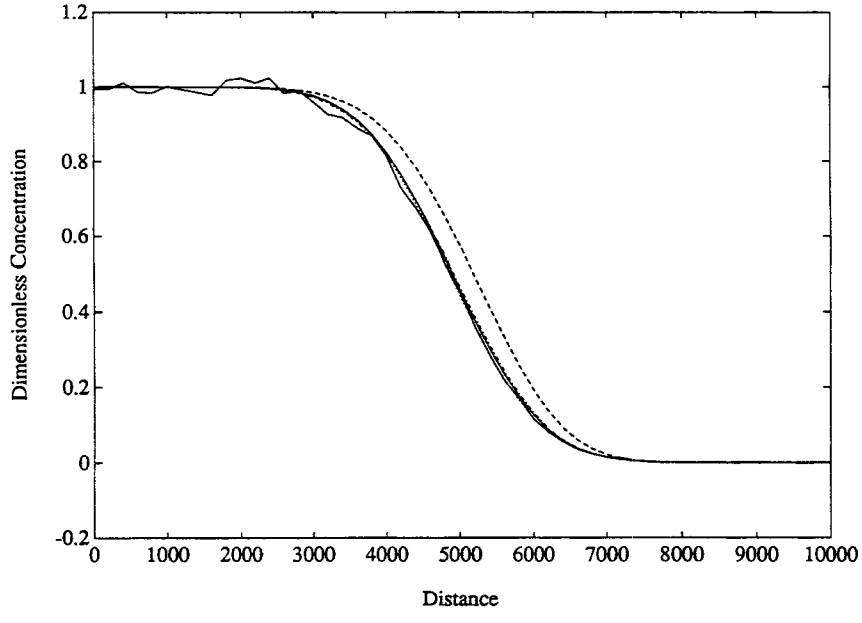

(b)

Figure 2-11. Concentration versus distance for the advancing front problem. Smooth solid line: analytical; noisy solid line; particle; (a) dashed line: CFD; dotted line: UFD; dashed-dotted line: LW; and (b) dashed line: FR; dotted line: PPM; dashed-dotted line: FCT.

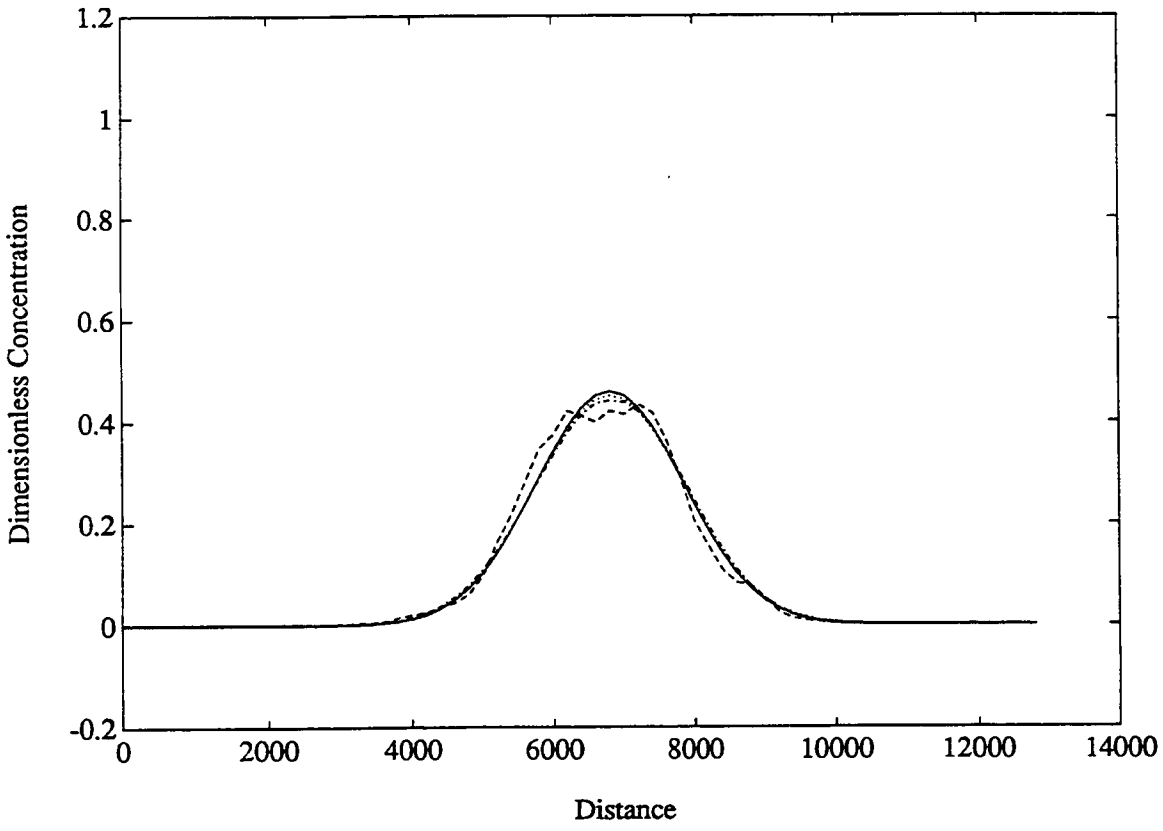

Figure 2-12. Concentration versus distance for the rectangular wave propagation problem. Smooth solid line: analytical; noisy dashed line: particle; dotted line: PPM; dashed-dotted line: FCT.

It should be noted that the stabilizing effect of the implicit method is often beneficial for nonlinear problems.

One important and widespread use of solute transport models involves management decisions when concentrations are at or near the maximum acceptable (or action) concentration level (MCL). Management decisions are often controlled by the MCL and by predictions of the effects induced by a number of possible clean-up methods on concentration. The latter are often obtained using numerical models. Therefore, numerical errors committed for concentrations near the MCL have great impact on the decision-making process. Dougherty and Bagtzoglou (1993) provide a discussion of this particular issue in greater detail.

This perspective suggests that we revisit the results given in Figures 2-11 and 2-12. Consider the difference between the numerical concentration and the analytical (true) concentration, relative to the analytical concentration, at different spatial locations for time T. Figures 2-13 and 2-14 show this error-to-signal (or noise-to-signal) ratio for the two test problems. The error-to-signal ratio is virtually constant and negligible for a wide range of x. However, at large x, where the concentration c is small, the error grows in all classical methods to large values [the Random Walk Particle Method (RWPM) is a special case due to its Lagrangian formulation]. It is clear from panels (a) and (b) of Figure 2-13 that

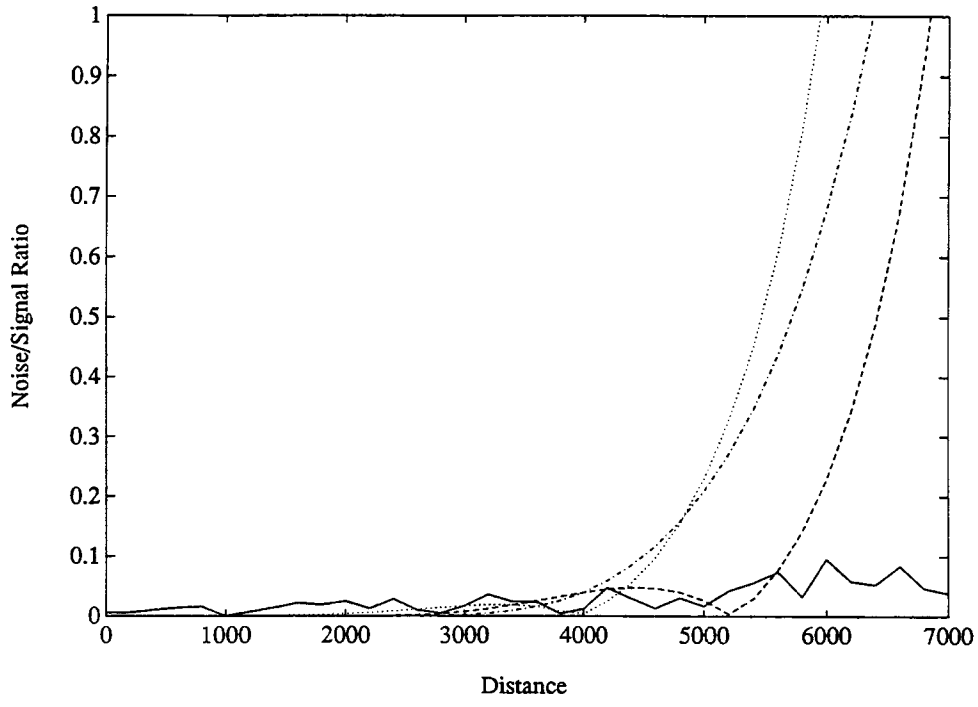

(a)

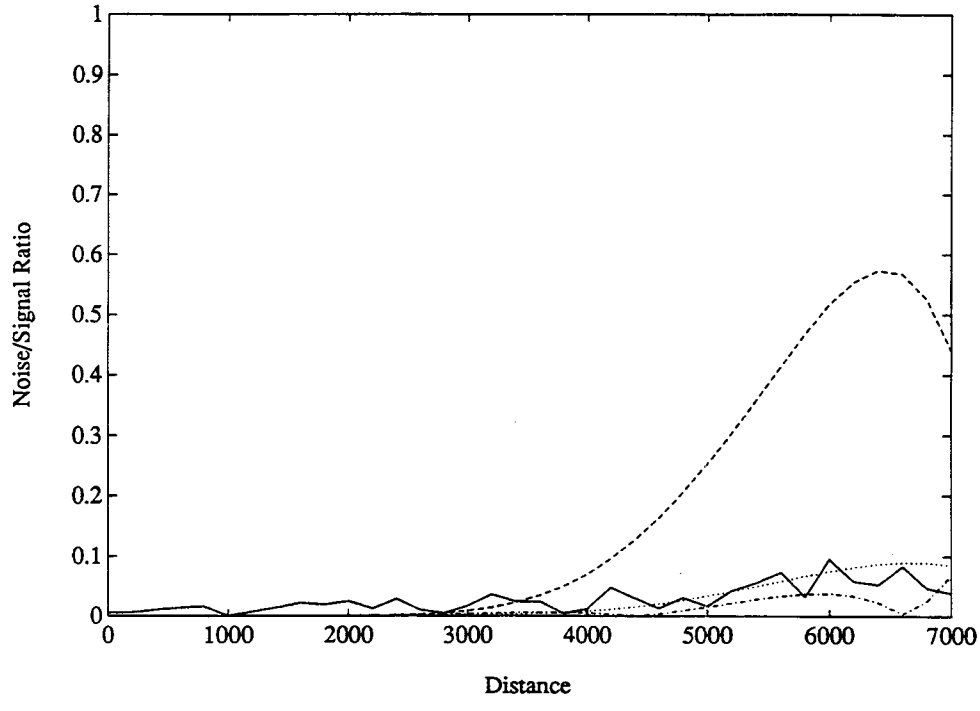

(b)

Figure 2-13. Noise-to-signal ratio versus distance for the advancing front problem. Solid line: particle; (a) dashed line: CFD; dotted line: UFD; dashed-dotted line: LW; and (b) dashed line: FR; dotted line: PPM; dashed-dotted line: FCT.

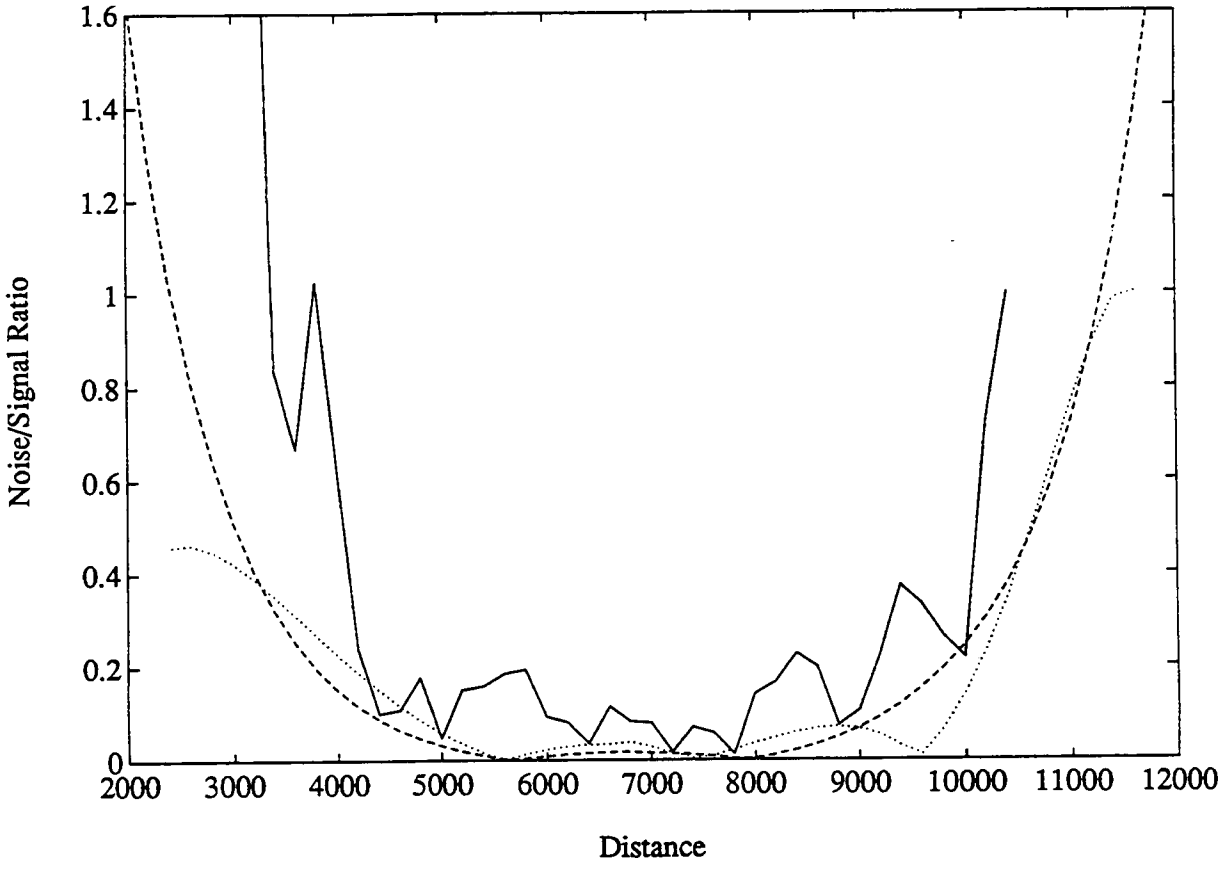

Figure 2-14. Noise-to-signal ratio versus distance for the rectangular wave propagation problem. Solid line: particle; dotted line: PPM; dashed-dotted line: FCT.

numerical modeling errors using classical methods are largest where concentrations are the lowest. This implies that in regions of low dimensionless concentration, near the MCL, large relative errors can be expected. Figure 2-14 shows that the same type of behavior occurs for receding fronts as well as advancing ones.

Panel (b) of Figure 2-13 and Figure 2-14 also show that particle and modern methods provide significantly better solutions near the MCL. As velocity becomes more dominant, the particle method is better than FCT or PPM, as would be expected for a Lagrangian scheme. Since particle methods are also found to be computationally efficient for 3D transport in heterogeneous formations, they are the method of choice in this work.

3 DESCRIPTION OF THE FLOW AND TRANSPORT PROBLEM

The SUFLAT methodology is applied to a hypothetical flow system analogous, in some respects, to the Yucca Mountain site. Flow and transport simulations are conducted for a horizontal, two-layered system with stochastically generated hydraulic properties, similar to the Topopah Spring welded (TSw) and Calico Hills nonwelded-vitric (CHnv) interface. It is recognized that this two-layered representation is far from the actual geostratigraphy of the site. However, it is very much relevant to the suite of pathways a water particle may encounter between a release point in the vicinity of the host rock (TSw) and the compliance boundary (CHnv), taken here to be the water table. Furthermore, our interest here is the development and demonstration of a working methodology which can be applied at a later point in time when more data are available as a result of comprehensive site characterization.

3.1 HYDROGEOLOGICAL PROPERTY DESCRIPTION

3.1.1 Characteristic Curves

In the stochastic approach, the heterogeneity of the porous medium may be represented by a single realization of a statistically homogeneous random conductivity field in 3D space. Because conductivity is necessarily non-negative, a log-normal probability distribution is assumed for K_s and, accordingly, a Gaussian log-conductivity, lnK_s, is generated. The mean of this random field is constant and its two-point covariance depends only on the separation vector; these statistical moments determine entirely the spatial structure of the conductivity field. In practice, the TBM can be used to generate single or multiple realizations of $lnK_s(x)$ with the desired statistical properties on the nodes of the numerical grid. For a detailed discussion of the 3D TBM random field generator, see Tompson et al. (1989).

In the more general case of transient unsaturated flow, the governing equation is nonlinear and depends on two constitutive relations, the moisture retention curve relating moisture content to pressure head $\theta(h)$ and the hydraulic conductivity curve relating conductivity to pressure head $K(h)$. For a heterogeneous medium, these are functions of both pressure and spatial location. In the following we present the assumed analytical forms of these functional relationships used for the unsaturated flow simulations presented in this report; other functional relationships are available in BIGFLOW as well. Spatial dependence is modeled by taking some or all of the parameters in these nonlinear relations to be spatially variable as desired.

The unsaturated conductivity-pressure relation is assumed to be a truncated exponential function involving at most three spatially variable parameters, that is

$$K(h,x) = K_s(x) \exp\left\{\alpha(x)\left[h - h_b(x)\right]\right\} \qquad \text{if } h \le h_b(x)$$

$$K(h,x) = K_s(x) \qquad \text{if } h \ge h_b(x) \tag{3-1}$$

The parameters are K_s [saturated conductivity (L/T)], h_b [bubbling pressure or air entry pressure head (L)], and α [scaling parameter, (L^{-1})]. Each or all of them can be taken spatially variable as desired in three spatial dimensions.

For a given length scale of interest, L, the product αL represents an advection/diffusion ratio. The inverse $\alpha^{-1}=\lambda_\theta$ is a moisture dispersivity length scale (Ababou, 1991). Alternatively, λ_θ can also be interpreted as a pore size distribution index (Yeh et al., 1985a,b,c) or an equivalent capillary fringe thickness (White and Sully, 1987). A survey of the literature indicates that the exponential conductivity model is in good agreement with measured conductivity curves in a variety of soils, at least within a moderate range of soil water pressures (Ababou 1981, Bresler 1978). In their stochastic solutions, Mantoglou and Gelhar (1987a,b,c) used the exponential model with random $K_s(x)$ and $\alpha(x)$, and zero bubbling pressure $(h_b=0)$.

For the soil moisture retention curve $\theta(h,x)$, BIGFLOW allows a choice between several functional forms, including the van Genuchten function (van Genuchten, 1980). These relations are also allowed to accommodate spatially variable parameters. For instance, the van Genuchten function is modified and generalized as follows to accommodate the case of spatially variable parameters

$$\theta(h,x) = \theta_r(x) + \frac{\theta_s(x) - \theta_r(x)}{\left\{1 + \left[-\beta(x)\,h\right]^{n(x)}\right\}^{1-\frac{1}{n(x)}}} \qquad \text{if } h \le 0 \tag{3-2}$$

$$\theta(h,x) = \theta_s(x) \qquad \text{if } h \ge 0$$

where n is a dimensionless shape factor (a real number, not an integer), β is an inverse pressure head scale factor (L^{-1}), θ_s is the saturated water content or effective porosity of the medium, and θ_r is the residual water content at very high or infinite negative pressure. Parameter θ_r is an empirical adjustment which is usually taken equal to zero unless a better fit to experimental data is obtained by using some nonzero value. Finally, note that Eqs. (3-1) and (3-2) are only meant to describe the nonlinear relationships that were used in the particular applications discussed in this report. The numerical model itself is by no means limited to these particular functional forms. In fact, more recent versions of BIGFLOW incorporate a more extensive set of multiparameter, spatially variable, nonlinear relations $K(h,x)$ and $\theta(h,x)$ in the form of additional modules.

3.1.2 Hydraulic Properties

A TSw/CHnv flow system, of size 250×250×500 m, is discretized in 18,081 computational cells each with a grid block size of $\Delta x=12.5$ m. It is recognized that the proposed HLW repository extends to an area much larger than the flow system studied in this work. Our work is based, among other reasons, on the testing of the premise that the flow will be predominantly vertically oriented. If this is indeed found to be the case, then compartmentalization of the repository area and independent 1D flow simulations may be sufficient for the study of the site. If, on the other hand, the results of the simulations presented in this work showed strong lateral or focused flow behavior, then a fully 3D representation and simulation of the site will be required in the future. An exponential covariance spatial correlation is assumed for all properties, and the correlation length is assumed isotropic in the horizontal directions ($\lambda_X=\lambda_Y=37.5$ m). A correlation scale anisotropy of 3 is taken to represent a mild stratification, consistent with the depositional nature of tuffaceous rocks (i.e., $\lambda_Z=12.5$ m). This is based on the findings of Russo and Bouton (1992), who studied soil cores and established statistical anisotropy in the covariance

functions of log-saturated conductivity and the parameters of the Gardner-Russo and van Genuchten models. The hydraulic properties used in this study, their distributions and cross-correlations (where established and found to be statistically significant) are presented in Table 3-1. Data for matrix tuffaceous materials were obtained from Peters et al. (1984) for samples taken from USW G-4 and USW GU-3 (Table A-2 of the report by Peters et al., 1984). The hydraulic properties for the fault zone were freely assumed and modified from the work of Rockhold et al. (1992).

The isotropic discretization interval of 12.5 m yields three nodes and one node per correlation scale in the horizontal and vertical directions, respectively. This discretization imposes a high-wave number cutoff in the corresponding spectrum employed to generate the 3D properties in the TBM code (Tompson et al., 1987a). Therefore, the actual stochastic description employed here does not have the rich high-wave number characteristic of an exponential covariance function. This is, in part, a remedy to the zero micro-scale assumption described in Section 2.1 [see Kapoor (1993) for a detailed discussion]. The large range of hydraulic-conductivity values encountered in this problem can be seen in Figures 3-1 and 3-2. These figures depict the sensitivity of $lnK(h)$ to various van Genuchten parameters, namely the n and β parameters for the TSw unit.

As is evident, the parameter β greatly affects the unsaturated hydraulic conductivity. In simulations a Gardner model is assumed for the unsaturated hydraulic conductivity versus suction relationship. Therefore, a linearization fitting process is implemented and the transformed (Figure 3-1 and 3-2) were analyzed further. A summary form of the range of unsaturated hydraulic conductivities, spanned in our simulations, is depicted in Figure 3-3 for both the fault zone and TSw and CHnv units. In this figure, the symbols "*" and "o" correspond to the hydraulic conductivity function for the mean K_S and α parameters for the TSw and CHnv layers, respectively. The upper dashed line corresponds to a K_S one standard deviation larger than its mean, and α one standard deviation smaller than its mean, for the TSw unit. The lower dashed line corresponds to a K_S one standard deviation smaller than its mean, and α one standard deviation larger than its mean, for the TSw unit. Similarly, the range of hydraulic conductivity for the CHnv layer is bounded by the solid lines. Finally, the characteristic curve for the fault zone is depicted by the "+" symbol. It is worthwhile noticing a number of crossing points in the mean curves, and their associated bounds, of the fault zone and the TSw and CHnv units. This, as will be seen later, affects greatly the flow behavior of the system in the case of faulting.

The hydraulic parameters used to describe the relation between unsaturated conductivity and pressure, such as saturated conductivity, K_S, and slope of relative conductivity curve (Gardner α) are, in general, significantly cross-correlated (Ababou, 1991; Ababou, 1993). Moderate coefficients of variation in the Gardner α-parameter produce highly heterogeneous moisture plumes (as theoretically predicted by Yeh et al. 1985b). Furthermore, GWTT estimates were found to exhibit a significant dependence on the Gardner α-parameter for the case of persistent discontinuities (Bagtzoglou et al., 1993). When the various hydraulic properties are uncorrelated, highly heterogeneous (perhaps even physically unrealistic) moisture patterns develop (Yeh, 1989). It is, therefore, extremely important that, when available or attainable, such property cross-correlations are taken into account for the generation of physically meaningful stochastic representations of hydraulic parameter fields. Wang and Narasimhan (1988) strongly advocated the use of such correlations, especially in the case of saturated hydraulic conductivity and partially saturated characteristic parameters. Other similar efforts include the work of Rautman and Robey (1993) who established cross-variable correlations between saturated conductivity, K_S, and porosity, and the work of Robey (1993) who established such cross-correlations between: (i) K_S, porosity, and the average pore size; and (ii) the Brooks-Corey constant and porosity. In these efforts

Table 3-1. Hydraulic properties used for modeling the faulted TSw/CHnv layered system and their correlations with K_S, when found to be statistically significant

Property	Distribution	Mean	Std. Deviation	Correlation
Topopah Spring (Welded)				
K_S (m/s)	Lognormal	−25.7000	1.3430	N/A
θ_S	Normal	0.0925	0.0185	0.7350
α (m^{-1})	Lognormal	−4.0300	0.5500	—
β (m^{-1})	Lognormal	−4.9300	0.0045	—
n	Normal	1.7664	0.2000	0.7100
θ_R	Normal	0.0067	0.0011	—
Calico Hills (Nonwelded-Vitric)				
K_S (m/s)	Lognormal	−15.5000	3.1526	N/A
θ_S	Normal	0.3950	0.0603	0.9690
α (m^{-1})	Lognormal	−2.5400	0.7500	—
β (m^{-1})	Lognormal	−3.8300	0.5041	—
n	Normal	4.2028	0.7807	—
θ_R	Normal	0.0316	0.0093	—
Fault Zone				
K_S (m/s)	Constant	−11.5000	N/A	N/A
θ_S	Constant	0.0750	N/A	N/A
α (m^{-1})	Constant	0.1000	N/A	N/A
β (m^{-1})	Constant	1.0000	N/A	N/A
n	Constant	5.0000	N/A	N/A
θ_R	Constant	0.0300	N/A	N/A

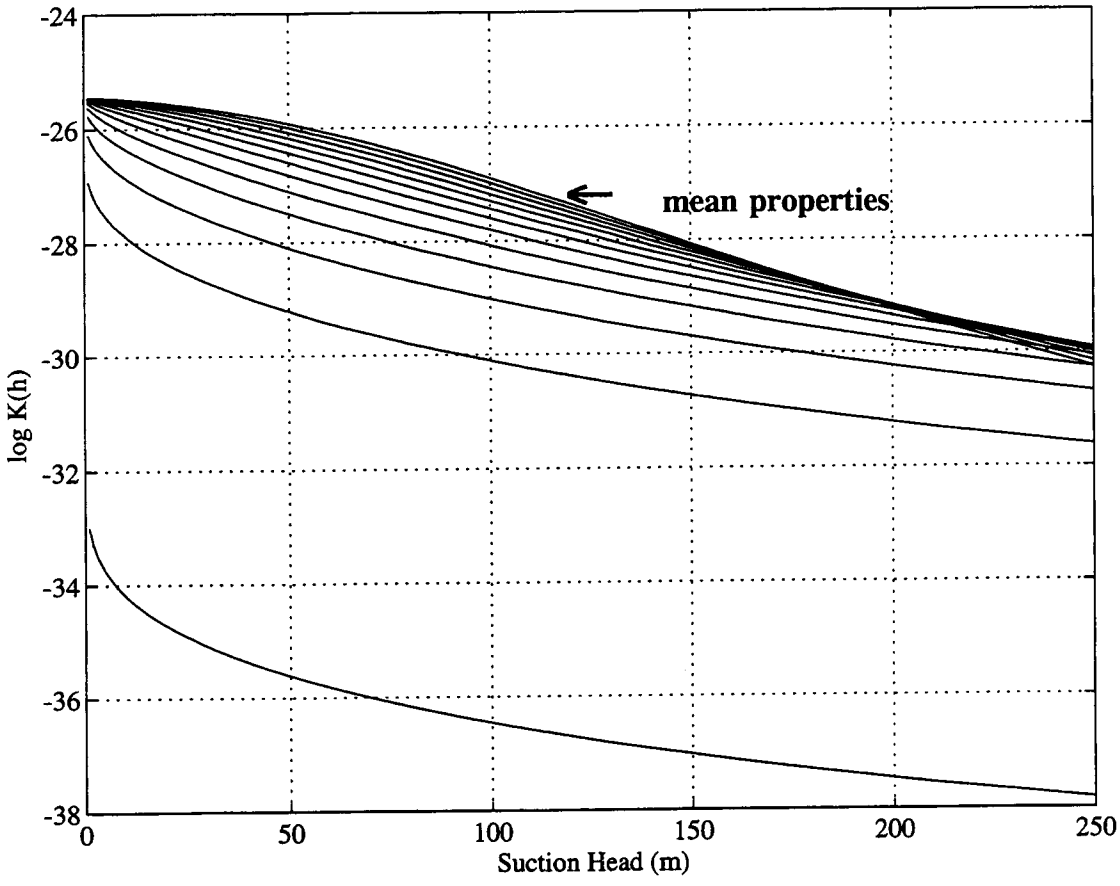

Figure 3-1. Sensitivity of unsaturated hydraulic conductivity on van Genuchten *n* for the TSw unit. Range of *n* is ± 3 standard deviations.

(Rautman and Robey, 1993; Robey, 1993), one-to-one singular behavior was avoided by adding a spatially uncorrelated Gaussian random noise component to the value computed by the cross-correlation relationships (Rautman and Robey, 1993).

In this work, spatially autocorrelated, and point-wise cross-correlated, hydraulic properties are generated by considering them to be linearly dependent on the saturated hydraulic conductivity. Reasons for doing so include: (i) the term lnK_S has been, by far, the primary variable of interest in all types of research efforts, deterministic/stochastic or saturated/unsaturated; (ii) spatial variability and covariance structure analyses of K_S have been routinely conducted over the years; and (iii) for ease of comparison, since employing lnK_S is consistent with previously reported, related work (Yeh et al., 1985a,b,c; Mantoglou and Gelhar, 1985, 1987a,b,c; and Yeh, 1989).

Thus, each hydraulic property is assumed linearly dependent on lnK_S and an independent autocorrelated random field, suitably weighted, is used to produce the desired correlation coefficient. The assumption of log-normality is made for properties such as the saturated hydraulic conductivity and the Gardner α-parameter, as indicated in Table 3-1. This assumption is supported by the measurements of White and Sully (1992). All of the input random fields are assumed to have the same spatial persistence structure.

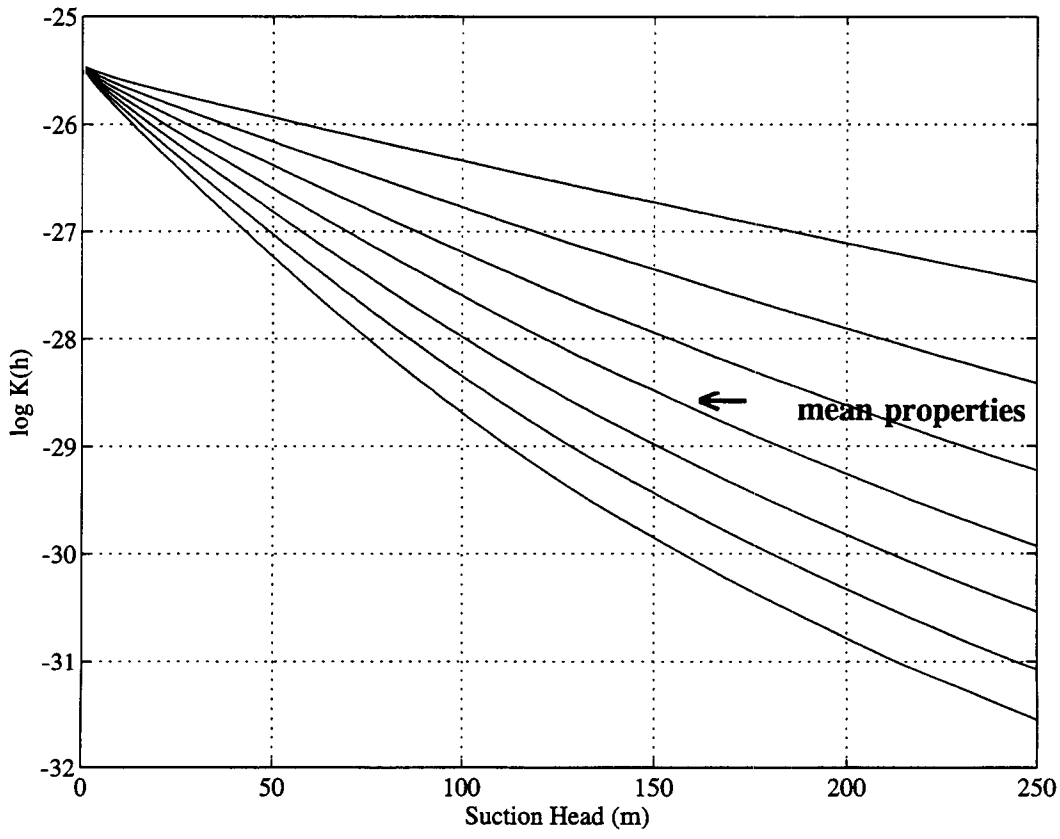

Figure 3-2. Sensitivity of unsaturated hydraulic conductivity on van Genuchten β for the TSw unit. Range of β is $\pm$ 1 standard deviation.

3.1.3 Generation of Cross-Correlated Random Fields

In this study, a method of direct generation of spatially correlated, cross-correlated hydraulic properties is employed, as advocated by Ababou (1993). Consider the random field parameters $F(x)$ and $A(x)$, assumed to be, for example, jointly Gaussian random fields. Assume, further, that they both correspond to lognormally distributed physical properties such as the saturated hydraulic conductivity and the Gardner α-parameter. Therefore, $F=ln(K_S)$ and $A=ln(\alpha)$. Decomposing each of the Gaussian random fields as:

$$F(x) = \langle F \rangle + \tilde{F}(x) \tag{3-3}$$

and

$$A(x) = \langle A \rangle + \tilde{A}(x) \tag{3-4}$$

where the symbols $\langle\ \rangle$ and $\sim$, associated with fields A and F, denote the ensemble mean and the zero-mean random field perturbations. These perturbations have standard deviations σ_A and σ_F, respectively. Assume that the perturbation in field A is a linear combination of two independent replicates

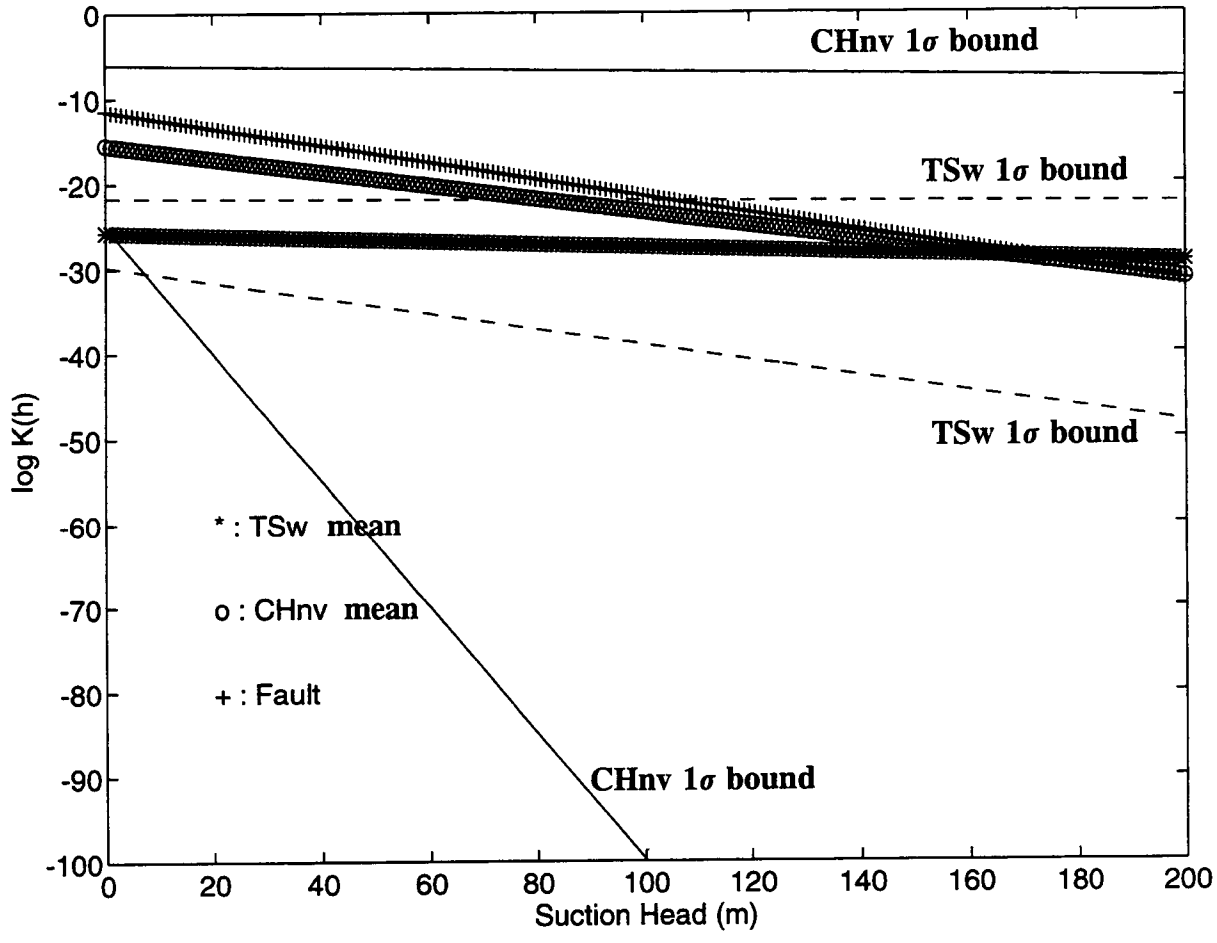

Figure 3-3. Range of unsaturated hydraulic conductivities for the fault zone and the TSw and CHnv units

of the perturbation in field F. Assume, further, that $G(x)$ is a normally distributed zero-mean, unit-variance random field, with the same structure as $F(x)$. Then, the perturbations in fields F and A can be constructed from two independent replicates of $G(x)$, namely $g_1(x)$ and $g_2(x)$ as:

$$\tilde{F}(x) = \sigma_F \; g_1(x) \tag{3-5}$$

and

$$\tilde{A}(x) = \sigma_A \; [\rho \, g_1(x) + \sqrt{1-\rho^2} \, g_2(x)] \tag{3-6}$$

where ρ is a measure of cross-correlation between A and F. By definition, the two random fields, A and F, are jointly Gaussian. They also honor a cross-covariance tensor which can be expressed as (Ababou, 1993):

$$R_{AF}(\xi) = \begin{bmatrix} R_{AA}(\xi) & R_{AF}(\xi) \\ R_{FA}(\xi) & R_{FF}(\xi) \end{bmatrix} = \begin{bmatrix} \dfrac{\sigma_A^2}{\sigma_F^2} & \dfrac{\rho \sigma_A}{\sigma_F} \\ \dfrac{\rho \sigma_A}{\sigma_F} & 1 \end{bmatrix} R_{FF}(\xi) \tag{3-7}$$

where ξ is the distance between two space locations. Note that both random fields are defined fully based on the spatial covariance of one of them, in this case $R_{FF}(\xi)$, the covariance of the saturated hydraulic conductivity field. Furthermore, the correlation coefficient ρ establishes a unique cross-correlation between the two random fields.

Figure 3-4 depicts a verification of this methodology, as implemented in the MKPROP module of SUFLAT. The cross-correlation relationships were developed using the Las Cruces Trench data (Wierenga et al., 1989) for saturated conductivity and van Genuchten β (also known as α in the literature). All 27,000 nodal values generated by MKPROP are plotted together with the 410 experimental data points. The statistical equivalence of the two data sets, as evidenced by the two indistinguishable best linear fits, serves as a verification of the MKPROP generator. The approach to generate cross-correlated property fields was applied to data of tuffaceous materials representative of Yucca Mountain, obtained from Peters et al. (1984), and cross-correlations between various properties were investigated. In this work the Gardner and van Genuchten models were assumed for the unsaturated hydraulic conductivity and moisture retention relationship, respectively. For example, there is an excellent correlation (ρ=0.969) between the saturated conductivity and porosity values for the CHnv unit. Similarly, a lack of any significant correlation between the shape parameters of the van Genuchten model and saturated hydraulic conductivity is evident for the same unit. This is consistent with observations made by Polmann (1990) for Maddock soil. The relationship established for the means of porosity and saturated hydraulic conductivity for the CHnv unit is:

$$\langle \theta_S \rangle = 0.9439 + 0.0308 \, ln \left(\langle K_S \rangle \right) \tag{3-8}$$

Rautman and Robey (1993) established a similar relationship based on data from drill holes N-54 and N-55, augmented by surface transect data and other sources. Their relationship between porosity and conductivity is:

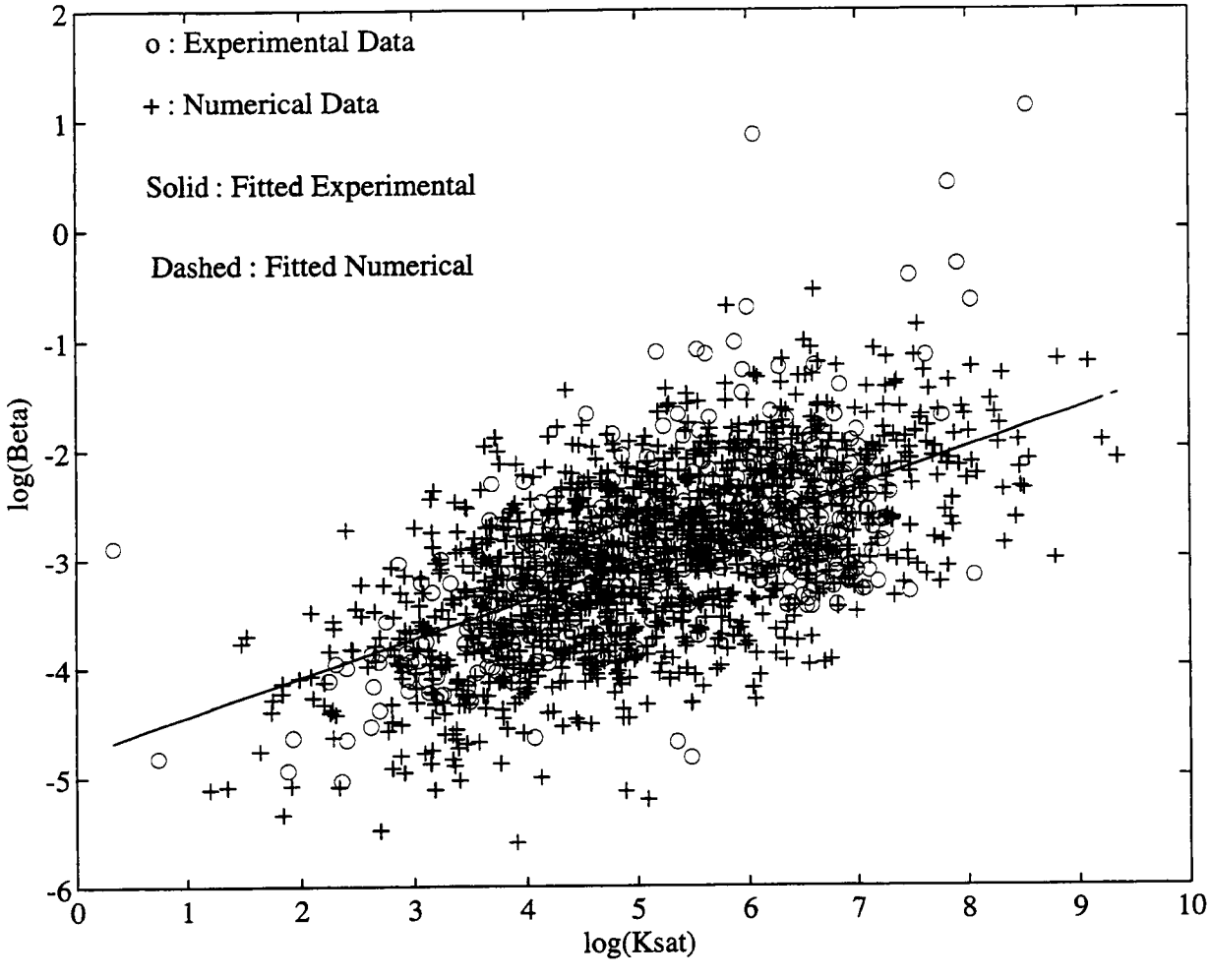

Figure 3-4. Verification of cross-correlation between K_S and van Genuchten β for Las Cruces trench data

$$\langle \theta_s \rangle = 1.0275 + 0.0385 \, ln \left(\langle K_s \rangle \right) \tag{3-9}$$

with a correlation coefficient of ρ=0.860. The similarity between Eqs. (3-8) and (3-9) is apparent.

Figure 3-5 presents a 3D perspective view of two vertical cross-sections in the logarithm of saturated hydraulic conductivity and porosity fields. The two layers are clearly defined and the greater variability in the CHnv unit is clearly perceptible due to a ratio in the values of σ_Y of 2.34. Also perceptible are the areas where high-hydraulic conductivity values coincide with high-porosity values. This is more frequently observed in the CHnv unit as a consequence of the larger correlation coefficient value (ρ=0.969 versus 0.735 for the TSw unit).

3.2 FLOW AND TRANSPORT SYSTEM DESCRIPTION

The unsaturated flow problem, represented by Richards equation, is solved with the BIGFLOW numerical code (Ababou and Gelhar, 1988; Ababou and Bagtzoglou, 1993). A detailed description can be found in Section 2.2 and in the work of Ababou and Bagtzoglou (1993); however, a brief discussion is included here for the sake of completeness. In BIGFLOW, an implicit, low-order, seven-point centered finite difference scheme is implemented and steady-state solutions are attained by time-stepping to sufficiently long times. In the simulations presented herein, the unsaturated conductivity-pressure relation $K(h,x)$ is assumed to be a truncated exponential function. For the soil moisture retention curve $\theta(h,x)$ a van Genuchten function is assumed. Both characteristic curves are allowed to include 3D spatially-variable parameters.

The thicknesses of the TSw and CHnv layers are 350 m and 150 m, respectively. The unsaturated flow problem is solved with the BIGFLOW numerical code, and steady-state solutions are attained by time-stepping to sufficiently long times, or until some mass balance criteria are satisfied. The SUFLAT methodology is implemented and multiple realizations of material properties and the corresponding flow problem solutions are obtained. The lateral boundaries of the system are no-flow, the bottom boundary is a water table condition, and the top boundary has a specified spatially uniform flux of 0.5 mm/yr. The computational domain spans 7 correlation lengths in the horizontal direction and 40 in the vertical. The choice of a water table boundary condition at the bottom of the domain has been questioned and subsequently investigated to determine whether it provides a free-drainage condition. This issue is of importance, especially under heterogeneous conditions, since a localized area of positive pressure immediately above the water table would result in a nonplausible, unrealistic blocking of water pathways.

In order to address this question, a detailed flow simulation was conducted with hydraulic properties characteristic of the TSw unit, which is substantially more prone to develop such a pressure buildup. An extremely fine resolution was implemented and 144,648 computational cells were used. A statistical analysis of the 1,681 (41×41) vertical transects revealed that this problem is very likely to occur in the TSw unit. Figure 3-6 depicts results from this analysis. In this figure the ensemble mean (of the 1,681 transects) and ± three standard deviation bounds of pressure head are shown as dashed-dotted and dashed lines, respectively. A typical realization (in this case the vertical transect in the middle of the domain) is also depicted as the solid line. Also depicted in this figure are the USGS borehole UZ-16 data within the TSw unit. These data were taken from the work of Wittmeyer et al. (1993) who determined the van Genuchten model parameters for each set of water retention data, based on a Levenberg-Marquardt nonlinear least squares procedure. Wittmeyer et al. (1993) mapped the van

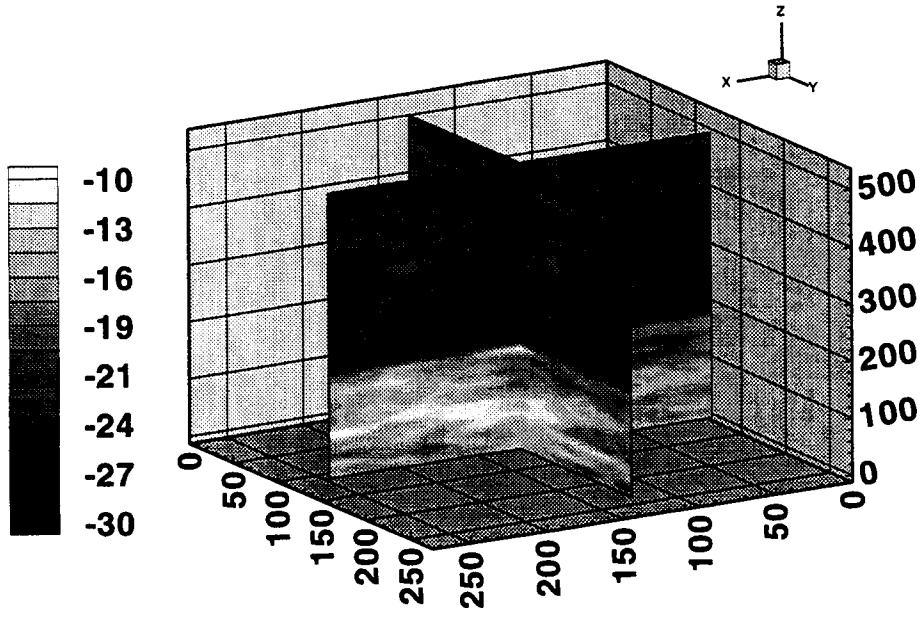

(a)

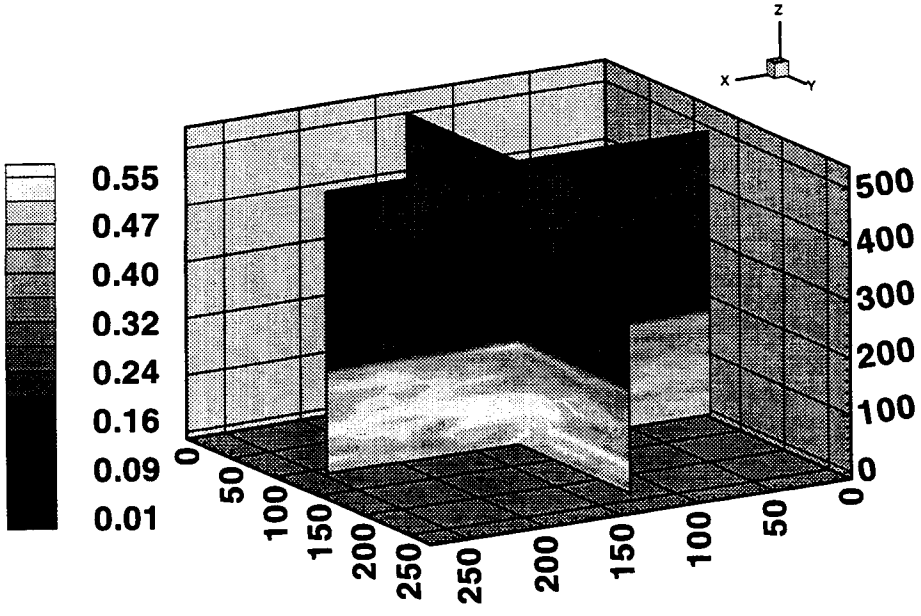

(b)

Figure 3-5. A 3D perspective view of representative hydraulic property fields for a single realization (#5), (a) Saturated hydraulic conductivity; (b) porosity.

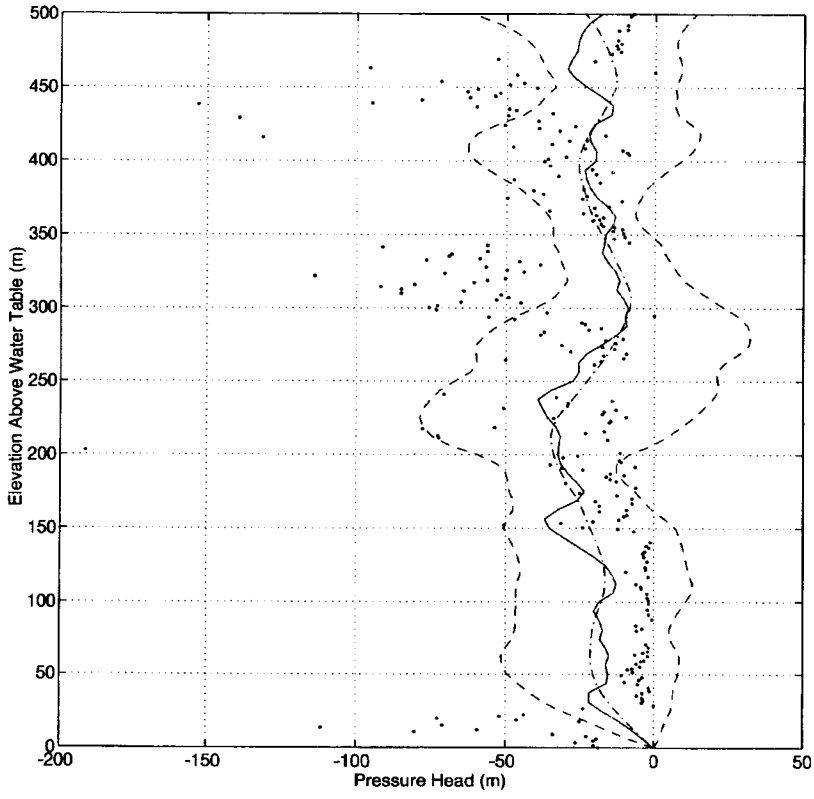

Figure 3-6. Variation of pressure head with elevation above the water table. Solid: vertical transect at X = 125 m, Y = 125 m; dashed dotted: ensemble mean; dashed: mean ± three standard deviations of pressure head; black dots: UZ-16 data for the TSw unit.

Genuchten model parameters to a 24-layer hydrostratigraphic description of UZ-16 by correlating lithologic descriptions and porosity values. UZ-16 saturation values as a function of depth were also provided by Mr. W. Ford of the NRC. From the saturation values, and based on the matrix hydraulic parameters for the 24-layer UZ-16 model of Wittmeyer et al. (1993) and Baca et al. (1994), pressure head values were calculated and plotted in Figure 3-6 as black dots. Note that in order to make the two data sets comparable, the UZ-16 data points have been scaled, so that instead of spanning a distance of 309.5 m they now span a distance of 500 m. There are several observations that can be made: (i) there is a good agreement between the vertical transect in the middle of the domain and the ensemble mean, providing confidence that the simulations presented herein satisfy the ergodic hypothesis; (ii) there is a substantial variability among the 1,681 vertical transects, as it is evident by the range of pressure heads spanned by the three standard deviation bounds; (iii) the results of the simulations presented in this work are in a fair qualitative agreement with the UZ-16 data, even though there exist data points which are very much out of the three standard deviation bounds; (iv) for the majority of the ensemble of vertical transects, the pressure head profile is very close to hydrostatic up to an elevation of 30 to 50 m above the water table.

This last observation deserves some further discussion, the pertinent question being "what is the probability of positive pressure heads developing at any given point within the layer?" Assuming that: (i) a total of 1,681 vertical transects is a good statistical sample; and (ii) pressure head variations follow

a normal distribution, then it is expected that within the three standard deviation bounds 99.87 percent of variability is captured. With this premise, the probability of occurrence of a positive pressure head at any arbitrary point along a vertical transect within the TSw unit can be estimated by the ratio of the area corresponding to positive pressure heads over the area bounded by the three standard deviation bounds. Using the data presented in Figure 3-6, this ratio is calculated to be 16.8 percent. As this represents an extreme upper bound on the amount of positive pressure head occurrences that might be expected in the CHnv unit, it is concluded that the water table boundary condition does not significantly contradict the desired free-drainage property.

Transport of conservative species is simulated by particle tracking with the numerical code SLIM (Tompson et al., 1987b). A large number of particles (10,000) is released instantaneously from a single cell located at the layer of cells adjacent to the top boundary and approximately at the center of the domain. Particle projection functions are used to obtain particle densities from particle cloud spatial configurations (Bagtzoglou et al., 1992a). Steady-state flow results are used for particle transport for three values of dispersivity; 0 for the purely advective case, and 0.1 m, and 1.0 m for the advective-dispersive cases. Within the context of this work, local dispersion is viewed as the manifestation of subcontinuum (grid block) variability, as it could be due to the presence of fractures in the rock. These values are in qualitative agreement with the dispersivity value of 0.44 m calculated from the results presented by Smith and Schwartz (1993) for flow and transport in saturated, discrete fracture networks. They are also bounded by the asymptotic longitudinal dispersivity value of 2.2 m deduced by Neuman et al. (1985) from the field results at the Oracle site. It should be noted that in the simulations presented in this work, transport is always advection dominated, insofar as the horizontal correlation scale-based Peclet number is 37.5, 375, and ∞ for dispersivity of 1.0 m, 0.1 m, and 0, respectively.

4 FLOW SIMULATION RESULTS

4.1 FLOW RESULTS FOR A TWO-LAYERED SYSTEM

Under the flow conditions described in Chapter 3 the steady-state pressure head solution is attained after approximately 1.5 M yr when the initial condition is assumed to be hydrostatic. The suction field obtained from the numerical simulations shows significant spatial variation. The impact of such suction variation on the overall flux of moisture and solute transport is discussed in great detail by Gelhar (1993), with a summary of analytical results and an overview of different approaches for analyzing unsaturated flow and transport. In our multiple SUFLAT flow simulations, the suction head solution from one realization is used as a wise initial guess for all subsequent simulations, yielding very rapid steady-state convergence. Harter and Yeh (1993) have addressed this issue by employing approximate spectral solutions as initial conditions to obtain fast convergence. The stochastic property fields are generated in such a manner that the flow domain spans at least 7 to 14 correlation lengths in the horizontal and vertical directions, respectively. Therefore, it is anticipated that all inherent variability in the fields is reflected in the solution of the flow problem and, consequently, subsequent flow simulations are closer, in an average sense, to their steady-state solution. To put this in perspective, one should note that a representative simulation is attained after 6 k yr. Figure 4-1 depicts a global mass balance-based steady-state convergence indicator as a function of time. It can be seen than for this particular realization a mass balance error of less than 2 percent is achieved in 6 k yr.

The steady-state pressure head solution for a representative simulation is shown in Figure 4-2. Several observations can be made: (i) the CHnv layer is predominantly under hydrostatic pressure conditions, at least for the first 100 m above the water table level; (ii) a zone of very high suction is formed at, or in the vicinity of, the interface, supporting the hypothesis of a capillary barrier existence; and (iii) a wedge-like zone of almost zero suction is formed above the interface. This zone extends up to a maximum of 30 m and is characterized by very high saturations, in the range of 95 to 98 percent.

These observations are very consistent with the results presented by Wittwer et al. (1993) who conducted 2D numerical simulations using the TOUGH2 code. These researchers identified a low capillary pressure zone (−22 bars) above the top layers of Calico Hills. They claim that "[*t*]his low capillary pressure zone is probably due to decreased vertical flow due to increased lateral flow in the upper layers of the Topopah Spring unit." The results presented in Figure 4-2 demonstrate the existence of a similar region; however, a low capillary pressure zone of only −16 bars was observed, possibly due to the 3D nature of the simulations discussed herein. Agreement exists also in the high liquid saturations estimated to occur in the Topopah Spring unit, which according to Wittwer et al. (1993) range between 0.78–0.93. These results are corroborated also by the work of Wittmeyer et al. (1993), who studied the water content profiles for borehole USW UZ-16. Figure 4-3 depicts the measured saturation values. It should be noted that the UZ-16 data are scaled in terms of depth in order to be comparable with the results of the simulations presented here. From Figure 4-2b it is estimated that a zone of approximately 50 m in thickness is at saturations greater than 97 percent, in fair agreement with the 100 m-thick zone of saturations greater than 93 percent of Figure 4-3.

The concept of extensive lateral unsaturated flow has not been investigated thoroughly to date (Lehman, 1992). However, there has been some recent progress made on theoretical, laboratory, and field studies of capillary barriers within the context of the soil physics literature. Zaslavsky and Sinai (1981), Ross (1990), and Kung (1990a,b) have studied various aspects of development and characteristics of

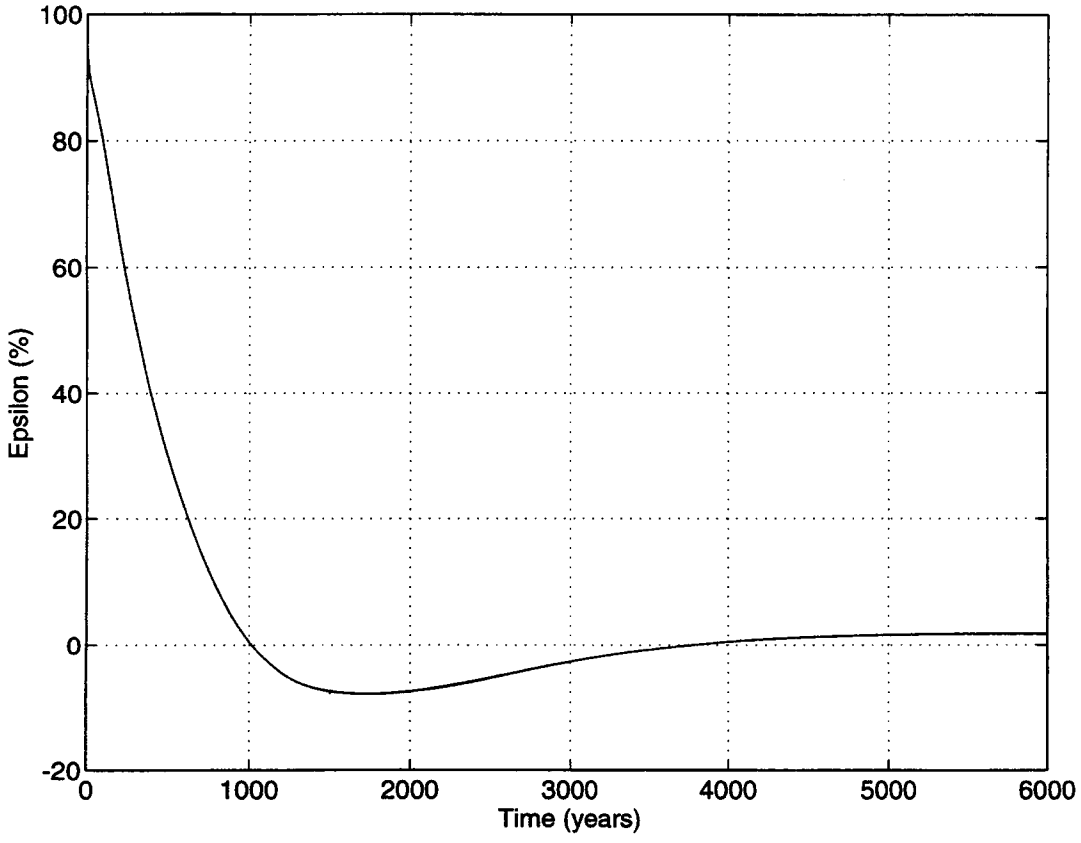

Figure 4-1. Global mass balance indicator as a function of time

capillary barriers. Oldenburg and Pruess (1993) conducted numerical modeling exercises, with careful consideration of space discretization and grid orientation effects, on the issue of capillary barriers. They performed an analysis of an idealized system, assuming the soils to have hydraulic conductivities which follow an exponential function and homogeneous properties on a per-layer basis. They based their analysis on a dimensionless index, equal to the ratio of the sorptive numbers of the fine over the coarse grained layers, and presented flow results demonstrating the capillary diversion and subsequent leakage through the barrier. The sorptive number (α) used by Oldenburg and Pruess (1993) is identical to the Gardner-α parameter used in the analyses presented herein. Therefore, the sorptive number ratio index is given by α/α^*, where α and α^* correspond to the fine and coarse grained layer properties, respectively. As this index decreased from 0.05 to 0.025, Oldenburg and Pruess found out that the flow break of the capillary barrier became more apparent and preferential.

The results of the work presented herein are in agreement with the analysis by Oldenburg and Pruess (1993). Figure 4-4 depicts the scalar magnitude of the water velocity. Notable is the overall contrast between the two distinct layers, with the lower layer acting as a capillary barrier (natural logarithm of velocity, in m/sec, is in the range of -45 to -39) as predicted by some U.S. Department of Energy researchers (Loeven, 1993). The formation of capillary barriers when coarse "homogeneous" porous media are overlain by fine "homogeneous" porous media is well known, and so is the existence

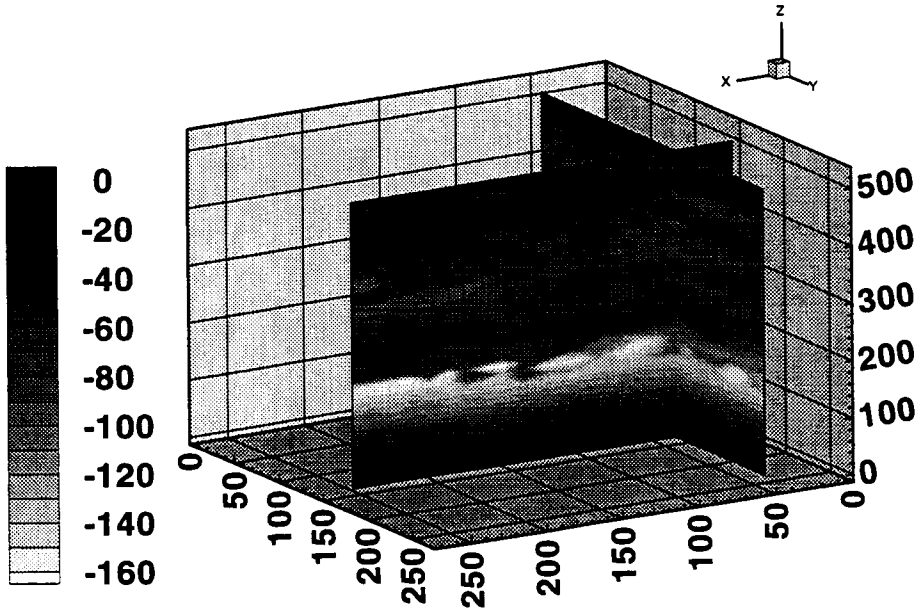

(a)

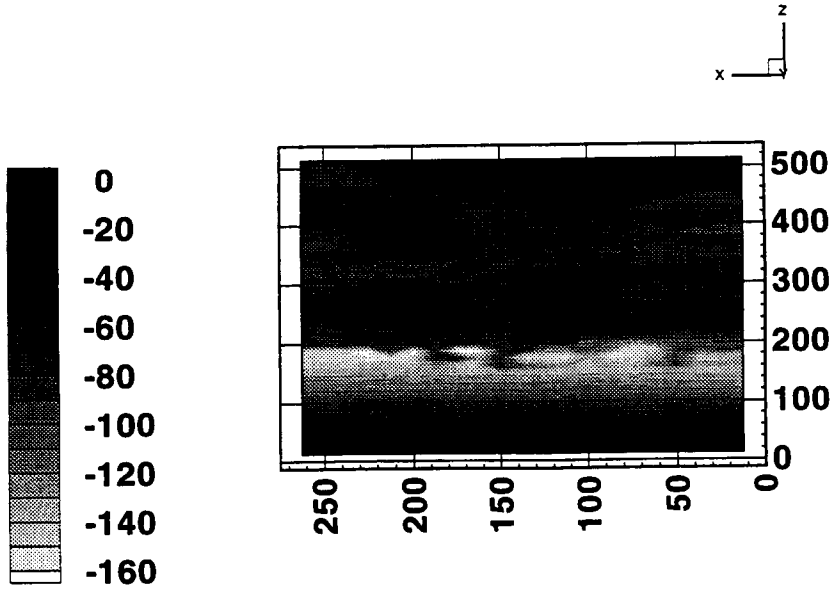

(b)

Figure 4-2. Steady-state pressure head results for the hydraulic property fields of Figure 3-5, (a) 3D perspective view, (b) 2D cross-sectional view at Y=125 m

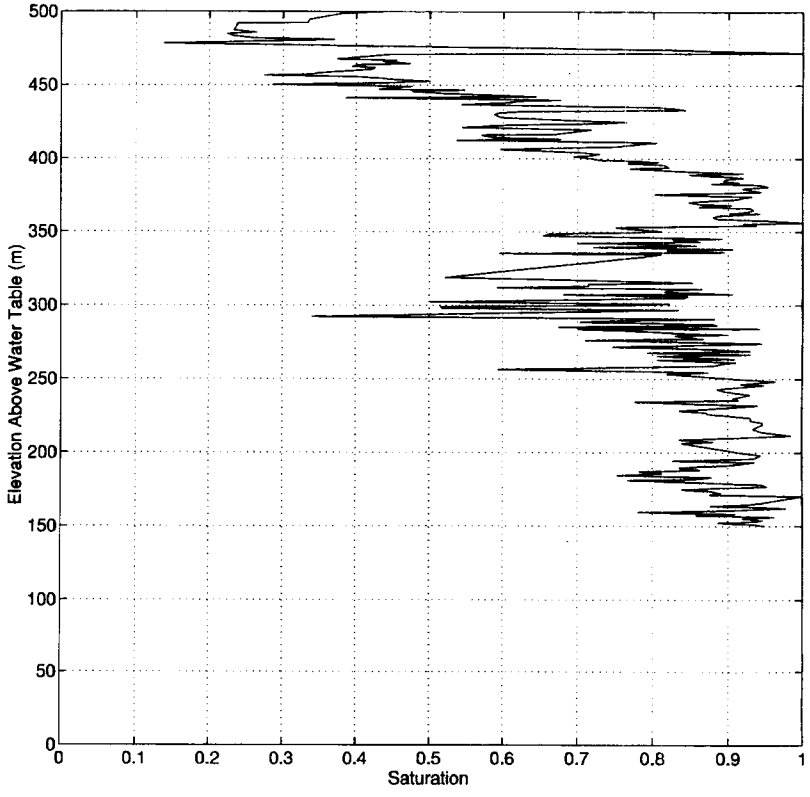

Figure 4-3. Measured saturation profile for UZ-16 (derived from Wittmeyer et al., 1993)

of the phenomenon of capillary barrier breaching by rapidly moving fingers of water (Baker and Hillel, 1990; and references therein). The work presented here demonstrates this phenomenon under the influence of high degrees of porous media heterogeneity. Whether such a capillary barrier can unequivocally maintain its integrity, thus diverting the flow laterally at infinite lengths, is a very important question. This is of particularly great interest for heterogeneous media. Smith and Schwartz (1981) presented a discussion on the subject of capillary barriers whereby the within-layer heterogeneities may, when large compared to the layer contrast, reduce the effect of the layering induced capillary barriers.

This is also consistent with the findings of Tchelepi et al. (1993) who studied numerically and experimentally the development of viscous fingering. One of their most important conclusions is that heterogeneities cannot be necessarily associated with the development of unstable displacements. As Neuman (1994) points out, stability depends greatly on: (i) the pressure gradient developing immediately above the wetting front; and (ii) the heterogeneity of the two media, as expressed by the variance σ^2 and correlation scale λ. Based on theoretical and numerical (Monte Carlo) analyses, it is concluded that in the case of unstable conditions (based on pressure gradients alone) a mild heterogeneity has a "pronounced stabilizing effect," whereas a "strong heterogeneity has a destabilizing effect." A low degree of heterogeneity may be enough to "dissipate the energy" trying to pass through the layer

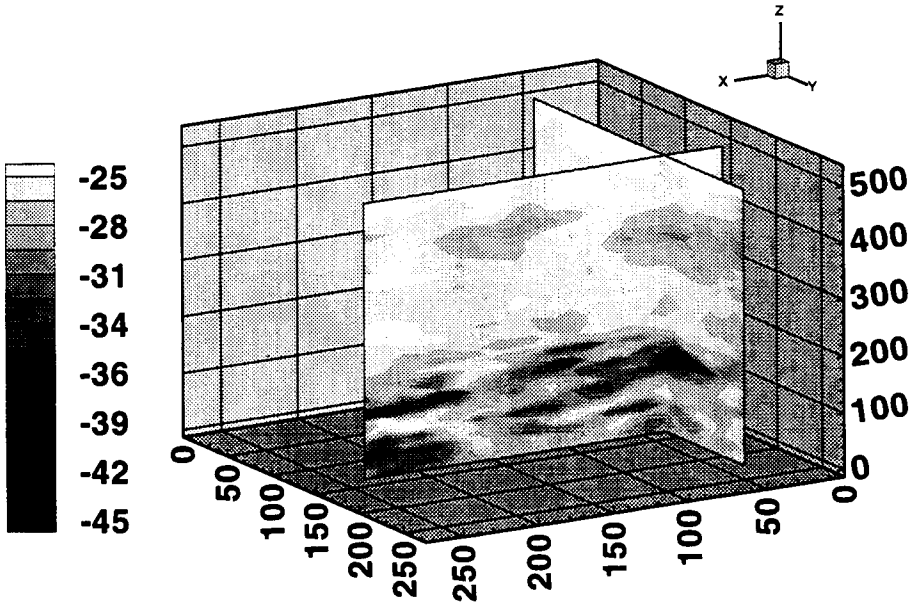

Figure 4-4. Steady-state magnitude of flow velocity, in *ln* (m/sec), for typical realization (#5)

interface. A higher degree of within-layer heterogeneity can very well act as the instigating mechanism for preferential flow pathways to develop, thus contributing to instabilities. This perception is in close agreement with Neuman's preliminary findings. Therefore, the breaching of a capillary barrier under the presence of substantial within-layer heterogeneity is an issue which cannot be settled without explicitly incorporating heterogeneity into the analysis. In this particular case, for example, the results demonstrate that this breaching does exist. In Figure 4-4 one can see that high-velocity zones bypass the barrier in some regions (velocity magnitude is approximately four orders of magnitude greater than those of the surroundings). The locations of these regions are hypothesized to be determined by the nature of the heterogeneity of the porous medium and are related to the range of suction-based crossing points in the unsaturated conductivity curves (shown in Figure 3-3). Note that there exists a substantial range in the suction head (greater than 80 m) over which the TSw layer property outliers are more conductive than the CHnv layer average properties.

Moreover, the sorptive number ratio index is bounded by 2×10^{-6} and 0.5 with an average value of 0.224 for the simulations presented in this work. Therefore, these results are again in agreement with Oldenburg and Pruess (1993) since there exists a plethora of potential barrier breaching points where the sorptive number ratio index is near the 0.025 value which, in their calculations, was related to strongly breaking flows. Finally, a more detailed representation of Figure 4-4 can be viewed in Figure 4-5, where velocity vectors are depicted together with streamlines at a vertical plane of $X=50$ m. The very strong,

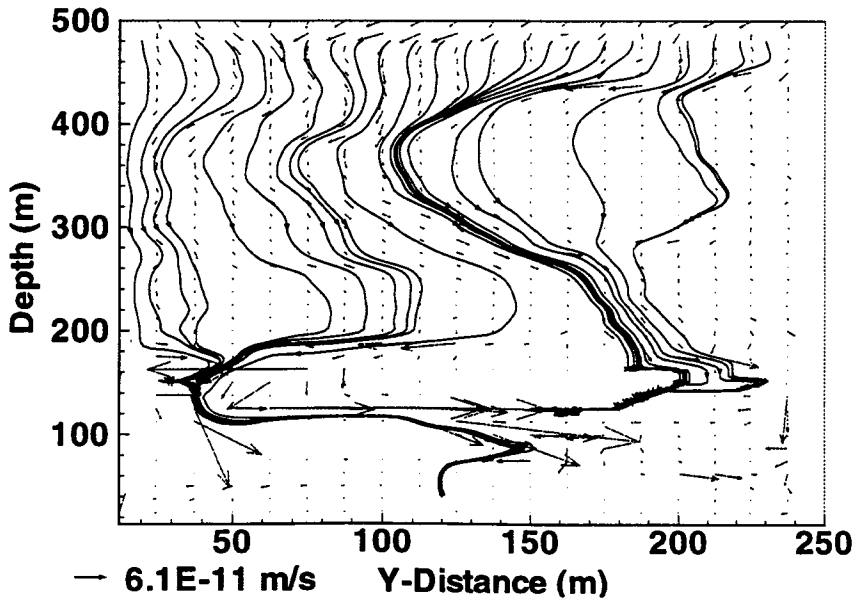

Figure 4-5. Velocity field and streamlines for a *Y-Z* plane at $X=50$ m

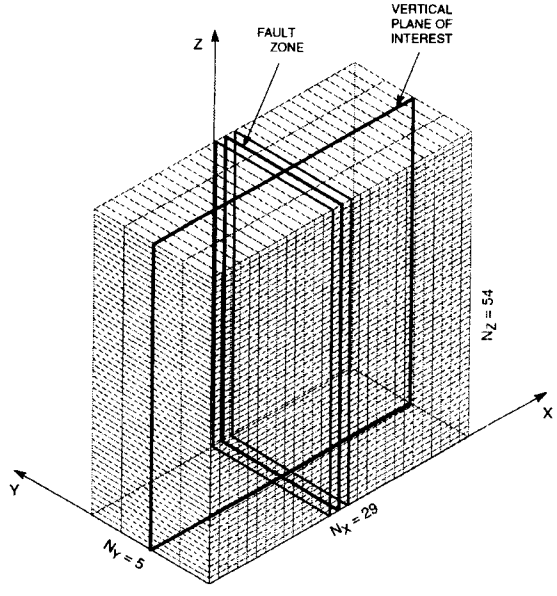

Figure 4-6. Computational grid used in the study by Bagtzoglou et al. (1993)

lateral flow velocities (order of 10 to 20 mm/yr) and very localized breaching area are characteristic of extensive lateral flow along the layer interface. Our results are a direct answer to the philosophical questions asked by Pruess and Tsang (1994) as to whether existing performance assessment models are unable to represent highly localized effects, including channelized flow along preferential paths.

4.2 FLOW RESULTS IN THE PRESENCE OF FAULTING

The exact mechanism through which fault zones convey water is unclear. It is hypothesized that because fault zones are filled with highly fractured rocks they may act as preferential pathways for groundwater. It has also been hypothesized that in some cases, when natural mineral cement is present, they may inhibit water flow. Monastersky (1994) quotes R.W. Spengler, a United States Geological Survey (USGS) scientist, as to a potential explanation of the hydraulic role of fault zones: "[t]he basic question that remains unanswered is whether or not any of the faults are barriers to the transport of fluids and gases or whether they are conduits."

The significantly different behavior of the flow system in the presence of a persistent discontinuity such as a fault zone was studied for a homogeneous layer case by Bagtzoglou et al. (1993). In the work of Bagtzoglou et al. (1993), five layers of approximately equal thicknesses spanned a total depth of 530 m, down to an assumed water table. The computational domain used in these simulations had dimensions of 1,230 m, 80 m, and 530 m in the X-,Y- and Z-directions, respectively. The domain was discretized into 7,830 nodes as shown in Figure 4-6. Also depicted in this figure is the location of the fault zone arbitrarily modeled as a three-cell wide, YZ planar zone in the middle of the domain. Figure 4-7 shows the velocity vectors and particle plots for two cases of contrast in the slope of the unsaturated conductivity curve. When the fault conductivity slope is comparatively much larger than that of the matrix $(\alpha_m=0.022\ m^{-1},\ \alpha_f=0.100\ m^{-1})$, higher fluxes are observed in the matrix resulting in a moisture front which lags within the fault zone. When the contrast is milder ($\alpha_m=0.022\ m^{-1}$, $\alpha_f=0.035\ m^{-1}$), the opposite behavior is observed. The fluxes within the fault zone are greater, but they point towards the matrix. This creates a frontal shape that continuously expands outwards from the fault zone.

As an illustration of the effects of faulting, one realization of the material property fields is modified to incorporate a highly conductive zone of $\Delta x \times 5\Delta y$ in areal extent, penetrating the full depth of the domain. The hydraulic properties of the fault zone were described in Chapter 3. Figure 4-8 depicts the steady-state pressure head solution, corresponding to Figure 4-2b, resulting from the superimposition of a homogeneous fault zone on the realization depicted in Figure 3-5. The dramatic change in the flow system behavior from Figure 4-3 to Figure 4-8 is apparent. Even though the fault zone extends only one computational cell in the X-direction, its effect is felt over almost 100 m. Also, the fault reduces the saturations along the layer interface. Bodvarsson et al. (1994) predicted similar behavior in their modeling efforts, dealing with homogeneous layers. It is also very interesting to notice the variation of pressure head along the fault between dry and wet conditions. This change occurs at approximate depths of 100, 170, and 290 m below the top of the domain (or at elevation of 400, 330, and 210 m above the water table). This complex behavior occurs because the fault conductivity and the mean curves of the two layers are nearly identical in the range of 60 to 160 m suction, while the layer property fields have excursions above and below the fault's properties.

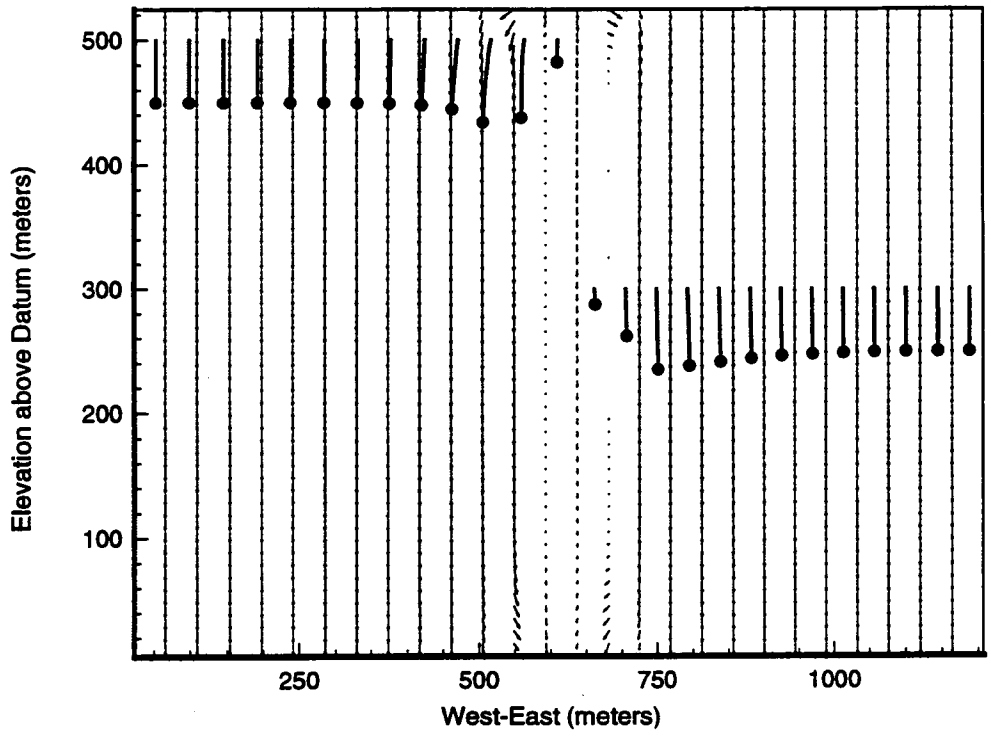

(a)

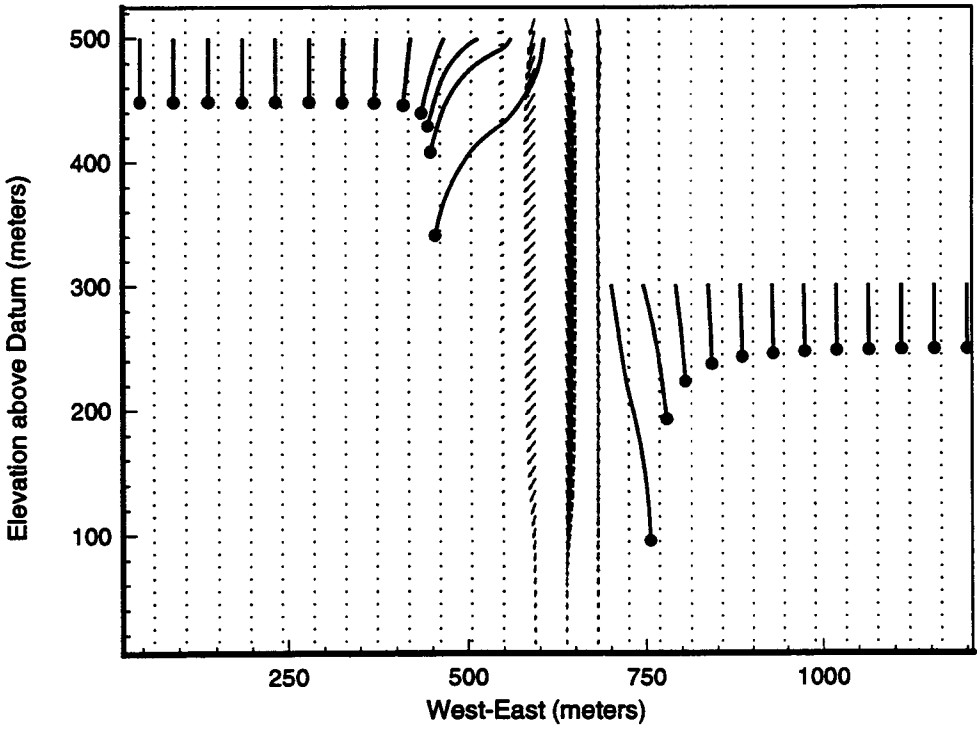

(b)

Figure 4-7. *X-Z* **plane velocity field and particle plot, (a)** α_f**=0.100 m**$^{-1}$ **(b)** α_f**=0.035 m**$^{-1}$ **(from Bagtzoglou et al., 1993)**

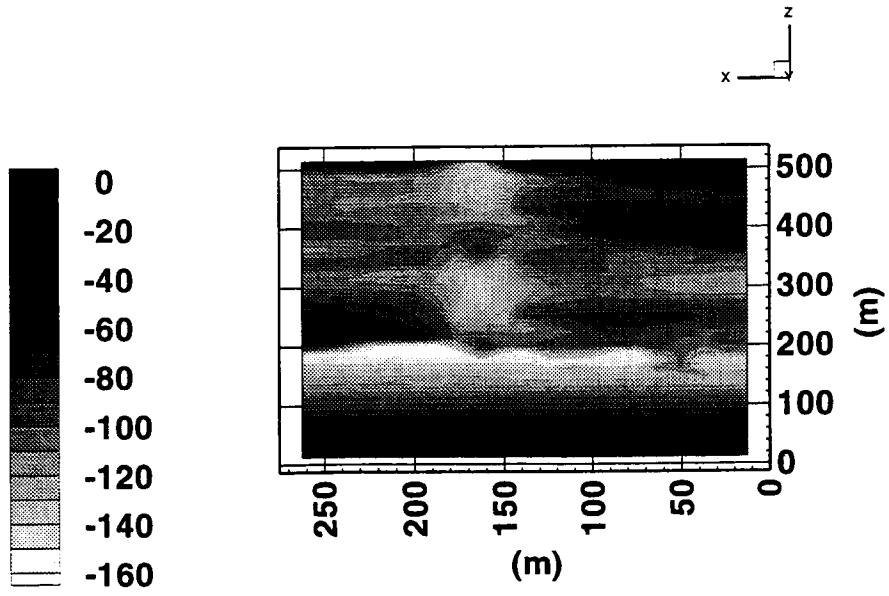

Figure 4-8. Steady-state pressure head results for a layered system in the presence of faulting

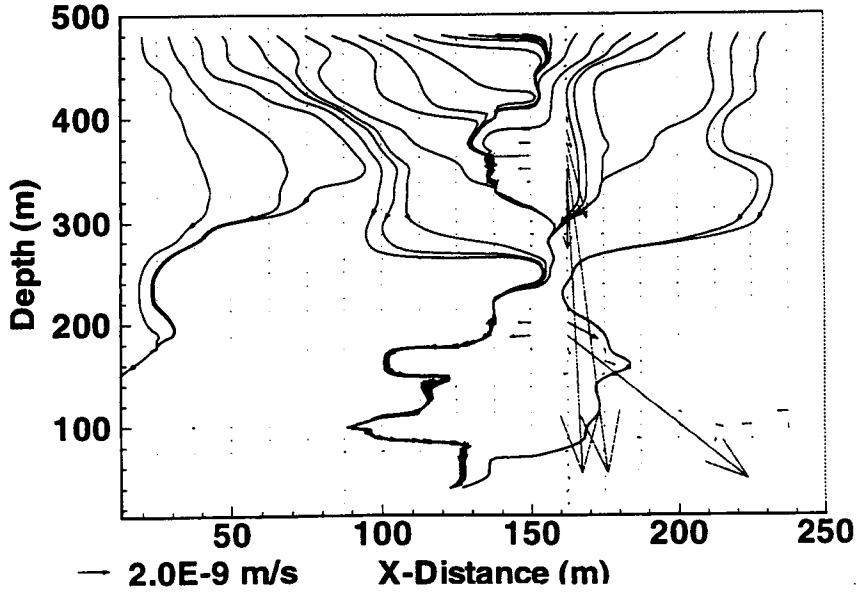

Figure 4-9. Velocity field and streamlines for a *X-Z* plane at $Y=150$ m for a layered system in the presence of faulting

Similar observations are made for the velocity fields and streamlines. Figure 4-9 presents velocity vectors and streamlines along a vertical plane at Y=150 m. Even though the capillary barrier is still functioning, the flow is now pretty much concentrated through the fault zone (velocity of 670 mm/yr), with some recirculatory flow patterns being perceptible in the vicinity of the crossing-point regions. These results are in disagreement with Tsang et al. (1993) who concluded that a "large saturated permeability of the Ghost Dance fault will play little role in channeling water into the fault or in enhancing the flow of water down the fault." The results presented herein, however, are in good agreement with Wittwer et al. (1993) who reported a very low-liquid saturation (3 percent) in the fault zones as one very dominant feature of their simulations. The analyses presented here predict a maximum saturation of 5 percent within the fault zone. Bodvarsson et al. (1994) estimate similar levels of saturation in the immediate vicinity of the Ghost Dance fault zone; however, for uniform areal infiltration of 0.1 mm/yr they calculated the normalized vertical moisture fluxes (given as a percentage of the infiltration at the ground surface) to be less than 290 percent. The apparent disagreement between the results presented herein and the work of Bodvarsson et al. (1994) can be attributed to the fact that the work of Bodvarsson et al. does not incorporate within-layer heterogeneity, and deals with an infiltration signal five times less than the one used in the present study.

5 TRANSPORT SIMULATION RESULTS

In this chapter, the detailed evaluation of advection-dispersion of solute in unsaturated heterogeneous porous media is simulated to understand transport processes in the far-field of a two-layer system. Velocity fields, used in the analyses, are obtained as described in Chapter 4. Conservative transport is simulated by particle tracking with the numerical code SLIM. Ten thousand particles are released in independent locations within a single cell, which is located in the layer of cells adjacent to the top boundary, and approximately at the center of the domain for each of the 20 simulations conducted. This could be envisioned to represent a potential repository location. Therefore, a total of 200,000 independent particle flights contribute to the statistics. The mean and variance of the concentrations of solute undergoing advection-dispersion in the flow fields are calculated. Moreover, particle breakthrough curves at the bottom boundary, considered here as the compliance boundary water table, provide an elegant way of presenting GWTT estimates. For example, the first particle to cross this boundary corresponds to the GWTT. Other measures, such as the 50th percentile of particles crossing the boundary can be used as well. Also, uncertainty in GWTT estimates can be readily calculated by performing statistical analyses over the realization ensemble space. It is recognized that an ensemble of 20 different realizations is a small statistical sample. However, our flow analyses involve quite a substantial amount of variability ($7\times7\times40$ correlation lengths), and the transport analyses involve a very large number of particles (10,000) which, since they are released randomly over a prescribed finite volume, sample numerous pathlines for every realization.

The SUFLAT methodology has been applied in the past for saturated systems (Bagtzoglou and Baca, 1994). Figure 5-1 depicts the cumulative distribution function for travel time for 200,000 particle flights in a saturated medium. As discussed in Section 2.3, SUFLAT not only provides estimates of GWTT but also measures of the uncertainty associated with these estimates. There exists a one-to-one relationship between solute concentrations and particle density functions. Therefore, the use of either terminology is a matter of semantics. What is important to keep in mind is that $\langle c(x,t)\rangle$, the expected value of the particle density for a series of random hydraulic property field realizations, can be calculated readily. A particle released at t=0 from within the release region has some probability ending up in any specific point within a specific volume of interest. To account for the particle ending up at any possible point within the same volume, one has to calculate the integral:

$$P(X \in V) = \int_V f_X(X, t=T)\,dV \tag{5-1}$$

where, in the general case, V stands for the volume of interest.

As there may be considerable variation in the concentration field from realization to realization, the important issue of quantifying this variability is raised. Kapoor (1993), Kapoor and Gelhar (1994a), and Harter (1994) have defined a useful measure of inter-realization variability, the concentration coefficient of variation (CV):

$$CV = \frac{\sigma_c}{\langle c \rangle} \tag{5-2}$$

where σ_c and $\langle c \rangle$ are the standard deviation and expected value of concentration at a particular point in space.

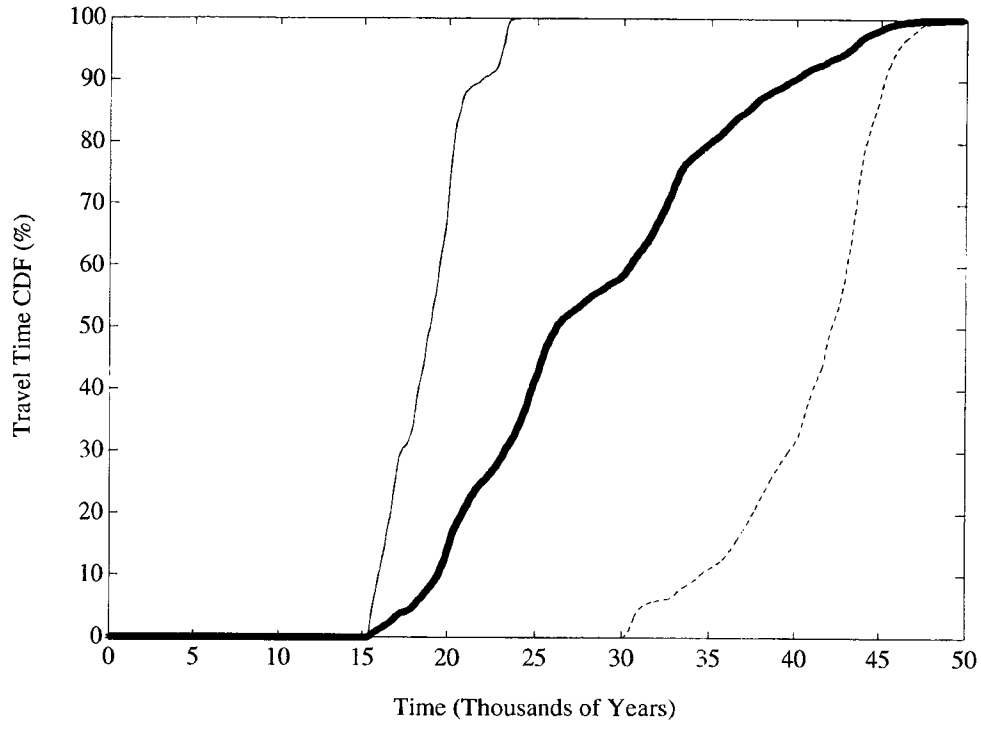

Figure 5-1. Cumulative distribution function for particle arrival time for σ_Y=0.90, and 200,000 particle flights (from Bagtzoglou and Baca, 1994). Thick solid line: ensemble mean; solid line: earliest particle arrival; dashed line: latest particle arrival.

5.1 ADVECTIVE TRANSPORT

Results from representative, purely advective transport simulations are depicted in Figures 5-2, 5-3, and 5-4 for the particle density mean, standard deviation, and CV, respectively. These figures show snapshots of the aforementioned variables at time T=100 and 300 k yr. There is a substantial amount of information one can deduce from these plots. For example, at T =300 k yr one can estimate the most probable location of the water particles to be at a depth 300 m below the top of the domain. However, as is evident by some relatively high values in the mean particle density near the bottom of the domain, there exist realizations that are very close in breaking through the water table. Finally, Figure 5-4 provides a measure of uncertainty in these predictions. Note for example, the most-probable ending location for a particle is associated with a low (CV=1.0 to 1.5) coefficient of variation, indicating a reliable prediction. This is in direct contrast to the high value (CV ≥ 3.0) associated with the perceptible mean near the bottom of the domain. Note also the rapid increase in the values of the coefficient of variation near the exterior boundary of the particle cloud. This result is very similar to the increase in noise far from the mean values for the noise-to-signal ratio discussed in Section 2.3.5.2. Figure 5-5 presents results from breakthrough analyses at the bottom boundary. The number of particles exiting the domain through this boundary is expressed as a percentage of the total number of particles released, and plotted as a function of time. Only five of the twenty realizations have particles that break through the bottom boundary within the prescribed time, thus providing a tremendous variability in the estimates of first arrivals, as calculated from this graph.

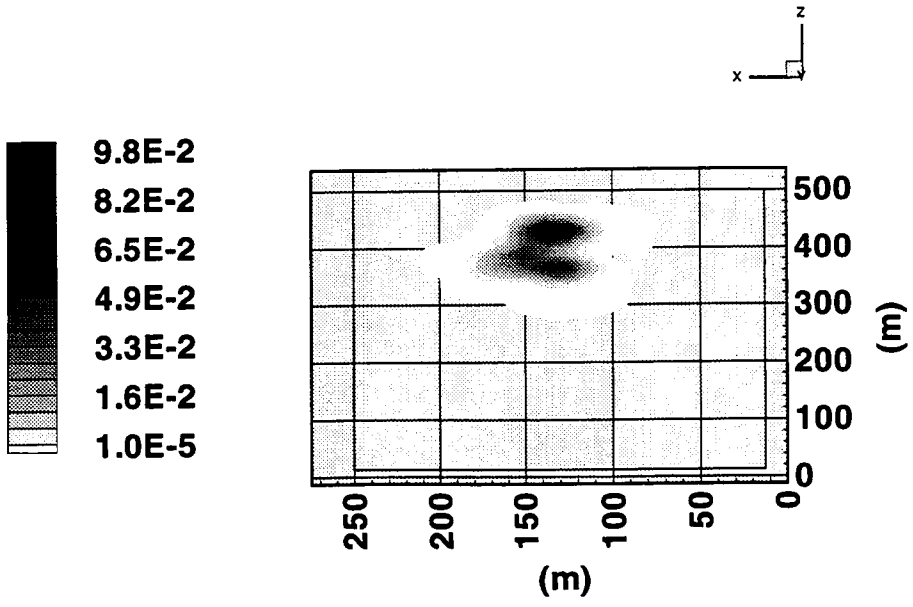

(a)

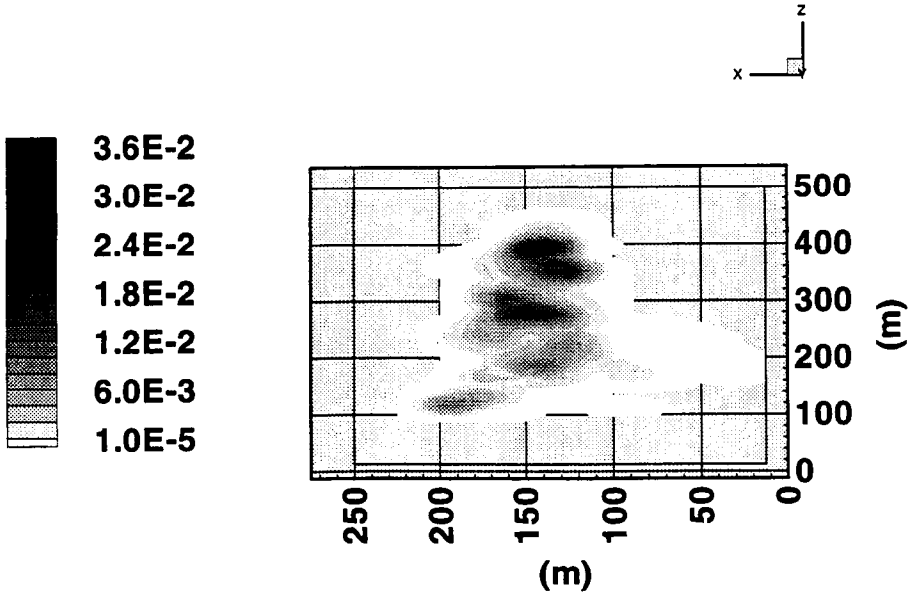

(b)

Figure 5-2. Mean particle density for advective transport at: (a) T=100 k yr, (b) T=300 k yr

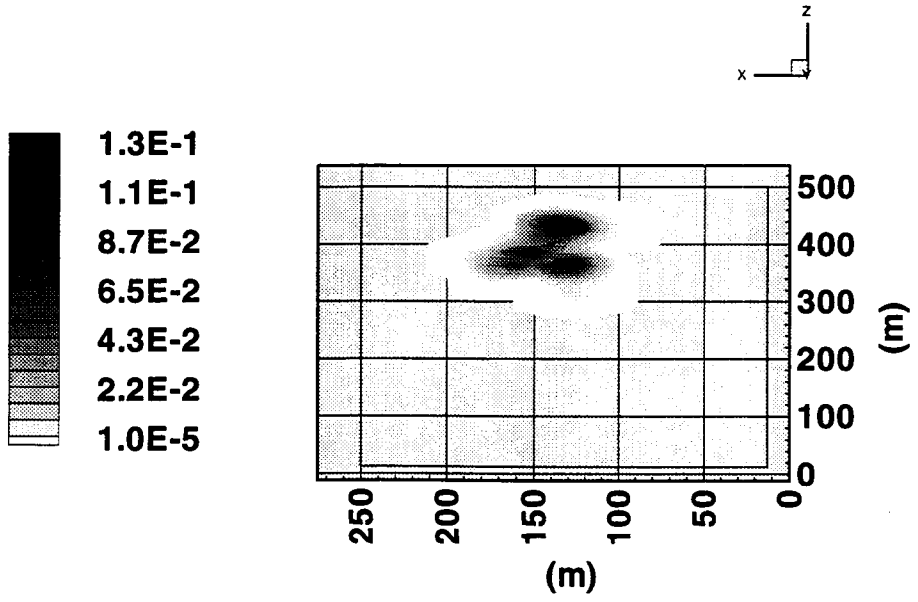

(a)

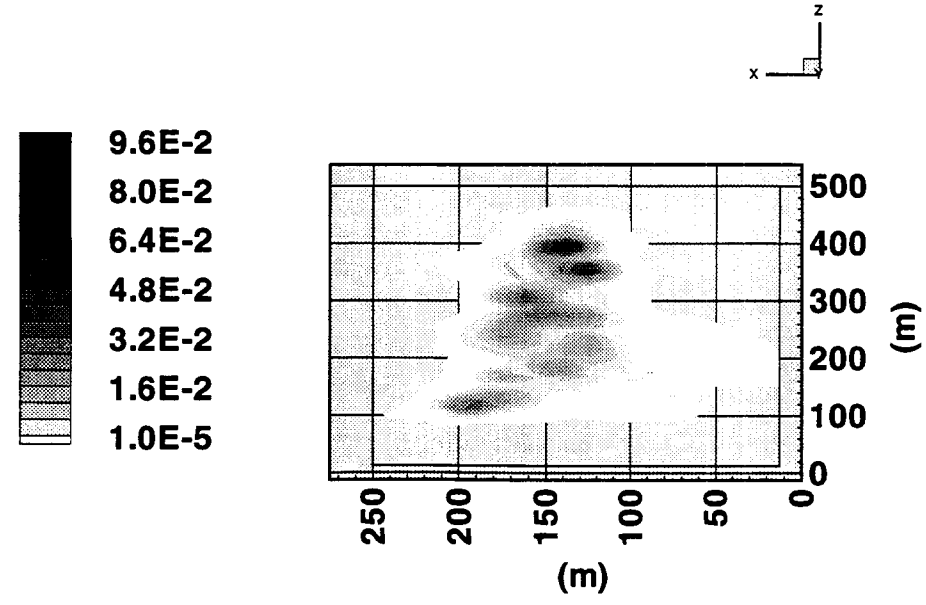

(b)

Figure 5-3. Standard deviation of particle density for advective transport at: (a) T=100 k yr, (b) T=300 k yr

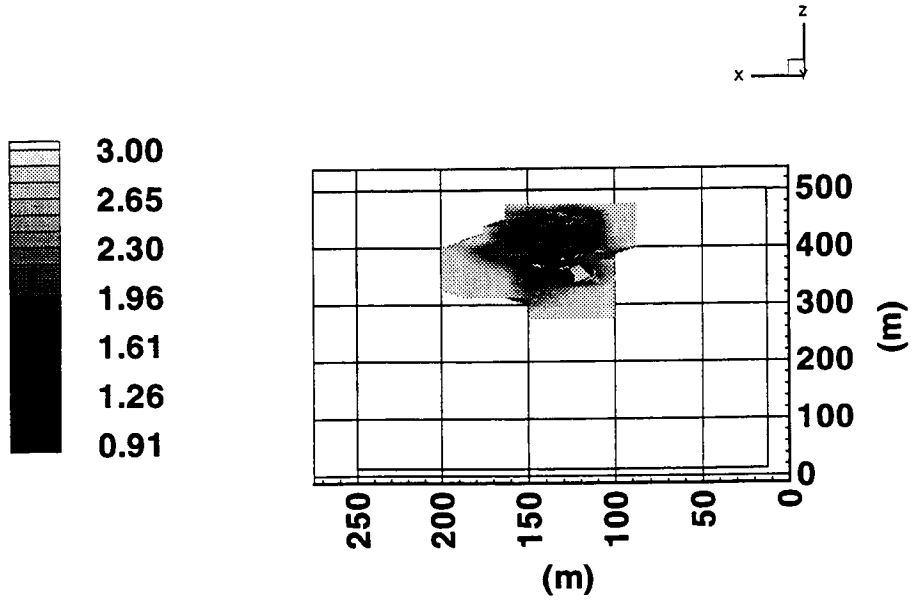

(a)

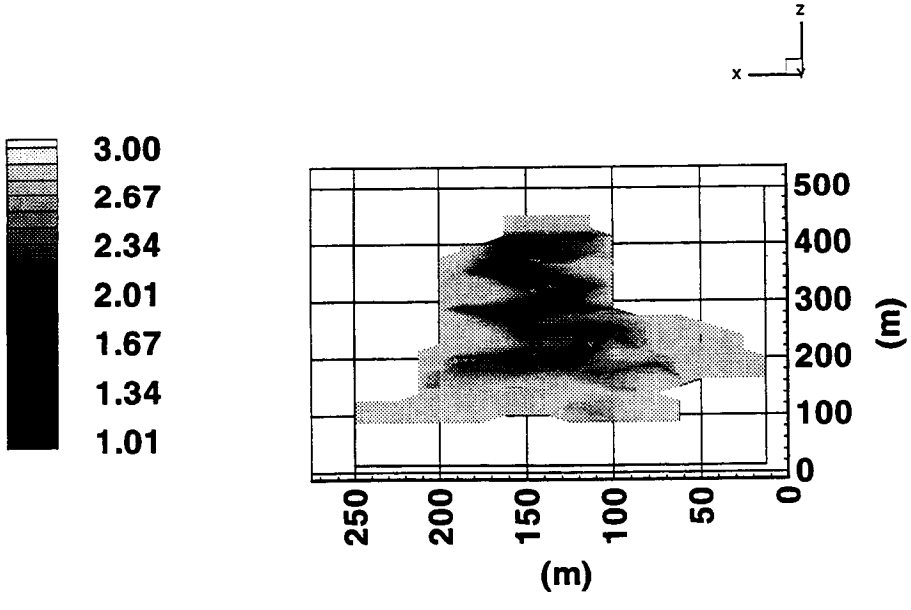

(b)

Figure 5-4. Coefficient of variation of particle density for advective transport at: (a) T=100 k yr, (b) T=300 k yr

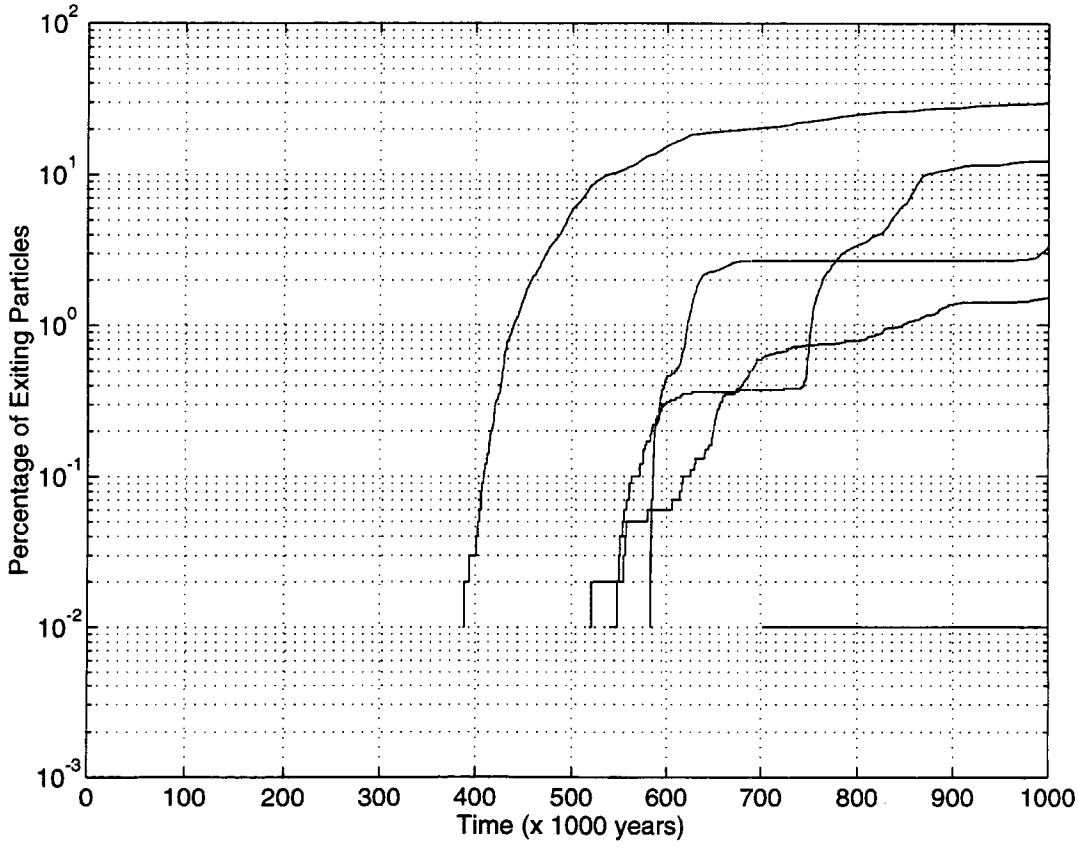

Figure 5-5. Cumulative distribution function of exiting particles at the bottom boundary for advective transport. Only five out of twenty realizations break through the bottom boundary.

5.2 ADVECTIVE-DISPERSIVE TRANSPORT

The simulations presented in this section are identical to those in Section 5.1, except that dispersive transport is implemented using the random walk process discussed in Section 2.3.3. Two values of isotropic dispersivity are used, namely 1.0 and 0.1 m. It is worthwhile observing the coefficient of variation results for these two levels of dispersion. Figures 5-6a and 5-6b depict the CV of concentration at $T = 100$ k yr for dispersivity values of 0.1 and 1.0 m, respectively.

Comparing Figures 5-6a,b and 5-4a, one can easily conclude that as the local dispersion is increased, the level of certitude in our transport simulations improves. This is attributed to: (i) the volumetric extent of the low CV region (e.g., $\mathbf{CV} \leq 1.0$), and (ii) the range of CV in the domain of interest. For example, the minimum CV is 0.91, 0.87, and 0.49 for dispersivity of 0.0, 0.1, and 1.0 m, respectively. One could challenge the validity of this assertion by posing the question: "How can a random process, and its associated lack of information at a certain scale, render the transport simulations more reliable?" The key in answering this question is to first perceive *reliability* as *repeatability*. This is, at least under a Monte Carlo framework, relevant since the higher the frequency of an occurrence, the more reliable is the prediction of this occurrence. Physically, *reliability* is very much related to the results presented in Chapter 2 regarding the numerical stability of the covariance matrix systems.

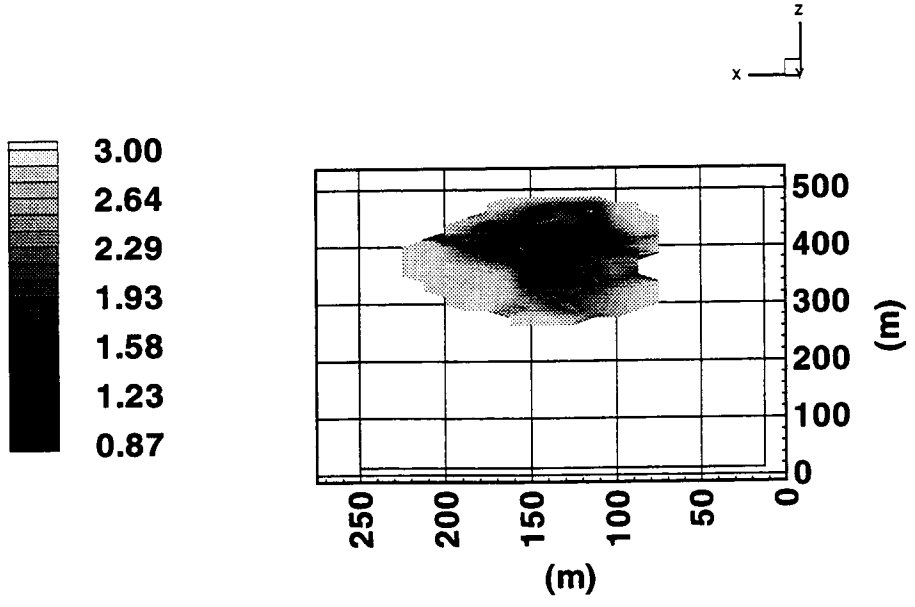

(a)

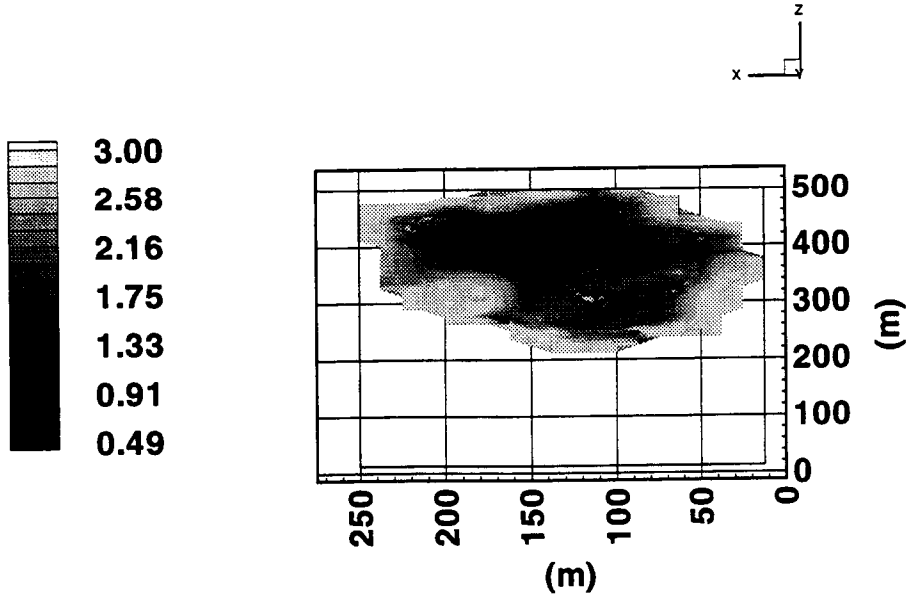

(b)

Figure 5-6. Coefficient of variation of concentration for advective-dispersive transport at T=100 k yr for: (a) dispersivity of 0.1 m; (b) dispersivity of 1.0 m

Microvariability serves as an extra mechanism which "shepherds" solute through a greater variety of pathways, thus sampling (on the average) more streamlines. Advective transport, on the other hand, is much more preferential. From one realization of the ensemble space to the next, solute particles travel through drastically different channels. Figure 5-7 presents results of the breakthrough analysis for the case of dispersivity equal to 1.0 m. Only 10 out of the total of 20 connecting realizations are depicted in Figure 5-7 for reasons of clarity. There is a much narrower envelope in the GWTT distribution (the realizations with fastest and slowest first-particle arrivals are included in the ten realizations shown in Figure 5-7) when compared to the purely advective transport case. To put this in perspective, note that (even excluding the 15 realizations which did not break through), in the case of advective transport, a mean GWTT of 546 k yr and a standard deviation in GWTT of 115 k yr are calculated. This is in contrast to the GWTT mean and standard deviation of 310 and 85 k yr for the dispersive case. The accelerated behavior of the GWTT (310 versus 546 k yr or 43 percent faster) for the dispersive case is viewed as logical, since some degree of fracturing is expected to yield faster travel times.

In order to demonstrate the pronounced variability in the flow behavior of the system, some results that deal with independent realizations are presented. One can visualize the actual tortuous pathways followed by the solute as it travels downward while, at the same time, undergoing advection and dispersion. These simulations correspond to the case of modest dispersivity (0.1 m). Figure 5-8 depicts a series of concentration snapshots at time T=50, 75, 100, 150, 200, and 250 k yr for the fifth realization. The elevation above the water table of the centroid of the plume is also calculated and presented. Several observations can be made. First, at early times (100 k yr) the particle cloud is impeded by a zone of relatively small flow velocities (with a contrast of one order of magnitude) near the top of the domain (see Figure 4-4). After some time, the solute plume finds its way around this obstacle and continues its downward travel. Second, at some time before 200 k yr, the interface between the two stratigraphic units is reached and a clear lateral movement is observed. This is consistent with the flow velocity results presented in Chapter 4. Third, at time equal to 250 k yr, the plume continues to spread laterally across the interface, consistent with observations by Yeh et al. (1994) who studied the wicking effect in liner systems. However, finger-like plume patterns have developed and passed through the interface. These patterns clearly serve to dispel the concept of an unequivocal and infinitely extensive capillary barrier.

The variability from one realization to the next is demonstrated through Figures 5-9 and 5-10. In Figure 5-9 the pressure head field at a vertical cross-section is depicted for the first realization. It is worthwhile noticing (while comparing to Figure 4-2b) that there exists no zone of saturation immediately above what appears to be a persistent zone of high suction at, or near, the layer interface. Figure 5-10 presents a series of concentration snapshots at time T=50, 75, 100, 150, 200, and 250 k yr for the first realization. When compared to Figure 5-8 one can quickly comprehend the tremendous variability sampled in these simulations. One could also possibly speculate on the role of the close-to-saturation zone above the interface and its effect on the overall transport phenomena occurring in the system. One should note that the concentration plume travels downward at a much slower pace in realization 1 (close-to-saturation zone does not exist) than in realization 5 (close-to-saturation zone exists).

A simple statistical analysis of the breakthrough curves for the case of modest dispersivity (0.1 m) resulted in a mean GWTT of 333 k yr and an associated standard deviation of 77 k yr. Additional information on the behavior of the two cases is found in Figure 5-11. Shown in this figure is the number of particles which have exited the domain through the bottom boundary as a function of time for the first and fifth realization. After some initial time adjustments, the rate of particles exiting per unit time (i.e.,

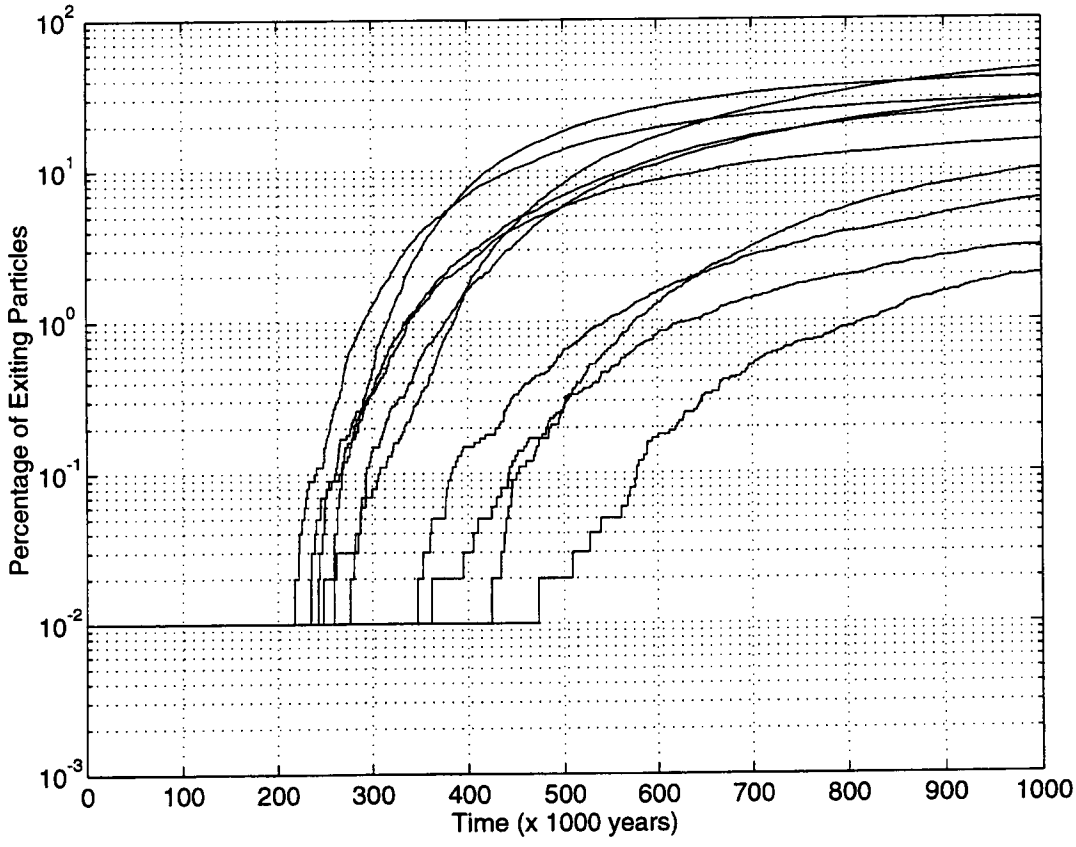

Figure 5-7. Cumulative distribution function of exiting particles at the bottom boundary for advective-dispersive (dispersivity of 1.0 m) transport. All twenty realizations break through the boundary; however, only ten are depicted for reasons of clarity.

the slope of the curve) becomes constant. It is clear from this figure not only that realization five produces the fastest arrival, but also provides a flux of particles exiting the domain approximately 2.4 times greater than that of realization one (3.33 versus 1.39 particles per k yr).

Breakthrough curves provide a measure of the behavior of the entire system over time. More detail on the spatial variability of the ensemble of realizations is found by considering the concentration coefficient of variation. Figure 5-12 depicts the spatial distribution of the concentration CV at time T = 250 k yr. The areas of the plot that are marked by light shades of gray-to-white correspond to a relatively high degree of uncertainty compared to the zones in gray or black. Once again, it is important to note that the persistence of the lateral movement across the interface is supported by the horizontal dark area above the 150-m elevation. Relatively high degree of repeatability in capillary barrier breaching is indicated by the coefficient of variation plot. Variations in concentration due to the complexity of the flow fields are large and should be acknowledged in assessing contaminant concentrations. The transport simulation results presented here support this very concept, first proposed by Russo (1991) for the case of unsaturated flow. The concentration estimates calculated by any large-scale mean transport model, neglecting advective heterogeneity, should have large error bars. The magnitude of the error bars, as a multiple of the mean concentration, increases with a decrease in the local dispersion value. The concentration CV keeps increasing with distance from the center of mass making the uncertainty around mean concentration predictions increasingly large multiples of the mean. The jaggedness of plumes as a

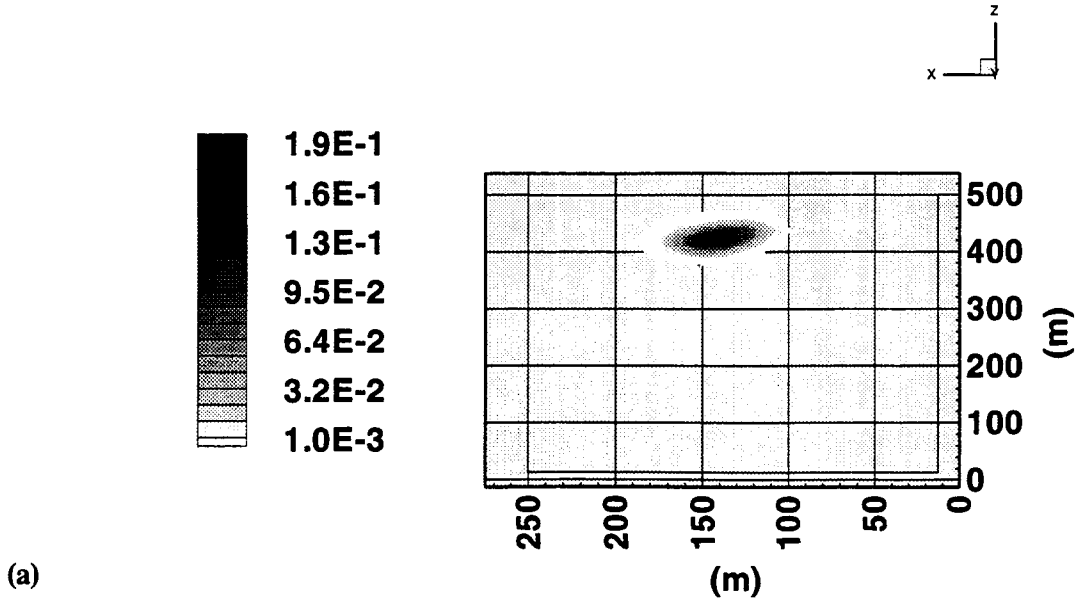

(a)

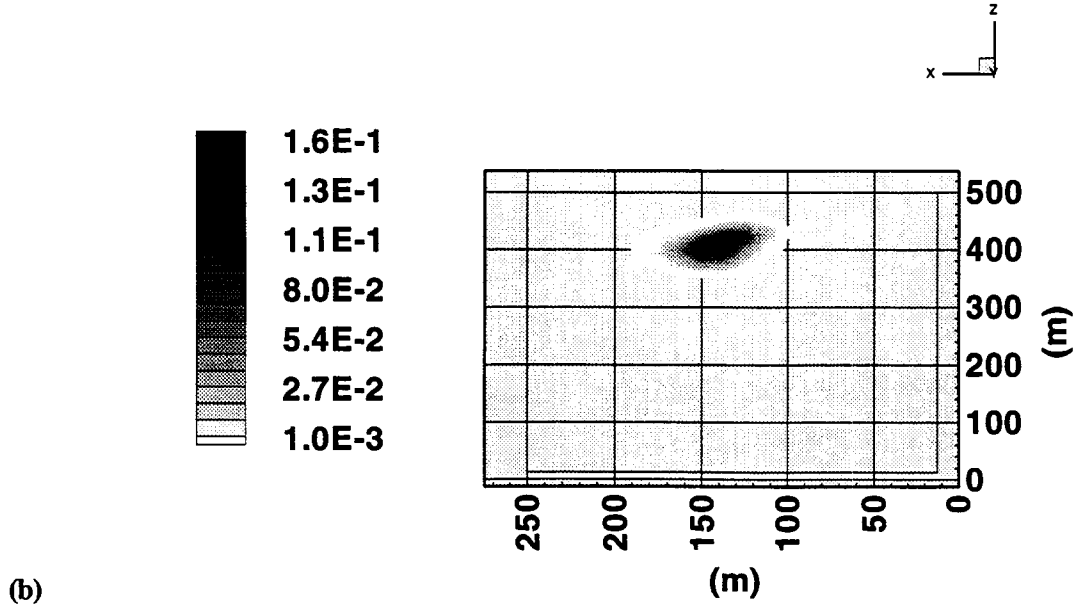

(b)

Figure 5-8. Concentration field at various times for a single realization (#5): (a) T=50 k yr, (Z_c=418.2 m), (b) T=75 k yr (Z_c=400.2 m)

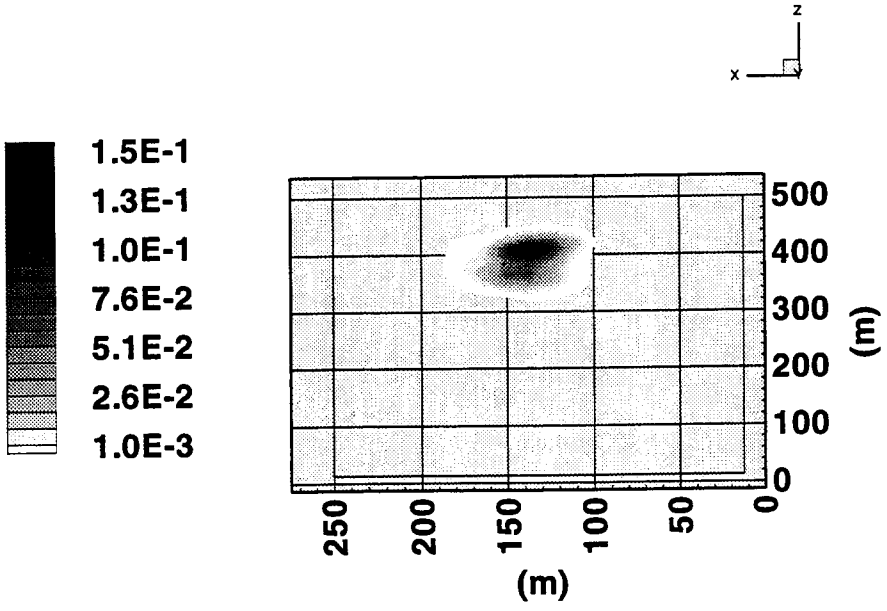

(c)

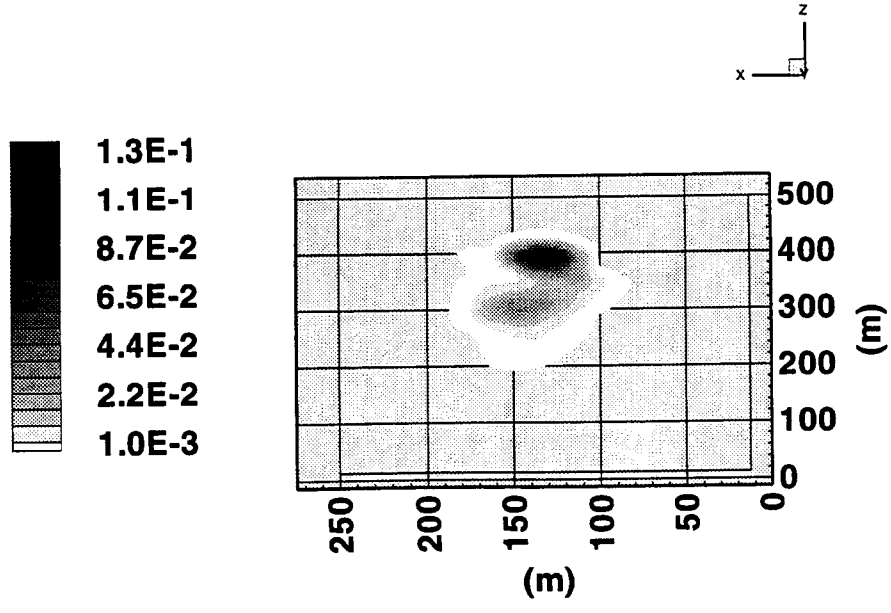

(d)

Figure 5-8. Concentration field at various times for a single realization (#5): (c) T=100 k yr, (Z_c=385.1 m), (d) T=150 k yr (Z_c=343.7 m) (cont'd)

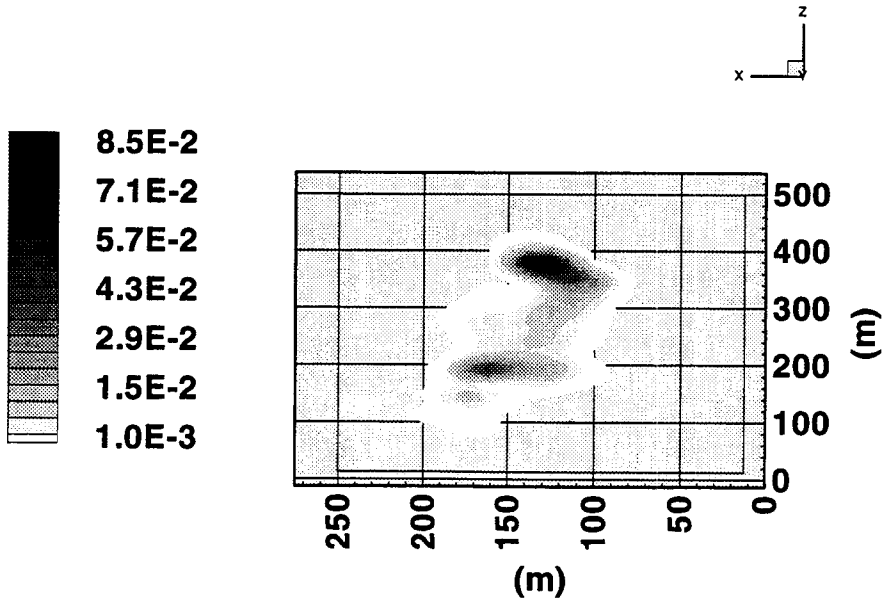

(e)

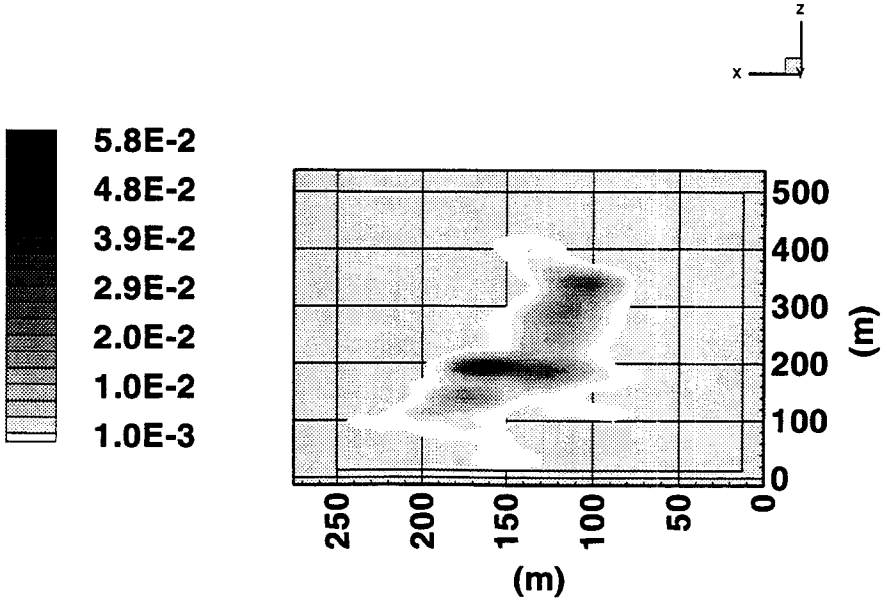

(f)

Figure 5-8. Concentration field at various times for a single realization (#5): (e) T=200 k yr, (Z_c=270.5 m), (f) T=250 k yr (Z_c=208.8 m) (cont'd)

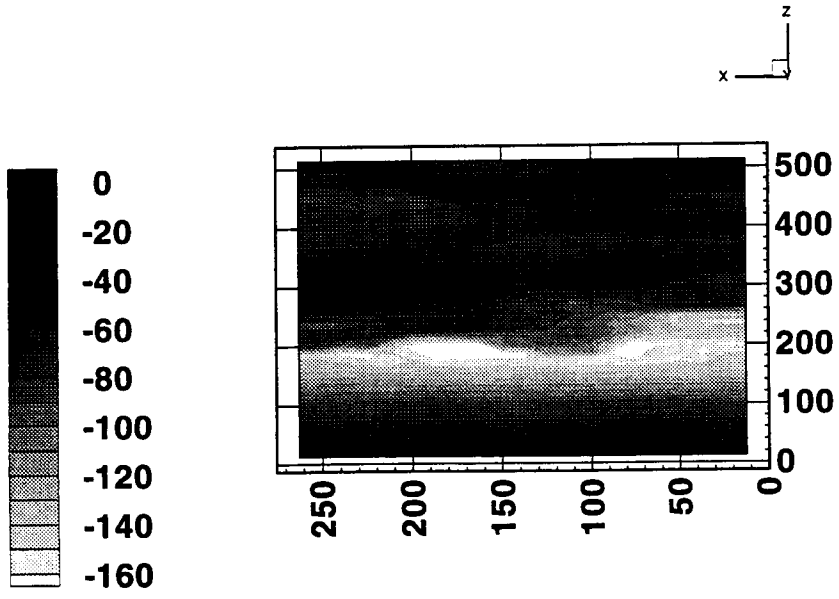

Figure 5-9. 2D cross-sectional view of steady-state pressure head results for realization #1, at $Y=125$ m

consequence of porous media heterogeneity needs to be appreciated in assessing contaminant exposure levels. Finally, a summary of the coefficient of variation analysis is presented in Figure 5-13 for the pure advection and the two advection-dispersion cases. This figure depicts the temporal evolution of the minimum (spatial) concentration CV, as presented in Bagtzoglou and Kapoor (1994).

At early times the zero-local dispersion CV grows more rapidly than the advective-dispersive cases. From a time of 150 k yr and on, in both advective-dispersive cases, the CV decreases with time. This is especially pronounced in the case of the dispersivity being 0.1 m. In contrast with this behavior, the zero-local dispersion case exhibits a mild increase in the CV with time from 150 to 300 k yr. This behavior was analytically predicted by Kapoor (1993) and Kapoor and Gelhar (1994a,b) for transport in 3D heterogeneous saturated porous media, and was corroborated by field data from the Cape Cod site. The numerical simulations presented here do not contradict their conclusion that some amount of dispersion is required to bring about a decrease in the concentration CV at large times. The concentrations derived from a zero-local-dispersion transport model are subject to unrealistically large relative degrees of uncertainty; thus the zero-local dispersion model is of little value in predicting or interpreting the asymptotic behavior of contaminant concentration in heterogeneous porous media.

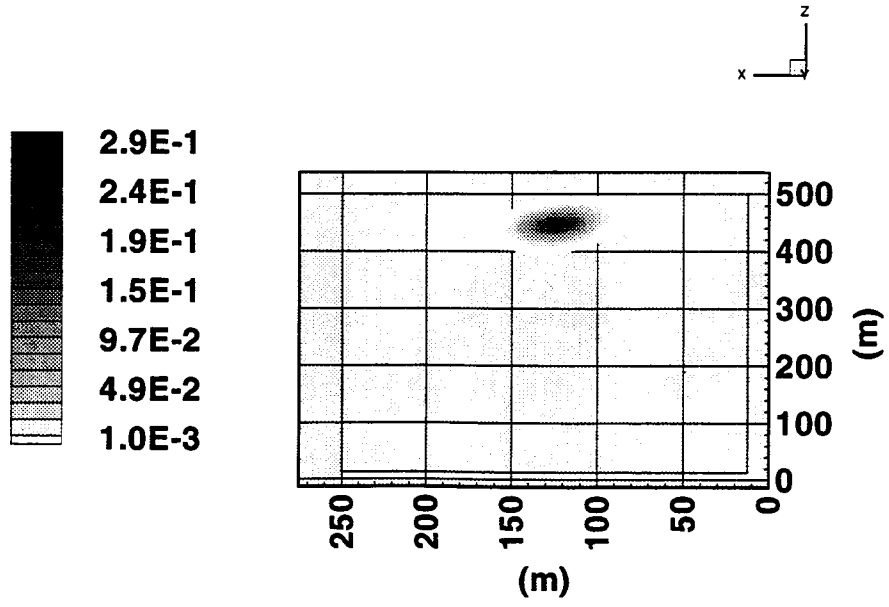

(a)

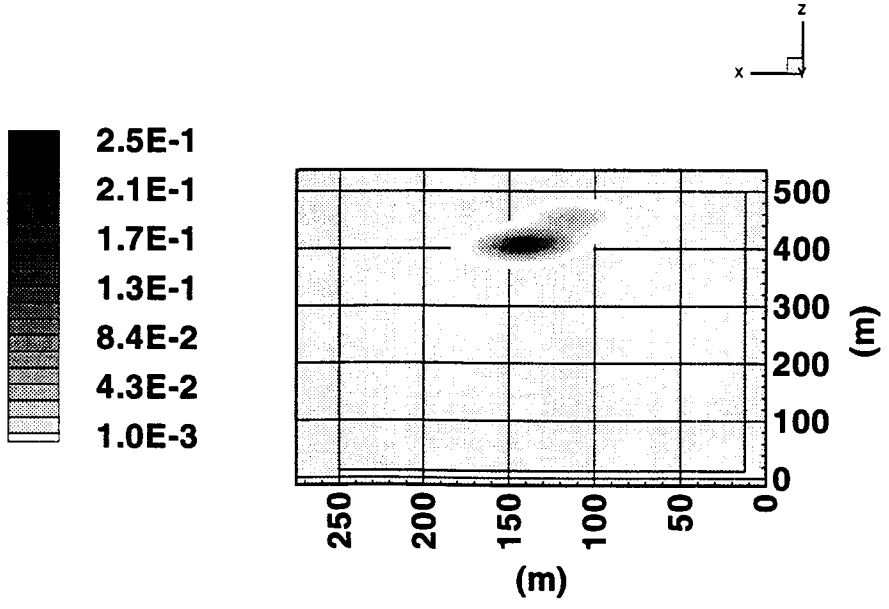

(b)

Figure 5-10. Concentration field at various times for a single realization (#1): (a) T=50 k yr, (b) T=75 k yr

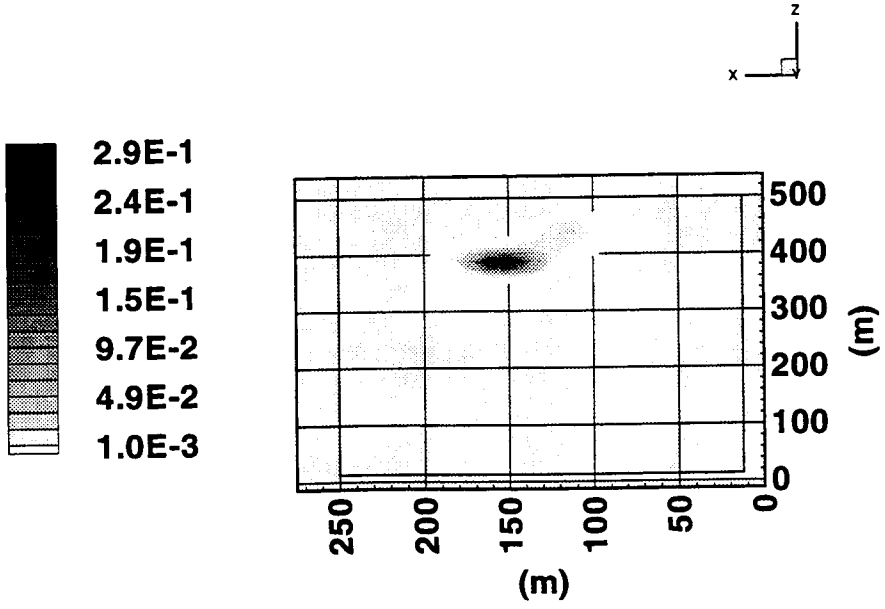

(c)

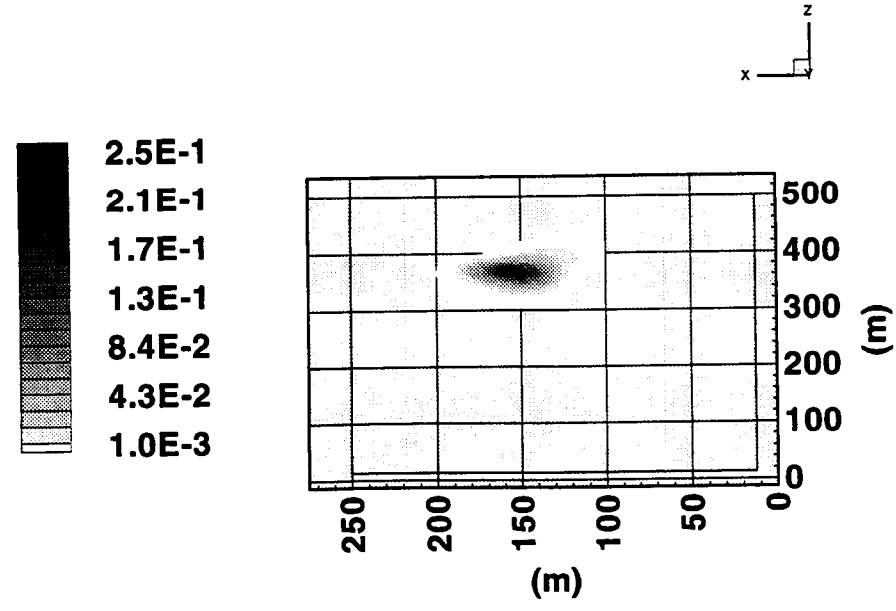

(d)

Figure 5-10. Concentration field at various times for a single realization (#1): (c) T=100 k yr, (d) T=150 k yr (cont'd)

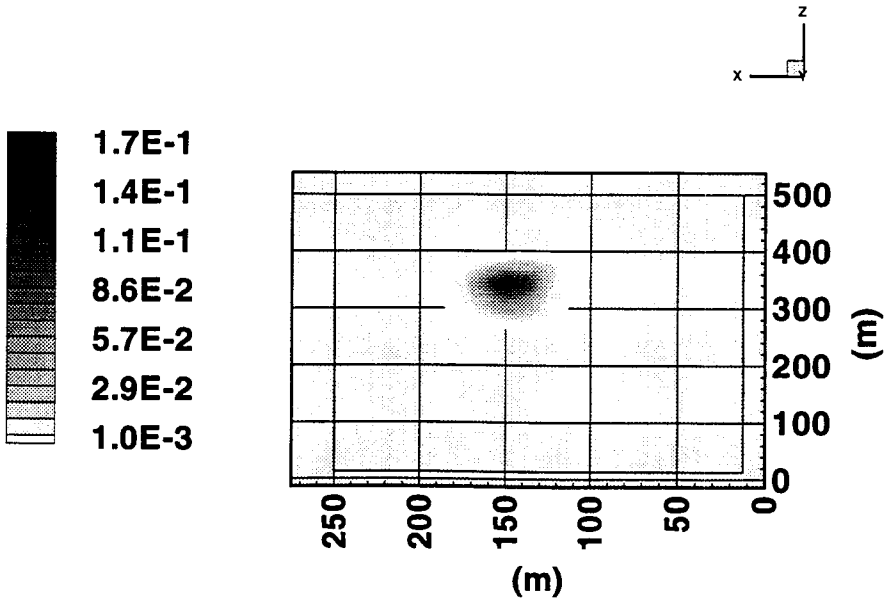

(e)

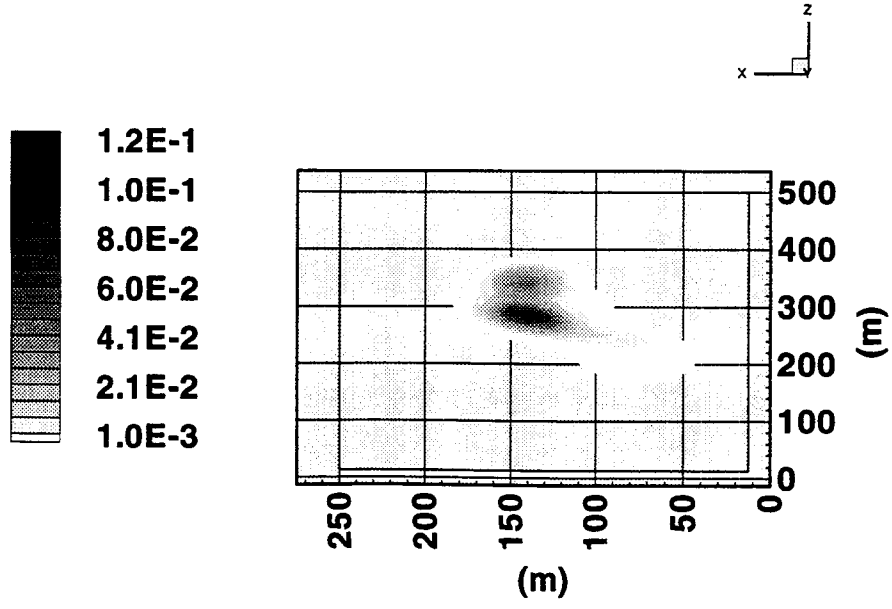

(f)

Figure 5-10. Concentration field at various times for a single realization (#1): (e) T=200 k yr, (f) T=250 k yr (cont'd)

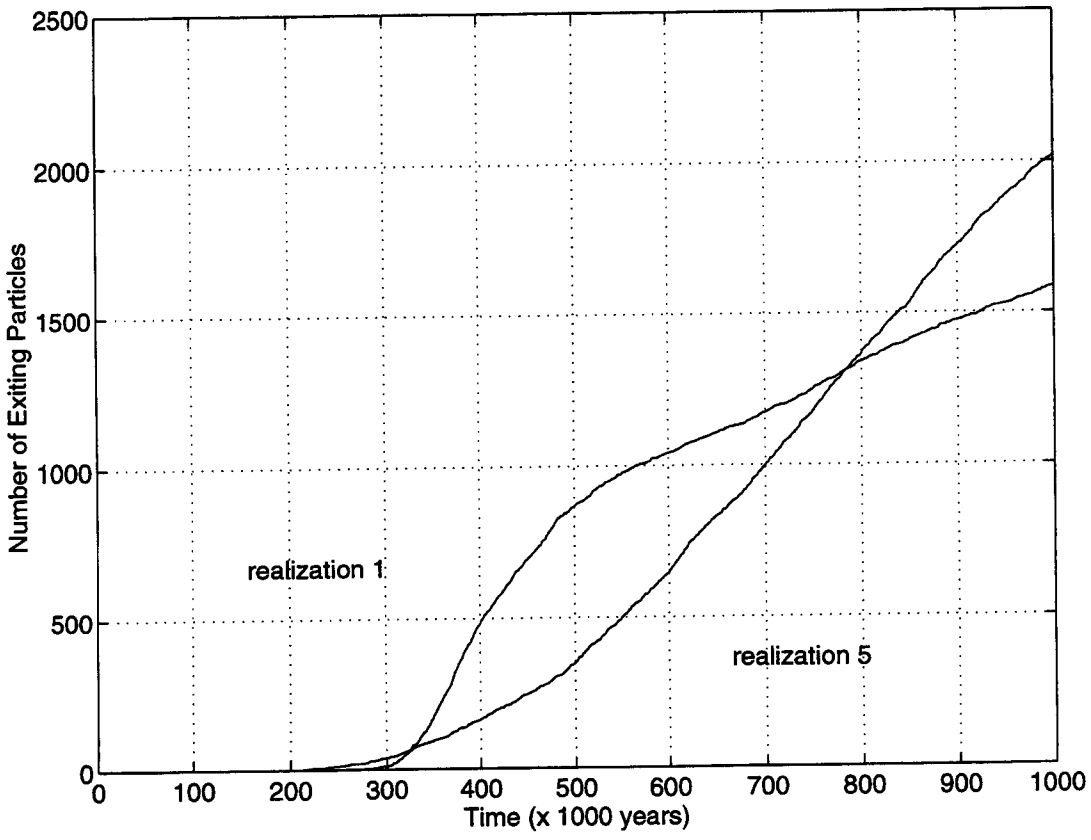

Figure 5-11. Cumulative number of exiting particles as a function of time for realization 1 and 5

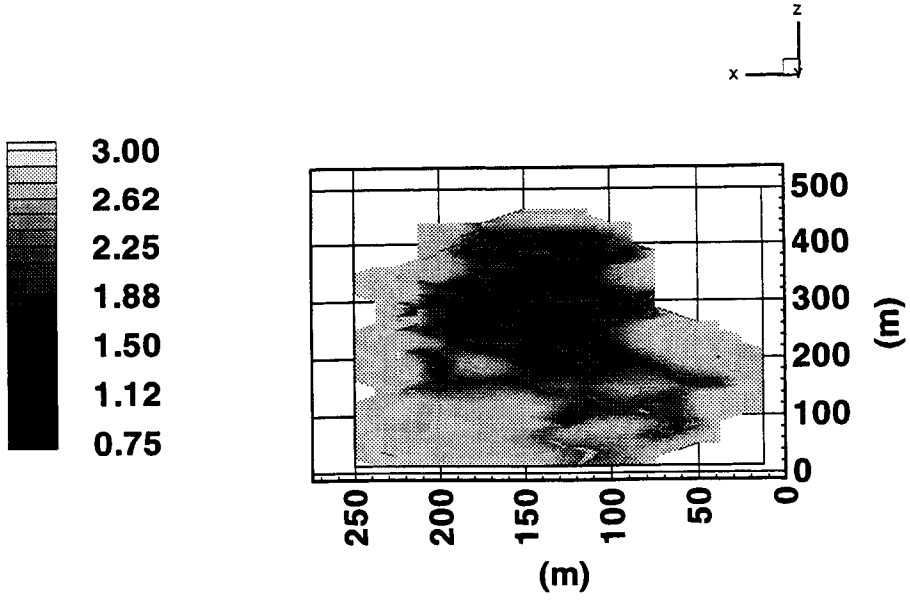

Figure 5-12. Concentration coefficient of variation field for dispersivity of 0.1 m at T=250 k yr (Z_c=208.8 m)

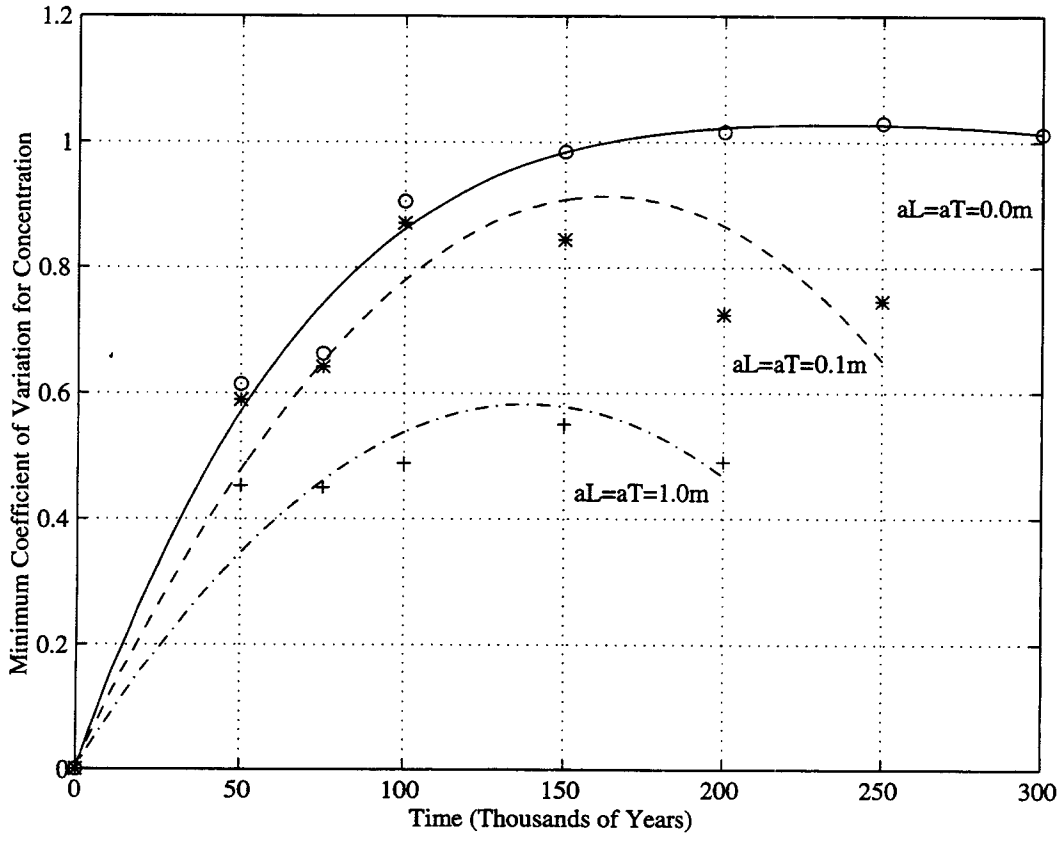

Figure 5-13. Temporal evolution of minimum concentration CV for three levels of dispersion

6 SUMMARY AND CONCLUSIONS

Modeling the flow and transport processes in the vadose zone at Yucca Mountain, Nevada, requires that the effects of various types and levels of heterogeneity be accounted for. Some of the most important geological features are stratification, faulting, and fractures. Bagtzoglou et al. (1994b) presented a review of several approaches and advocated the use of a hybrid approach whereby heterogeneity is accounted for in conjunction with the incorporation of persistent discontinuities in the conceptual models of flow. There is field evidence to corroborate the existence of both preferential flow pathways through vertical channels (fissures, faults, etc.) and extensive lateral spread along the interfaces of horizontal or dipping strata. It is known that the hydraulic properties of unsaturated media are pressure-dependent. Moreover, these properties become anisotropic as a function of moisture (Ababou, 1991). Detailed characterization of unsaturated constitutive relationships is a daunting task, and it will be limited to selected locations. Ababou (1991) strongly advocated cross-property correlations be used to ease the task of estimating the spatial structure of material properties which are difficult or impossible to measure.

This approach has been implemented in the present work. A general purpose executive numerical code has been developed and applied to the simulation of large-scale flow and transport. The code SUFLAT provides for the generation of a suite of hydraulic property fields honoring certain geostatistical identifiers [e.g., first two moments, variogram, layering (Deutsch and Journel, 1992)] in a manner that establishes cross-correlations between properties, where available. Then, SUFLAT typically solves the unsaturated flow equation, post-processes all outputs to calculate saturations and velocity fields and, finally, solves the transport problem *via* particle tracking in a repeated mode. In the simulations presented in this work, explicit incorporation of the effects of fractures on flow and transport is neglected. Microvariability was shown to be related, in some respects, to the existence of fractures or sub-grid heterogeneity and its effects were incorporated *via* dispersive transport. It is hypothesized that explicit representation of discrete fractures, embedded in a matrix continuum (deterministic or stochastic), will have a profound effect on the overall behavior of the system. However, such an endeavor was not a part of the research efforts reported herein. SUFLAT is modular and, in principle, allows for specific modules to be interchanged, upgraded, or substituted readily. As such, it is anticipated that this methodology will be modified in the future so that some of its limitations be dealt with. Specifically, it is envisioned that conditional simulations and multiphase flow processes will be incorporated within the SUFLAT methodology structure.

This report presented a relatively thorough, but by no means exhaustive, literature review on the subject of stochastic flow. It described, in some detail, the structure of SUFLAT and its components. Several assumptions inherent in the application of the current version of the code were discussed and supported by some auxiliary analyses (e.g., the choice of an exponential covariance structure and of particle tracking methods for the solution of the transport problem). A description of the hydrogeologic parameters used for the simulations presented in this report followed, and was supplemented by a verification of the cross-correlation algorithm with data from the Las Cruces trench site. Flow and transport analyses with and without the presence of a fault zone concluded the report.

This work demonstrated that stochastic-theory-based methodologies have real potential for application to environmental impact assessments for real world waste disposal problems. A working methodology and all associated numerical tools have been put to work to conduct large-scale flow and transport simulations for a layered system analogous, in some respects, to Yucca Mountain. The results presented here serve to accomplish the following. The unequivocal existence of a laterally-infinite diversive capacity for

capillary barriers forming along strata interfaces is dispelled. It is shown that stochastic approaches provide a natural platform to infer the likelihood of perched zone development. The need to account for large variations in concentrations, due to the complexity of the unsaturated flow fields, in the assessment of contaminant concentrations is emphasized. It is shown that matrix-flow conceptual models lead to large travel times; however, these travel times are associated with large standard deviations, or uncertainties. The results exemplify the very peculiar role of fault zones. Contrary to popular beliefs, vertical fault zones are neither flow conduits nor barriers. Their behavior depends very much on the layering and the within-layer heterogeneous, hydraulic properties of the surrounding material. The results shown here, for example, indicate the existence of recirculatory flow patterns. The results also provide corroborating evidence of the effect of heterogeneity on the development of capillary barrier breaches.

7 REFERENCES

Ababou, R. 1981. *Modelisation des Transfers Hydriques dans le Sol en Irrigation Localisee*. Dr -Ing ed. Thesis. Grenoble, France: Institute de Mecanique de Grenoble: 218.

Ababou, R. 1988. *Three-Dimensional Flow in Random Porous Media*. Ph.D. Thesis. Cambridge, MA: Massachusetts Institute of Technology: Department of Civil Engineering 2: 833.

Ababou, R. 1991. *Approaches to Large Scale Unsaturated Flow in Heterogeneous, Stratified, and Fractured Geologic Media*. NUREG/CR-5743. Washington, DC: Nuclear Regulatory Commission.

Ababou, R. 1993. Stochastic analysis of unsaturated flow and transport. *Report on Research Activities for Calendar Year 1991*. NUREG/CR-5817. Washington, DC: Nuclear Regulatory Commission.

Ababou, R., and L.W. Gelhar. 1988. A high-resolution finite difference simulator for 3D unsaturated flow in heterogeneous media. *Computational Methods in Water Resources*. Elsevier and Computational Mechanics Publications 1: 173–178.

Ababou, R., and A.C. Bagtzoglou. 1993. *BIGFLOW: A Numerical Code for Simulating Flow in Variably Saturated, Heterogeneous Geologic Media (Theory and User's Manual—Version 1.1)*. NUREG/CR-6028. Washington, DC: Nuclear Regulatory Commission.

Ababou, R., A.C. Bagtzoglou, and E.F. Wood. 1994. On the condition number of covariance matrices in kriging, estimation, and simulation random fields. *Mathematical Geology* 26(1): 99–133.

Ackerer, P. 1988. Random-walk method to simulate pollutant transport in alluvial aquifers or fractured rocks. *Groundwater and Quality Modelling*. E. Custodio et al., eds. D. Reidel Publishing Co.: 475–486.

Adams, E.E., and L.W. Gelhar. 1992. Field study of dispersion in a heterogeneous aquifer 2. Spatial moment analysis. *Water Resources Research* 28(12): 3,293–3,307.

Ahlstrom, S., H. Roote, R. Arnett, C. Cole, and R. Serne. 1977. *Multicomponent Mass Transport Model: Theory and Numerical Implementation*. Report BNWEL 2127. Richland, VA: Batelle Pacific Northwest Laboratories.

Allen, M.B., and M.C. Curran. 1989. Adaptive local grid refinement algorithms for finite-element collocation. *Numerical Methods for Partial Differential Equations* 5: 121–132.

Andricevic R., and E. Foufoula-Georgiou. 1990. A particle tracking method of kinetically adsorbing solutes in heterogeneous porous media. *Computational Methods in Surface Hydrology*. G. Gambolati, A. Rinaldo, C.A. Brebbia, W.G. Gray, and G.F. Pinder, eds. Berlin, Germany: Springer-Verlag: 429–435.

Baca, R.G., R.D. Manteufel, S. Mohanty, S.A. Stothoff, and G.W. Wittmeyer. 1994. *Chapter 7: Performance Assessment Research, NRC High-Level Radioactive Waste Research at CNWRA July—December 1993*. CNWRA 93-02S. San Antonio, TX. Center for Nuclear Waste Regulatory Analyses.

Bagtzoglou, A.C., and D.E. Dougherty. 1990. Numerical solution of Fisher's equation using particle methods. *Proceeding of the 10th AGU Hydrology Days*. H.J. Morel-Seytoux ed. Fort Collins, CO: Hydrology Days Publications: 28–38.

Bagtzoglou, A.C., and V. Kapoor. 1994. Unsaturated flow and advection-dispersion in three-dimensionally heterogeneous geologic media. In *Proceedings of X International Conference on Computational Methods in Water Resources*. A. Peters et al. eds: Kluwer Publishing Co. (in press).

Bagtzoglou, A.C., A.F.B Tompson, and D.E. Dougherty. 1991. Probabilistic simulation for reliable solute source identification in heterogeneous porous media. *Water Resources Engineering Risk Assessment*. J. Ganoulis, ed. Berlin and Heidelberg, Germany: Springer-Verlag: NATO ASI Series. G29: 189–201.

Bagtzoglou, A.C., A.F.B. Tompson, and D.E. Dougherty. 1992a. Projection functions for particle-grid methods. *Numerical Methods for Partial Differential Equations* 8: 325–340.

Bagtzoglou, A.C., A.F.B. Tompson, and D.E. Dougherty. 1992b. Application of particle methods to reliable identification of groundwater pollution sources. *Water Resources Management* 6: 15–23.

Bagtzoglou, A.C., R. Ababou, B. Sagar, and M.R. Islam. 1993. Effects of some common geological features on 2D variably saturated flow. *Scientific Basis for Nuclear Waste Management XVI* 294: Pittsburgh, PA: Materials Research Society: 929–936.

Bagtzoglou, A.C., and R.G. Baca. 1994. Probabilistic calculation of groundwater travel time in heterogeneous three-dimensional porous media. *Scientific Basis for Nuclear Waste Management XVII* 333: Pittsburgh, PA: Materials Research Society: 849–854

Bagtzoglou, A.C., M.R. Islam, and M. Muller. 1994a. Stochastic analysis of unsaturated flow and transport with the SUFLAT executive numerical code. *Proceedings of 5th International High Level Radioactive Waste Management Conference*. Las Vegas, NV: American Nuclear Society: 2,669–2,677.

Bagtzoglou, A.C., S. Mohanty, A. Nedungadi, T-C.J. Yeh, and R. Ababou. 1994b. *Effective Hydraulic Property Calculations for Unsaturated, Fractured Rock with Semi-Analytical and Direct Numerical Techniques: Review and Applications*. CNWRA 94-007. San Antonio, TX: Center for Nuclear Waste Regulatory Analyses.

Baker, R.S., and D. Hillel. 1990. Laboratory tests of a theory of fingering during infiltration into layered systems. *Soil Science Society of America Journal* 54: 20–30.

Baptista, A., P. Gresho, and E. Adams. 1988. Reference problems for the convection-diffusion forum. *Proceedings of the VII International Conference on Computational Methods in Water Resources*. Cambridge, MA.

Bellin, A., P. Salandin, and A. Rinaldo. 1992. Simulation of dispersion in heterogeneous porous formations: Statistics, first-order theories, convergence of computations. *Water Resources Research* 28(9): 2,211–2,227.

Bentley, L.R., G.F. Pinder, and I. Herrera. 1989. Solution of the advective-dispersive transport equation using a least squares collocation, Eulerian-Lagrangian method. *Numerical Methods for Partial Differential Equations* 5: 227–240.

Bhattacharya, R.N., and V.K. Gupta. 1983. A theoretical explanation of solute dispersion in saturated porous media at the Darcy scale. *Water Resources Research* 19(4): 938–944.

Bodvarsson, G., G. Chen, C. Wittwer. 1994. Preliminary analysis of Three-Dimensional moisture flow within Yucca Mountain, Nevada. *Proceedings of the Fifth International Conference on High-Level Radioactive Waste Management*. Las Vegas, NV: American Nuclear Society and American Society of Civil Engineers: 2,038–2,047.

Boggs, J.M., S.C. Young, L.M. Beard, L.W. Gelhar, K.R. Rehfeldt, and E.E. Adams. 1992. Field study of dispersion in a heterogeneous aquifer 1. Overview and site description. *Water Resources Research* 28(12): 3,281–3,291.

Bonano, E.J., P.A. Davis, R.L. Bras, and P.K. Kitanidis. 1989. *Methodology for Estimating Groundwater Travel Times at a Nuclear Waste Repository Using a Physically Based Geostatistical Approach*. Technical Report 3-11-89. Cambridge, MA: Department of Civil Engineering, Massachusetts Institute of Technology.

Boris, J.P., and D.L. Book. 1973. Flux-corrected transport. I. SHASTA: A fluid transport algorithm that works. *Journal of Computational Physics* 11: 38–69.

Bouloutas, E.T. 1989. *Improved Numerical Approximations for Flow and Transport in the Unsaturated Zone*. Ph.D. Thesis. Cambridge, MA: MIT: Department of Civil Engineering.

Bresler, E. 1978. Analysis of trickle irrigation with application to design problems. *Irrigation Science* 1(1): 3–17.

Butters, G.L., and W.A. Jury. 1989. Field scale transport of bromide in an unsaturated soil. 2 Dispersion modeling. *Water Resources Research* 25(7): 1,583–1,589.

Cady, R., and S.P. Neuman. 1985. Advection-dispersion with adaptive Eulerian-Lagrangian finite elements. *Proceedings of the NATO Advanced Study Institute on Fundamentals of Transport Phenomena in Porous Media*. Newark, DE.

Celia, M.A., I. Herrera, E. Bouloutas, and J.S. Kindred. 1989. A new numerical approach for the advective-diffusive transport equation. *Numerical Methods for Partial Differential Equations* 5: 203–226.

Celia, M.A., E.T. Bouloutas, and R.L. Zarba. 1990. A general mass-conservative numerical solution for the unsaturated flow equation. *Water Resources Research* 26(7): 1,483–1,496.

Cheng, R.T., V. Casuli, and S.N. Milford. 1984. Eulerian-Lagrangian solution of the convection-dispersion equation in natural coordinates. *Water Resources Research* 20(7): 944–952.

Chin, D.A. 1989. Diagnostic model of dispersion in porous media. *Journal of Hydraulic Engineering* 115(2): 210–227.

Christakos, G. 1984. On the problem of permissible covariance and variogram models. *Water Resources Research* 20(2): 251–265.

Chu, W., E.W. Strecker, and D.P. Lettenmaier. 1987. An evaluation of data requirements for groundwater contaminant transport modeling. *Water Resources Research* 23(3): 408–424.

Clifton, P.M., and S.P. Neuman. 1982. Effects of kriging and inverse modeling on conditional simulation of the Avra Valley aquifer in southern Arizona. *Water Resources Research* 18(4): 1,215–1,234.

Clifton, P.M., B. Sagar, and R.G. Baca. 1985. Stochastic groundwater travel time modeling using a Monte Carlo technique. Tucson, AZ. In *International Association of Hydrogeologists Memoirs: Hydrogeology of Rocks of Low Permeability* 17(1): 319–329.

Collela P., and P.R. Woodward. 1984. The piecewise parabolic method (PPM) for gas-dynamical simulations. *Journal of Computational Physics* 54: 174–201.

Cvetkovic, V.D., and A.M. Shapiro. 1989. Solute advection in stratified formations. *Water Resources Research* 25(6): 1,283–1,289.

Dagan, G. 1982a. Stochastic modeling of groundwater flow by unconditional and conditional probabilities: 1. Conditional simulation and the direct problem. *Water Resources Research* 18(4): 813–833.

Dagan, G. 1982b. Stochastic modeling of groundwater flow by unconditional and conditional probabilities 2: The solute transport. *Water Resources Research* 18(4): 835–848.

Dagan, G. 1984. Solute transport in heterogeneous formations. *Journal of Fluid Mechanics* 145: 151–177.

Dagan, G. 1985. A note on higher-order corrections of the head covariances in steady aquifer flow. *Water Resources Research* 21: 573–578.

Dagan, G. 1987. Review of stochastic theory of transport in groundwater flow. *Proceeding of the NATO Advanced Study Institute on Groundwater Flow and Quality Modelling*. Lisbon, Portugal.

Dagan, G. 1988. Time-dependent macrodispersion for solute transport in anisotropic heterogeneous aquifers. *Water Resources Research* 24(9): 1,491–1,500.

Dagan, G. 1989. *Flow and Transport in Porous Formations*. Heidelberg, Germany: Springer-Verlag.

Dagan, G., and V. Nguyen. 1989. A comparison of travel time and concentration approaches to modeling transport by groundwater. *Journal of Contaminant Hydrology* 4: 79–91.

Delhomme, J.P. 1979. Spatial variability and uncertainty in groundwater flow parameters: A geostatistical approach. *Water Resources Research* 15(2): 269–280.

de Marsily G. 1986. *Quantitative Hydrogeology*. Orlando, FL: Academic Press.

Deutsch, C.V., and A.G. Journel. 1992. *GSLIB: Geostatistical Software Library and User's Guide*. New York, NY: Oxford University Press.

Dougherty, D.E., and A.F.B. Tompson. 1990. Implementing the particle method on the iPSC/2. *Computational Methods in Surface Hydrology*. G. Gambolati, A. Rinaldo, C.A. Brebbia, W.G., Gray, and G.F. Pinder, eds. Berlin, Germany: Springer-Verlag: 473–478.

Dougherty, D.E., and A.C. Bagtzoglou. 1993. A caution on the regulatory use of numerical solute transport models. *Ground Water* 31(6): 1,007–1,010.

Einstein, A. 1926. *Investigations on the Theory of the Brownian Movement*. New York, NY: Dover Publications.

Eckstrom, M.P. 1973. A spectral characterization of the ill-conditioning in numerical deconvolution. *Institute of Electrical and Electronic Engineers* Transactions AU-21(4): 344–348.

Follin, S. 1992. *Numerical Calculations on Heterogeneity of Groundwater Flow*. Ph.D. Dissertation. Stockholm, Sweden: Royal Institute of Technology.

Freyberg, D.L. 1986. A natural gradient experiment on solute transport in a sand aquifer 2. Spatial moments and the advection and dispersion of nonreactive tracers. *Water Resources Research* 22(13): 2,031–2,046.

Freeze, R.A. 1975. A stochastic-conceptual analysis of one-dimensional groundwater flow in nonuniform homogeneous media. *Water Resources Research* 11(5): 725–741.

Garabedian, S.P., D.R. LeBlanc, L.W. Gelhar, and M.A. Celia. 1991. Large-scale natural-gradient tracer test in sand and gravel, Cape Cod, Massachusetts: 2 Analysis of tracer moments for a nonreactive tracer. *Water Resources Research* 27(5): 911–924.

Gardiner, C. 1985. *Handbook of Stochastic Methods for Physics, Chemistry and the Natural Sciences*. 2nd ed. Heidelberg, Germany: Springer Verlag.

Gelhar, L.W. 1986. Stochastic subsurface hydrology: From theory to applications. *Water Resources Research* 22(9): 1,35S–1,45S.

Gelhar, L.W. 1993. *Stochastic Subsurface Hydrology*. Engelwood Cliffs, NJ: Prentice-Hall, Inc.

Gelhar, L.W., and C.L. Axness. 1983. Three-dimensional stochastic analysis of macrodispersion in aquifers. *Water Resources Research* 19(1): 161–180.

Golub, G.H., and C.F. Van Loan. 1989. *Matrix Computations*. Baltimore, MA: The John Hopkins University Press: 2: 642.

Gómez-Hernández, J.J., and S.M. Gorelick. 1989. Effective groundwater model parameter values: Influence of spatial variability of hydraulic conductivity, leakage, and recharge. *Water Resources Research* 25(3): 405–419.

Gotway, C.A. 1994. The use of conditional simulation in nuclear-waste-site performance assessment. *Technometrics* 36(2): 129–141.

Gutjahr, A.L. 1984. Stochastic models of subsurface flow: Log-linearized Gaussian models are "exact" for covariances. *Water Resources Research* 20: 1,909–1,912.

Gutjahr, A.L. 1992. Chapter 4: Hydrology. in *Techniques for Determining Probabilities of Geologic Events and Processes*. R.L. Hunter and C.J. Mann, eds. New York, NY: Oxford Press: 75–98.

Gutjahr, A.L., and R.L. Bras. 1993. Spatial variability in subsurface flow and transport: A review. *Reliability Engineering and System Safety* 42: 293–316.

Güven, O., F.J. Molz, and J.G. Melville. 1984. An analysis of dispersion in a stratified aquifer. *Water Resources Research* 20(10): 1,337–1,354.

Guzman, A., S.P. Neuman, and C. Lohrstorfer. 1993. Multiscale air permeability measurements in unsaturated fractured tuff. *Workshop VI: Flow and Transport Through Unsaturated, Fractured Rocks*. University of Arizona. Tucson, AZ: (unpublished proceedings).

Haken, H. 1983. *Advanced Synergetic: Instability Hierarchies of Self-Organizing Systems and Devices*. New York, NY: Springer Verlag.

Harlow, F.H. 1964. The particle in cell computing method for fluid dynamics. B. Adler et al., eds. *Methods in Computational Physics* 3: 319–343.

Harr, M.E. 1987. *Reliability-Based Design in Civil Engineering*. New York, NY: McGraw-Hill.

Harter, T. 1994. *Unconditional and Conditional Simulation of Flow and Transport in Heterogeneous Variably Saturated Porous Media*. Ph.D. Dissertation. Tucson, AZ: University of Arizona.

Harter, T., and T.-C.J. Yeh. 1993. An efficient method for simulating steady unsaturated flow in random porous media: Using an analytical perturbation solution as initial guess to a numerical model. *Water Resources Research* 29(12): 4,139–4,149.

Hockney, R.W., and J.W. Eastwood. 1988. *Computer Simulation Using Particles*. Bristol, United Kingdom: Adam Hilger.

Hoeksema, R.J., and P.K. Kitanidis. 1985. Analysis of the spatial structure of properties of selected aquifers. *Water Resources Research* 21(4): 563–572.

Hopmans, J.W., H. Schukking, and P.J.J.F. Torfs. 1988. Two-dimensional steady state unsaturated water flow in heterogeneous soils with autocorrelated soil hydraulic properties. *Water Resources Research* 24: 2,005–2,017.

Isaaks E.H., and R.M. Srivastava. 1989. *An Introduction to Applied Geostatistics*. New York, NY: Oxford University Press.

Jones, L. 1990. Explicit Monte Carlo simulation head moment estimates for stochastic confined groundwater flow. *Water Resources Research* 26(6): 1,145–1,153.

Journel, A.G., and C.J. Huijbregts. 1978. *Mining Geostatistics*. San Diego, CA: Academic Press.

Journel, A.G. 1983. Nonparametric estimation of spatial distributions. *Mathematical Geology* 15: 445.

Journel, A.G. 1989. *Fundamentals of Geostatistics in Five Lessons*. Washington, DC: American Geophysical Union.

Journel, A.G., F. Alabert. 1989. Non-Gaussian data expansion in the earth sciences. *Terra Nova* 1: 123.

Kapoor, V. 1993. *Macrodispersion and Concentration Fluctuations in Three-Dimensionally Heterogeneous Aquifers*. Sc.D. Dissertation. Cambridge, MA: Massachusetts Institute of Technology.

Kapoor, V., and L.W. Gelhar. 1994a. Transport in three-dimensionally heterogeneous aquifers: 1. Dynamics of concentration fluctuations. *Water Resources Research* 30(6): 1,775–1,788.

Kapoor, V., and L.W. Gelhar. 1994b. Transport in three-dimensionally heterogeneous aquifers: 2. Predictions and observations of concentration fluctuations. *Water Resources Research* 30(6): 1,789–1,801.

Kinzelbach, W. 1988. The random walk method in pollutant transport simulation. E. Custodio et al., eds. *Groundwater flow and Quality Modelling*: 227–245.

Kinzelbach, W. 1989. Methods for the simulation of pollutant transport in groundwater—A model comparison. *Proceedings of the NWWA Conference on Solving Groundwater Problems with Models*. Indianapolis, IN.

Konikow, L.F., and J.D. Bredehoeft. 1978. Computer modeling of two-dimensional solute transport and dispersion in groundwater. *Techniques of Water Resources Investigations of the United States Geological Survey*. Washington, DC: Book 7 Chapter C2: United States Government Printing Office.

Kozak, M.W., N.E. Olague, R.R. Rao, and J.T. McCord. 1993. *Evaluation of a Performance Assessment Methodology for Low-Level Radioactive Waste Disposal Facilities*. NUREG/CR-5927. Washington, DC: Nuclear Regulatory Commission.

Kung, K.-J.S. 1990a. Preferential flow in a sandy vadose zone: 1 Field observation. *Geoderma* 46: 51–58.

Kung, K.-J.S. 1990b. Preferential flow in a sandy vadose zone: 2 Mechanism and implications. *Geoderma* 46: 59–71.

LeBlanc, D.R., S.P. Garabedian, K.M. Hess, L.W. Gelhar, R.D. Quadri, K.G. Stollenwerk, and W.W. Wood. 1991. Large-scale natural gardietn tracer test in sand and gravel, Cape Cod, Massachusetts, 1: Experimental design and observed tracer movement. *Water Resources Research* 27(5): 895–910.

Lehman, L.L. 1992. Alternate conceptual model of groundwater flow at Yucca Mountain. *Proceedings of the 3rd International High-Level Radioactive Waste Management Conference*. Las Vegas, NV: American Nuclear Society: 310–320.

Lewis, J.P. 1987. Generalized stochastic subdivision. *ACM Transactions* 6(3): 167–190.

Loeven, C. 1993. *A Summary and Discussion of Hydrologic Data from the Calico Hills Nonwelded Hydrogeologic Unit at Yucca Mountain, Nevada*. LA-12376-MS. Los Alamos, NM: Los Alamos National Laboratory.

Mantoglou, A., and J.L. Wilson. 1982. The Turning Bands method for the simulation of random fields using line generation by a spectral method. *Water Resources Research* 18(5): 1,379–1,394.

Mantoglou, A., and L.W. Gelhar. 1985. *Large-scale Models and Effective Parameters of Transient Unsaturated Flow and Contaminant Transport Using Stochastic Methods*. Technical Report 299. Cambridge, MA: R.M. Parsons Lab, Massachusetts Institute of Technology.

Mantoglou, A., and L.W. Gelhar. 1987a. Stochastic modeling of large-scale transient unsaturated flow systems. *Water Resources Research* 23(1): 37–46.

Mantoglou, A., and L.W.Gelhar. 1987b. Capillary tension head variance, mean soil moisture content, and effective specific soil moisture capacity of transient unsaturated flow in stratified soils. *Water Resources Research* 23(1): 47–56.

Mantoglou, A., and L.W. Gelhar. 1987c. Effective hydraulic conductivities of transient unsaturated flow in stratified soils. *Water Resources Research* 23(1): 57–67.

Matalas, N. 1967. Mathematical assessment of synthetic hydrology. *Water Resources Research* 3: 937–945.

McCord, J.T. 1991. Application of second-type boundaries in unsaturated flow modeling. *Water Resources Research* 27(12): 3,257–3,260.

Monastersky, R. 1994. Faults found at Nevada nuclear waste site. *Science News* 145: 310.

Moreno, L. 1985. Analysis of some laboratory tracer runs in natural fissures. *Water Resources Research* 17(7): 951–958.

Morse, R.L. 1970. Multidimensional plasma simulation by the particle-in-cell method. B. Adler et al., *Methods in Computational Physics*: Academic Press: 213–239.

Naff, R.L. 1990. On the nature of the dispersive flux in saturated heterogeneous porous media. *Water Resources Research* 26(5): 1,013–1,026.

Neuman, S.P. 1981. A Eulerian Lagrangian scheme for the dispersion convection equation using conjugate space-time grids. *Journal of Computational Physics* 41: 270–294.

Neuman, S.P. 1990. Universal scaling of hydraulic conductivities and dispersivities in geologic media. *Water Resources Research* 26: 1,749–1,758.

Neuman, S.P. 1994. *Is Fingering and Wetting Front Instability an Issue*? NUREG/CR: Washington, DC: Nuclear Regulatory Commission: (in preparation).

Neuman, S.P., E.S. Simpson, P.A. Hsieh, J.W. Jones, and C.L. Winter. 1985. Statistical analysis of hydraulic test data from fractured crystalline rock near Oracle, Arizona. *Proceedings of Congress on Hydrogeology of Rocks of Low Permeability*. Tucson, AZ: International Association of Hydrogeologists XVII(1): 289–300.

Neuman, S.P., C.L. Winter, and C.M. Newman. 1987. Stochastic theory of field-scale Fickian dispersion in anisotropic porous media. *Water Resources Research* 23: 453–466.

Nichols, W.E., and M.D. Freshley. 1993. Uncertainty analyses of unsaturated zone travel time at Yucca Mountain. *Ground Water* 31(2): 293–301.

O'Dowd, R.J. 1991. Conditioning of coefficient matrices of ordinary kriging. *Mathematical Geology* 23(5): 721–739.

Ogata, A., and R.B. Banks. 1961. A solution of the differential equation of longitudinal dispersion in porous media. *U.S. Geological Survey Professional Paper* 411-A: A1–A9.

Oldenburg, C.M., and K. Pruess. 1993. On numerical modeling of capillary barriers. *Water Resources Research* 29(4): 1,045–1,056.

Oran, E.S., and J.P. Boris. 1987. *Numerical Simulation of Reactive Flow*. New York, NY: Elsevier Science Publishing Co.

Peters, R.R., E.A. Klavetter, I.J. Hall, D.C. Blair, P.R. Heller, and G.W. Gee. 1984. *Fracture and Matrix Hydrologic Characteristics of Tuffaceous Materials from Yucca Mountain, Nye County, Nevada*. SAND84-1471. Albuquerque, NM: Sandia National Laboratories.

Pinder, G.F., and H.H. Cooper. 1970. A numerical technique for calculating the transient position of the saltwater front. *Water Resources Research* 6(3).

Polmann, D.J. 1990. *Application of Stochastic Methods to Transient Flow and Transport in Heterogeneous Unsaturated Soils*. Ph.D. Thesis. Cambridge, MA: Massachusetts Institute of Technology.

Polmann, D.J., E.G. Vomvoris, D. McLaughlin, E.M. Hammick, and L.W. Gelhar. 1988. *Application of Stochastic Methods to the Simulation of Large-Scale Unsaturated Flow and Transport.* NUREG/CR-5094. Washington, DC: Nuclear Regulatory Commission.

Posa, D. 1989. Conditioning of the stationary kriging matrices for some well-known covariance models. *Mathematical Geology* 21(7): 755–765.

Press, W.H., B.P. Flannery, S.A. Teukolsky, and W.T. Vetterling. 1986. *Numerical Recipes: The Art of Scientific Computing*. Cambridge, UK: Cambridge University Press.

Price, W.E. 1974. Simulation of alluvial fan deposition by a random walk model. *Water Resources Research* 10(2): 263–274.

Prickett, T., T.G. Naymic, and C.G. Lonnquist. 1981. A random-walk solute transport model for selected groundwater quality evaluations. Illinois State Water Survey, Champaign, IL: *Bulletin 65*.

Pruess, K., and Y. Tsang. 1994. *Thermal Modeling for a Potential High-Level Nuclear Waste Repository at Yucca Mountain, Nevada*. LBL-35381. Berkeley, CA: Lawrence Berkeley Laboratory.

Rautman, C.A., and A.H. Treadway. 1991. Geologic uncertainty in a regulatory environment: An example from the potential Yucca Mountain nuclear waste repository site. *Environmental and Geological Water Science* 18(3): 171–184.

Rautman, C.A., and A.L. Flint. 1992. Deterministic geologic processes and stochastic modeling. *Proceedings of the Third International High-Level Radioactive Waste Conference*. La Grange Park, IL: American Nuclear Society: 1,617–1,624.

Rautman, C.A., and T.H. Robey. 1993. Recent developments in stochastic modeling and upscaling of hydrologic properties in tuff. *Proceedings of the Fourth International Conference on High-Level Radioactive Waste Management*. Las Vegas, NV: American Nuclear Society and American Society of Civil Engineers: 1,437–1,445.

Rautman, C.A., and T.H. Robey. 1994. Development of stochastic indicator models of lithology, Yucca Mountain, Nevada. *Proceedings of the Fifth International Conference on High-Level Radioactive Waste Management*. Las Vegas, NV: American Nuclear Society and American Society of Civil Engineers: 2,510–2,519.

Roache, P.J. 1976. *Computational Fluid Dynamics*. Albuquerque, NM. Hermosa Publishers.

Robertson, M. 1990. *A Statistical Continuum Approach for Mass Transport in Fractured Media*. M.A.Sc. Thesis. Vancouver, Canada: University of British Columbia.

Robey, T.H. 1993. Numerical methods for fluid flow in unsaturated heterogeneous Tuff. *Proceedings of the Fourth High-Level Radioactive Waste Management Conference*. Las Vegas, NV: American Nuclear Society and American Society of Civil Engineers: 138–145.

Rockhold, M.L. 1993. *Simulation of Unsaturated Flow and Nonreactive Solute Transport in a Heterogeneous Soil at the Field Scale*. NUREG/CR-5998. Washington, DC: Nuclear Regulatory Commission.

Rockhold, M.L., B. Sagar, and M.P. Connelly. 1992. *Three-Dimensional Modeling of Unsaturated Flow in the Vicinity of Proposed Exploratory Shaft Facilities at Yucca Mountain, Nevada*. PNL-7474. Richland, VA: Pacific Northwest Laboratory.

Rosenblatt, M. 1952. Remarks on a multivariate transformation. *The Annals of Mathematical Statistics* 23: 470–472.

Ross, B. 1990. The diversion capacity of capillary barriers. *Water Resources Research* 26(10): 2,625–2,629.

Rubin, Y. 1991. Transport in heterogeneous porous media: Prediction and uncertainty. *Water Resources Research* 27(7): 1,723–1,738.

Russo, D. 1991. Stochastic analysis of simulated vadose-zone solute transport in a vertical cross-section of heterogeneous soil during nonsteady water flow. *Water Resources Research* 27(3): 267–283.

Russo, D., and G. Dagan. 1991. On solute transport in a heterogeneous porous formation under saturated and unsaturated flows. *Water Resources Research* 27(3): 285–292.

Russo, D., and M. Bouton. 1992. Statistical analysis of spatial variability in unsaturated flow parameters. *Water Resources Research* 28(7): 1,911–1,925.

Sagar, B., P.M. Clifton. 1985. Stochastic groundwater flow modeling using the second-order method. Tucson, AZ. In *International Association of Hydrogeologists Memoirs: Hydrogeology of Rocks of Low Permeability* 17(1): 498–512.

Salandin, P., and A. Rinaldo. 1990. Numerical experiments on dispersion in heterogeneous porous media. *Computational Methods in Subsurface Hydrology*. G. Gambolati, A. Rinaldo, C.A. Brebbia, W.G. Gray, and G.F. Pinder eds. Berlin, Germany: Springer-Verlag: 495–501.

Schwartz, F.W. 1977. Macroscopic dispersion in porous media: The controlling factors. *Water Resources Research* 13(4): 743–752.

Schwartz, F.W., L. Smith, and A.S. Crowe. 1983. A stochastic analysis of macroscopic dispersion in fractured media. *Water Resources Research* 19(5): 1,253–1,265.

Seginer, I. 1969. Random walk and random roughness models of drainage networks. *Water Resources Research* 5(3): 591–607.

Shinozuka, M., and C.M. Jan. 1972. Digital simulation of random processes and its application. *Journal of Sound and Vibrations* 25(1): 111–128.

Simmons, C.S. 1982. A stochastic-convective transport representation of dispersion in one-dimensional porous media systems. *Water Resources Research* 18(4): 1,193–1,1214.

Smith, L., and R.A. Freeze. 1979a. Stochastic analysis of steady state groundwater flow in a bounded domain, 1: One-dimensional simulations. *Water Resources Research* 15(3): 521–528.

Smith, L., and R.A. Freeze. 1979b. Stochastic analysis of steady state groundwater flow in a bounded domain, 2: Two-dimensional simulations. *Water Resources Research* 15(6): 1,543–1,559.

Smith, L, and F.W. Schwartz. 1980. Mass transport 1. A stochastic analysis of macroscopic dispersion. *Water Resources Research* 16(2): 303–313.

Smith, L., and F.W. Schwartz. 1981. Mass transport 2. Analysis of uncertainty in prediction. *Water Resources Research* 17(2): 351–369.

Smith, L., and F.W. Schwartz. 1993. Solute transport through fracture networks. *Flow and Contaminant Transport in Fractured Rock*. J. Bear, C.-F. Tsang, and G. de Marsily, eds. San Diego, CA: Academic Press, Inc.: 129–167.

Soerjadi, R. 1981. An alternative development of the dispersion equation. *Water Resources Research* 17(6): 1,611–1618.

Sposito, G., A.W. Jury, and V.K. Gupta. 1986. Fundamental problems in the stochastic convection-dispersion model of solute transport in aquifers and fields soils. *Water Resources Research* 22(1): 77–88.

Srinivasan, S.K., and R. Vasudevan. 1971. *Introduction to Random Differential Equations and Their Applications*. New York, NY: American Elsevier Publishing Co.

Stone, H.L., and P.L.T. Brian. 1963. Numerical solution of convective transport problems. *American Institute of Chemical Engineering Journal* 9(5): 681–688.

Sudicky, E.A. 1986. A natural gradient experiment on solute transport in a sand aquifer: Spatial variability of hydraulic conductivity and its role in the dispersion process. *Water Resources Research* 22(13): 2,069–2,082.

Tang, D.H., and G.F. Pinder. 1977. Simulation of groundwater flow and mass transport under uncertainty. *Advances in Water Resources* 1(1): 25–29.

Tsang, Y.W., K. Pruess, and J.S.Y. Wang. 1993. The role of fault zone in affecting multiphase flow at Yucca Mountain. *Proceeding of the Fourth International High-Level Radioactive Waste Management Conference*. Las Vegas, NV: American Nuclear Society: 660–666.

Tchelepi, H.A., and F.M. Orr, Jr., N. Rakotomalala, D. Salin, and R. Wouméni. 1993. Dispersion, permeability heterogeneity, and viscous fingering: Acoustic experimental observations and particle-tracking simulations. *Physical Fluids* A5(7): 1,558–1,574.

Tidwell, V.C., J.D. Von Doemming, and K. Martinez. 1993. Scale dependence of effective media properties. *Proceedings of the Fourth High-Level Radioactive Waste Management Conference*. Las Vegas, NV: American Nuclear Society and American Society of Civil Engineers: 1,059–1,065.

Todorovic, P. 1970. A stochastic model of longitudinal diffusion in porous media. *Water Resources Research* 6(1): 211–222.

Todorovic, P. 1975. A stochastic model of dispersion of sediment particles released from a continuous source. *Water Resources Research* 11(6): 919–925.

Tompson, A.F.B., and D.E. Dougherty. 1988. On the use of particle tracking methods for modeling solute transport in porous media. M.A. Celia et al., eds. *Computational Methods in Water Resources* (2): Numerical Methods for Transport and Hydrologic Processes: 227–232.

Tompson, A.F.B., and L.W. Gelhar. 1990. Numerical simulation of solute transport in three-dimensional, randomly heterogeneous porous media. *Water Resources Research* 26(10): 2,541–2,562.

Tompson, A.F.B., and D.E. Dougherty. 1992. Particle-grid methods for reacting flows in porous media: Application to Fisher's equation. *Applied Mathematical Modelling* 16: 374–383.

Tompson, A.F.B., R. Ababou, and L.W. Gelhar. 1987a. *Application and Use of the Three-Dimensional Turning Bands Random Field Generator: Single Realization Problems*. Report 313. Ralph M. Parsons Laboratory. Cambridge, MA: Massachusetts Institute of Technology.

Tompson, A.F.B., E.G. Vomvoris, and L.W. Gelhar. 1987b. *Numerical Simulation of Solute Transport in Randomly Heterogeneous Porous Media: Motivation, Model Development, and Application.* UCID-21281. Livermore, CA: Lawrence Livermore National Laboratory.

Tompson, A.F.B., R. Ababou, and L.W. Gelhar. 1989. Implementation of the three-dimensional turning bands random field generator. *Water Resources Research* 25(10): 2,227–2,243.

Uffink, G. 1986. A random-walk simulation of dispersion at an interface between fresh and saline groundwater. *Proceeding of the 9th Salt Water Intrusion Meeting*. Delft, Netherlands.

Uffink, G. 1987. Modeling of solute transport with the random walk method. *NATO Advanced Workshop on Advances in Analytical and Numerical Groundwater Flow and Quality Modelling*. Lisbon, Portugal.

Ünlü, K., D.R. Nielsen, and J.W. Biggar. 1990. Stochastic analysis of unsaturated flow: One-dimensional Monte Carlo simulations and comparisons with spectral perturbation analysis and field observations. *Water Resources Research* 26(9): 2,207–2,218.

Valocchi, A.J. 1990. Numerical simulation of the transport of adsorbing solutes in heterogeneous aquifers. *Computational Methods in Subsurface Hydrology*. G. Gambolati, A. Rinaldo, C.A. Brebbia, W.G. Gray, and G.F Pinder eds. Berlin, Germany: Springer-Verlag: 373–382.

Valocchi, A.J., and H.A.M. Quinodoz. 1989. Application of the random walk method to simulate the transport of kinetically absorbing solutes, groundwater contamination. *Proceedings of the 3rd IAHS Scientific Assembly*. Baltimore, MD: IAHS Publ. No. 185: 35–42.

van Genuchten, M. 1980. A closed form equation for predicting the hydraulic conductivity of unsaturated soils. *Soil Science Society of America Journal* 44: 892–898.

van Genuchten, M., and W.J. Alves. 1982. Analytical solution of the one-dimensional convective-dispersive solute transport equation. Technical Bulletin No. 1661: Riverside, CA: *U.S. Department of Agriculture.*

Vanmarcke, E. 1983. *Random Fields: Analysis and Synthesis*. Cambridge, MA: The MIT Press.

Vauclin, M., R. Haverkamp, and G. Vachaud. 1979. *Résolution Numérique d' une Équation de Diffusion Non Linéaire*. Grenoble, France. Presses universitaires de Grenoble: 183.

Wang, J.S.Y., and T.N. Narasimhan. 1988. *Hydrologic Modeling of Vertical and Lateral Movement of Partially Saturated Fluid Flow Near a Fault Zone at Yucca Mountain*. SAND87-7070. Albuquerque, NM: Sandia National Laboratories.

Warren, J.E., and H.S. Price. 1961. Flow in heterogeneous porous media. *Society of Petroleum Engineering Journal* 1: 153–169.

White, I., and M.J. Sully. 1987. Macroscopic and microscopic capillary length and time scales from field infiltration. *Water Resources Research* 23(8): 1,514–1,522.

White, I., and M.J. Sully. 1992. On the variability and use of the hydraulic conductivity alpha parameter in stochastic treatments of unsaturated flow. *Water Resources Research* 28(1): 209–213.

Wierenga, P.J., A.F. Toorman, D.B. Hudson, J. Vinson, M. Nash, and R.G. Hills. 1989. *Soil Physical Properties at the Las Cruces Trench Site*. NUREG/CR-5441. Washington, DC: Nuclear Regulatory Commission.

Willardson, L.S., and R.L. Hurst. 1965. Sample size estimates in permeability studies. *ASCE Journal of the Irrigation and Drainage Division* 91(1): 1–9.

Wittmeyer, G., S. Mohanty, R. Codell, and T. McCartin. 1993 *Yucca Mountain Test Case: Predicted Water Content Profiles for Borehole USW UZ16*. Stockholm, Sweden: Proceedings of INTRAVAL Workshop.

Wittwer, C.S., G. Chen, and G.S. Bodvarsson. 1993. Studies of the role of fault zones in fluid flow using the site-scale numerical model of Yucca Mountain. *Proceeding of the 4th International High-Level Radioactive Waste Management Conference*. Las Vegas, NV: American Nuclear Society: 667–674.

Wollrath, J., and W. Zielke. 1990. Transport in fractured rock-particle tracking in stochastically generated fracture networks. *Computational Methods in Surface Hydrology*. G. Gambolati, A. Rinaldo, C.A. Brebbia, W.G. Gray, and G.F. Pinder, eds. Berlin, Germany: Springer-Verlag: 229–232.

Wu, Y.T., A.B. Gureghian, and B. Sagar. 1993. Sensitivity and uncertainty analyses applied to one-dimensional radionuclide transport in a layered fractured rock. Part II: Probabilistic methods based on the limit-state approach. *Nuclear Technology* 104: 297–308.

Yaglom, A.M. 1962. *Stationary Random Functions*. R. Silverman ed. New York, NY: A. Dover

Yeh, T.-C.J. 1989. One-dimensional steady state infiltration in heterogeneous soils. *Water Resources Research* 25(10): 2,149–2,158.

Yeh, G.T. 1990. A Lagrangian-Eulerian method with zoomable hidden fine-mesh approach to solving advection-dispersion equations. *Water Resources Research* 26(6): 1,133–1,144.

Yeh, T.-C.J., W.L. Gelhar, and A.L. Gutjar. 1985a. Stochastic analysis of unsaturated flow in heterogeneous soils 1. Statistically isotropic media. *Water Resources Research* 21(4): 447–456.

Yeh, T.-C.J., W.L. Gelhar, and A.L. Gutjahr. 1985b. Stochastic analysis of unsaturated flow in heterogeneous soils 2. Statistically anisotropic media with variable α. *Water Resources Research* 21(4): 457–464.

Yeh, T.-C.J., W.L. Gelhar, and A.L. Gutjahr. 1985c. Stochastic analysis of unsaturated flow in heterogeneous soils 3. Observations and applications. *Water Resources Research* 21(4): 465–471.

Yeh, T.-C.J., A. Guzman, R. Srivastava, and P.E. Gagnard. 1994. Numerical simulation of the wicking effect in liner systems. *Ground Water* 32(1): 2–11.

Zaslavsky, D., and G. Sinai. 1981. Surface hydrology: IV Flow in sloping layered soil. *Journal of Hydraulic Division of American Society Civil Engineering* 107: 53–64.

Zimmerman, D.A., K.K. Wahl, A.L. Gutjahr, and P.A. Davis. 1990. *A Review of Techniques for Propagating Data and Parameters Uncertainties in High-Level Radioactive Waste Repository Performance Assessment Models*. NUREG/CR-5393. Washington, DC: Nuclear Regulatory Commission.

APPENDIX A

A.1 Description of Numerical Schemes Used for Testing the Accuracy of the Particle Tracking Method

Consider the problem of finding an approximate solution of the 1D advection-diffusion-equation (ADE) at a point x_i and time t_{n+1} on a mesh that covers the domain of interest. We shall consider explicit methods (in time) only. The centered finite difference (CFD) method uses second-order, centered approximations for both the advection and diffusion operators. The resulting finite difference analog of the ADE is, therefore:

$$\frac{c_i^{n+1} - c_i^n}{\Delta t} = - v\frac{c_{i+1}^n - c_{i-1}^n}{2\Delta x} + \frac{D}{\Delta x^2}\left(c_{i+1}^n - 2c_i^n + c_{i-1}^n\right) \tag{A-1}$$

where c_i^n is the concentration at node i at time step n; v is the velocity; D is the dispersion coefficient; and Δx, Δt are the grid node spacing and time step, respectively. This method is characterized by extensive numerical smearing. When small timesteps are used, as a countermeasure, wiggles may appear in the solution. The upwind finite difference (UFD) scheme employs backward difference approximation in space for the advection term. The result is (assuming $v>0$)

$$\frac{c_i^{n+1} - c_i^n}{\Delta t} = - v\frac{c_i^n - c_{i-1}^n}{\Delta x} + \frac{D}{\Delta x^2}\left(c_{i+1}^n - 2c_i^n + c_{i-1}^n\right) \tag{A-2}$$

UFD resolves the oscillatory behavior problem, although it maintains numerical smearing in the solution. The Lax-Wendroff (LW) and Fromm (FR) schemes are developed from the pure advection problem, $D=0$, by examining the Taylor series for the derivative $\partial c/\partial t$. We start with the LW scheme. Including only the first- and second-order terms of a Taylor series for the time derivative:

$$\left.\frac{\partial c}{\partial t}\right|_i^n = \frac{c_i^{n+1} - c_i^n}{\Delta t} - \frac{1}{2}\Delta t \left.\frac{\partial^2 c}{\partial t^2}\right|_i^n \tag{A-3}$$

The second-order temporal derivative can be written as:

$$\frac{\partial^2 c}{\partial t^2} = \frac{\partial}{\partial t}\left[\frac{\partial c}{\partial t}\right] = \frac{\partial}{\partial t}\left[-v\frac{\partial c}{\partial x}\right] \tag{A-4}$$

Exchanging the order of temporal and spatial differentiation, substituting in Eq. (A-3), and making use of the centered, second-order finite difference approximation of the right-hand side, we get:

$$\left.\frac{\partial c}{\partial t}\right|_i^n = \frac{c_i^{n+1} - c_i^n}{\Delta t} - \frac{v^2\Delta t}{2\Delta x^2}\left(c_{i+1}^n - 2c_i^n + c_{i-1}^n\right) \tag{A-5}$$

Thus, a higher-order time-differencing scheme is being used.

The LW scheme employs a centered differencing approximation for the first-order spatial derivative of concentration. When diffusion is nonzero, its form is:

$$\frac{c_i^{n+1} - c_i^n}{\Delta t} = - \frac{v}{2\Delta x}\left(c_{i+1}^n - c_{i-1}^n\right) + \left[\frac{D}{\Delta x^2} + \frac{v^2\Delta t}{2\Delta x^2}\right]\left(c_{i+1}^n - 2c_i^n + c_{i-1}^n\right) \tag{A-6}$$

Fromm's scheme was developed by observing (using von Neumann analysis) that the LW scheme, D=0, has a lag in the phase. An upstream-biased scheme,

$$\frac{c_i^{n+1} - c_i^n}{\Delta t} = - \frac{v}{2\Delta x}\left(c_i^n - c_{i-2}^n\right) + \frac{v^2\Delta t - 2v\Delta x}{2\Delta x^2}\left(c_i^n - 2c_{i-1}^n + c_{i-2}^n\right) \tag{A-7}$$

has a leading phase error. A straightforward average of Eq. (A-6), with D=0, and Eq. (A-7), and then adding the central approximation for the diffusion term, leads to the Fromm scheme:

$$\begin{aligned}\frac{c_i^{n+1} - c_i^n}{\Delta t} = &- \frac{v}{4\Delta x}\left(c_{i+1}^n - c_{i-1}^n + c_i^n - c_{i-2}^n\right) + \left[\frac{D}{\Delta x^2} + \frac{v^2\Delta t}{4\Delta x^2}\right]\left(c_{i+1}^n - 2c_i^n + c_{i-1}^n\right) \\ &+ \frac{v^2\Delta t - 2v\Delta x}{4\Delta x^2}\left(c_i^n - 2c_{i-1}^n + c_{i-2}^n\right)\end{aligned} \tag{A-8}$$

The piecewise parabolic method (PPM), presented by Collela and Woodward (1984), is a nonlinear high-order Godunov method. It is based on the concept of representing the concentration (or any other attribute involved in the advection equation) on a grid as a piecewise parabolic interpolant. Collela and Woodward (1984) state that by using a parabolic interpolant a more correct representation of both steep and smooth gradients of concentration can be obtained. Furthermore, a fourth-order approximation is attained when sufficiently smooth initial conditions are imposed. The hyperbolic differential operator is approximated as:

$$\frac{c_i^{n+1} - c_i^n}{\Delta t} = \frac{v}{\Delta x}\left(f_{i-\frac{1}{2}} - f_{i+\frac{1}{2}}\right) \tag{A-9}$$

where

$$f_{i\pm\frac{1}{2}} = (v\Delta t)\, f^a_{i\pm\frac{1}{2},L} \tag{A-10}$$

and

$$f^a_{i\pm\frac{1}{2},L}(y) = \frac{1}{y}\int_{x_i\pm\frac{1}{2}-y}^{x_i\pm\frac{1}{2}} c(x)\,dx \tag{A-11}$$

is a measure of the mass flux in or out of each computation cell. The method ensures local monotonicity and mass balance within a computational cell. The effects of diffusion are calculated subsequently using a standard finite difference method according to the idea of operator splitting. A detailed description of the algorithm can be found in Collela and Woodard (1984).

The flux-corrected transport (FCT) scheme is a nonlinear, second-order monotone method presented by Boris and Book (1973). The FCT technique ensures positivity, mass conservation, and local monotonicity, thus resolving the overshoot/undershoot problem. The scheme consists of two parts, a numerically-diffusive convective step followed by an anti-diffusion correction part. In the latter step,

numerical smearing is limited by applying an anti-diffusion operator. For a uniform velocity field the FCT finite difference scheme is described by:

$$c_i^{\sim n+1} = c_i^n - \frac{C_o}{2}\left(c_{i+1}^n - c_{i-1}^n\right) + \omega\left(c_{i+1}^n - 2c_i^n + c_{i-1}^n\right) \qquad \text{(A-12)}$$

where ω is the numerical diffusion coefficient and $c_i^{\sim n+1}$ is the solution after the first step. To guarantee stability and positivity, the numerical diffusion coefficient has to be bounded. Oran and Boris (1987) and Boris and Book (1973) provide a detailed discussion of these bounding criteria. During the second part of the FCT algorithm, excessive numerical diffusion is corrected by introducing numerical anti-diffusion as follows:

$$c_i^{n+1} = c_i^{\sim n+1} - \mu\left(c_{i+1}^{\sim n+1} - 2c_i^{\sim n+1} + c_{i-1}^{\sim n+1}\right) \qquad \text{(A-13)}$$

where μ is a positive (or zero) numerical anti-diffusion coefficient. The anti-diffusion step should not generate new extrema and should not amplify the values of existing extrema. It is, therefore, imperative to limit the anti-diffusive fluxes. For the reference problem, μ was chosen to be $\omega - \frac{C_o^2}{2} = 0.0984$. Here, the effects of physical diffusion are introduced by augmenting the numerical diffusion coefficient, ω, by D. A detailed description of this limiting procedure can be found in Boris and Book (1973).